INFORMATION TO USERS

This manuscript has been reproduced from the microfilm master. UMI films the text directly from the original or copy submitted. Thus, some thesis and dissertation copies are in typewriter face, while others may be from any type of computer printer.

The quality of this reproduction is dependent upon the quality of the copy submitted. Broken or indistinct print, colored or poor quality illustrations and photographs, print bleedthrough, substandard margins, and improper alignment can adversely affect reproduction.

In the unlikely event that the author did not send UMI a complete manuscript and there are missing pages, these will be noted. Also, if unauthorized copyright material had to be removed, a note will indicate the deletion.

Oversize materials (e.g., maps, drawings, charts) are reproduced by sectioning the original, beginning at the upper left-hand corner and continuing from left to right in equal sections with small overlaps.

Photographs included in the original manuscript have been reproduced xerographically in this copy. Higher quality 6" x 9" black and white photographic prints are available for any photographs or illustrations appearing in this copy for an additional charge. Contact UMI directly to order.

Bell & Howell Information and Learning
300 North Zeeb Road, Ann Arbor, MI 48106-1346 USA
800-521-0600

Université d'Ottawa • University of Ottawa

Development and Implementation of Novel Numerical Techniques for Integrated Optics and Microwave Planar Structures

by

Chengkun Chen, B. Sc., M.Sc.

A thesis submitted to the
School of Graduate Studies and Research
in partial fulfillment of the requirements for the degree of

Master of Applied Science
In Electrical Engineering

Ottawa-Carleton Institute for Electrical and Computer Engineering
School of Information Technology and Engineering
Faculty of Engineering
University of Ottawa

May 2000

ABSTRACT

In this thesis, a novel numerical method for characterizing the electromagnetic modes supported by multilayer planar optical waveguides and a new formulation of the Method of Lines (MoL) for the static analysis of multi-conductor planar transmission line structures have been developed.

One purpose of this work is to develop an efficient and accurate numerical method to analyze planar lossless, lossy and active optical waveguides in anisotropic media. This method solves the dispersion equation in the complex plane via Cauchy's integration for a guided wave structure of interest. The method is applicable to lossless, lossy, active and ARROW waveguide structures and can handle both leaky and guided modes. Contrary to the methods currently published in the literature, which are based on a numerical derivative of the dispersion equation, we propose an analytical derivative for the latter. This has a double impact: improved accuracy and reduced CPU time. The specific integration contour for leaky modes is discussed. The results are in excellent agreement with several results published in the literature.

Another purpose of this work is to develop a new formulation useful for modeling the Quasi-TEM performance of multi-conductor transmission lines in inhomogeneous anisotropic media, including finite metallization thickness. A general Method of Lines (MoL) formulation for inhomogeneous anisotropic media and finite metallization thickness is derived. The method allows the accurate determination of the static parameters of the transmission line with great efficiency compared to methods available in the literature. Several numerical examples are shown for single and multi-conductor transmission lines including finite metallization thickness effect. Comparisons made with the results available from the literature validate the approach.

ACKNOWLEDGEMENT

I would like to express my deepest gratitude to my supervisor Dr. P. Berini for his constant guidance, inspiration, advice, and encouragement throughout this thesis project.

I would also like to thank Dr. D. Feng for his valuable suggestions on the numerical simulation and computer programming at Optiwave Corporation; Dr. V. P. Tzolov, Dr. Z. Jakubczyk, Dr. D. Feng and Dr. S. Tanev for their valuable suggestions and fruitful discussions on the Planar Optical Waveguides at Optiwave Corporation.

I would like to acknowledge the support of Optiwave Corporation, Canada and Communications and Information Technology Ontario (CITO), Canada.

I would also like to take this opportunity to thank my wife Fangyu for her continued support, understanding, love and patience during my studies and research.

TABLE OF CONTENTS

LIST OF FIGURES

LIST OF TABLES

CHAPTER 1

INTRODUCTION

1.1 BACKGROUND AND MOTIVATION

1.1.1 Numerical Analysis of Multilayer Planar Optical Waveguides

The notions of guided and leaky modes are fundamental concepts in optical waveguiding theory. A knowledge of mode propagation characteristics is essential to the design of numerous guided-wave optoelectronic devices, passive and active components such as semiconductor lasers, electro-absorption and electro-optic modulators, switches, photodetectors, filters and couplers, to name but a few. Numerical methods that can efficiently and accurately model planar optical waveguides are thus of obvious importance since they are used as a basic tool in the design process.

The transfer matrix method (TMM) [1,2], as one of the primary tools for multilayer planar optical waveguide analysis, can generate the dispersion equation of the TE and TM modes supported by such structures in a straightforward manner. In our formulation, the waveguides can consist of any combination of lossless, lossy (dielectric, semiconductor, metallic), active and anisotropic layers. By solving the dispersion equation, the mode propagation constant is

obtained, and the electromagnetic field distribution found. For the modes of lossy, active waveguides and leaky modes, the mode propagation constants, which are the roots of the dispersion equation, are complex numbers.

Traditional numerical zero-search algorithms, such as the downhill method [3], Newton's method and the one-dimensional scan method [4], cannot predict the number of propagating modes supported by the waveguides, and need an initial guess value close to the actual root. Therefore these methods are not efficient and reliable, especially for a general-purpose mode solver. There is a rigorous mathematical technique [5,6], which is capable of finding the zeros or poles of any analytic function in the complex plane. This technique is based on Cauchy's integration in the complex plane and can be used to solve the dispersion equation of a multilayer planar optical waveguide [7]-[9].

The new features that we present in this thesis include: (i) the formulation of the multilayer problem for anisotropic media characterized by a diagonal permittivity tensor, (ii) the derivation and use of an analytical derivative for the dispersion equation, and (iii) the selection of a new integration contour used in conjunction with Cauchy's integration method for locating leaky modes. Using an analytical derivative improves the accuracy of the method and greatly reduces the CPU time required to find modes. Our new integration contour improves the efficiency of the adaptive integration calculation. Moreover, our method is applicable to lossless, lossy and ARROW (AntiResonant Reflecting Optical Waveguide) waveguide [10] structures in anisotropic media and can handle both leaky and guided modes. Based on the method, object oriented software has been developed for the analysis of multilayer planar optical waveguides.

1.1.2 The Method of Lines for the Quasi-TEM Analysis of Multi-Conductor Transmission Lines

The quasi-TEM analysis of multi-conductor transmission lines such as (coupled) microstrip lines and (coupled) coplanar waveguides is of significant practical importance to the design of monolithic microwave integrated circuits (MMIC's) and high-speed optoelectronic devices such as travelling-wave photodetectors and modulators. The need for accurate and fast computer-aided design (CAD) tools that can model the quasi-TEM performance of multi-conductor transmission lines having a finite metallization thickness and embedded in inhomogeneous anisotropic media is manifest. It is desirable that a numerical technique forming the basis of such a CAD tool be robust and operate with limited computing resources as well as rapidly provide accurate solutions to a wide range of transmission line problems.

Numerous methods have been proposed for the quasi-TEM analysis of transmission lines. Commonly encountered methods include the boundary element method [11], [12]; the finite element method [13], [14]; the mode matching method [15]-[18]; the spectral domain method [19], [20]; the conformal mapping method [21]; the finite difference method [22]; the moment method [23], [24]; and the method of lines [25], [26]. Of the methods listed above, only the finite element and finite difference methods can perform the quasi-TEM analysis of transmission lines comprised of conductors of finite thickness embedded in inhomogeneous anisotropic dielectric media. However, both of these methods suffer from the same well-known drawbacks stemming from the fact that they are based on a full domain discretization.

The method of lines (MoL), formulated for the full-wave analysis of microwave and optical waveguides, is well-developed [27], [28], and is well-known for its numerical performance, that

is, its high accuracy, rapid speed of computation and minimal memory requirements. In a 2-D problem, the numerical performance of the MoL is due mainly to the fact that only one of the dimensions of the computational domain is discretized while generalized analytical solutions are introduced along the remaining dimension as part of the solution process. The MoL however has not been widely used for the quasi-TEM analysis of transmission lines, perhaps due to the fact that a formulation that can handle finite thickness conductors embedded in inhomogeneous anisotropic dielectric media is unavailable.

When a transmission line is used at frequencies where geometrical dispersion can be neglected, that is when the quasi-TEM approximation holds, then an expensive full-wave analysis of the structure may be wasteful. Furthermore, a quasi-TEM numerical method can be much more robust and numerically efficient compared to its full-wave counterpart and thus more suitable for introduction into commercial CAD packages. The main advantage of the quasi-TEM MoL, compared to the full-wave MoL, is that in the end a small inhomogeneous matrix problem is generated and solved directly via matrix inversion or using an efficient matrix solver. In the full-wave MoL, a homogeneous matrix problem is generated and solved by locating a zero of the determinant of the matrix, a procedure difficult to automate in a robust manner if the method is to be incorporated into a CAD package.

1.2 OBJECTIVE OF THE THESIS

A primary objective of the thesis is to develop a versatile, efficient, and accurate numerical tool to analyze multilayer planar optical waveguides. The numerical tool should be able to:

- Generate the propagation constant of guided and leaky modes of multilayer planar optical waveguides with arbitrary lossless, lossy and active materials.
- Generate the field distributions of guided and leaky modes within arbitrary waveguide profiles, and find the power in each layer for guided modes in lossless waveguides.
- Handle isotropic and anisotropic (diagonal permittivity tensor) media.
- Be suitable for integration into commercial integrated optics CAD tools.

Another primary objective of the thesis is to develop a new formulation of method of lines for the Quasi-TEM analysis of finite-thickness multi-conductor transmission lines embedded in inhomogeneous anisotropic dielectrics. The numerical method should be able to:

- Handle finite-thickness multi-conductor transmission lines and accurately determine the static parameters of transmission lines with great numerical efficiency.
- Generate the charge density distributions, potential distributions and fields distributions of the finite-thickness multi-conductor transmission lines structures.
- Handle inhomogeneous anisotropic dielectrics.
- Be suitable for integration into commercial CAD tools

1.3 THESIS ORGANIZATION

The remainder of the thesis is organized as follows. In Chapter 2, some background on electromagnetic field theory in waveguides is presented to introduce and better understand the TEM mode, TE mode and TM mode in planar optical waveguides and microwave transmission lines.

Chapter 3 consists of the numerical analysis of multilayer planar optical waveguides. Section 3.1 gives an Introduction. In section 3.2, the transfer matrix method is discussed. Transfer matrix, dispersion equation and field profiles in waveguides are derived in anisotropic media for both TE and TM modes. The power equation for guided modes in lossless structures is obtained. Cauchy's integration method is presented in section 3.3. The argument principle, numerical derivative, numerical integration, Laguerre's method to locate the root of polynomial and using Muler's method to further locate the accurate roots of a function are fully discussed in this section. Section 3.4 gives the analytical derivative of the dispersion equations. The analytical derivatives of the transfer matrix and dispersion equation for TE and TM modes are derived. Numerical results and discussion are given by section 3.5. Numerous examples for various waveguide structures are shown in this section. The results that aimed using this method are discussed and compared with the literature.

Chapter 4 presents a new formulation of the method of lines for the electrostatic analysis of transmission lines. This chapter is organized as follows. Section 4.2 presents the formulation of the quasi-TEM MoL for the analysis of multi-conductor transmission lines embedded inhomogeneous anisotropic media. Section 4.3 extends the formulation to handle conductors of finite thickness. Section 4.4, 4.5 and 4.6 describe how to handle abrupt dielectric discontinuities

along the transverse dimension, the non-equidistant discretization scheme and open structure along vertical dimensions. Section 4.7 presents some numerical results obtained by using the formulation and discusses them.

Finally, conclusions from this research and suggestions for further research are presented in chapter 5.

In addition to formulation presented in the thesis, the author has implemented a mode solver for the multilayer planar optical waveguides and a numerical engine for the finite-thickness multi-conductor transmission lines based on the novel numerical techniques presented in this thesis. They are being integrated into commercial CAD software packages for integrated optics.

CHAPTER 2

REVIEW OF ELECTROMAGNETIC FIELDS IN TRANSMISSION LINES AND WAVEGUIDES

2.1 INTRODUCTION

The electromagnetic wave propagation in an arbitrary medium can be described rigorously by Maxwell's equations and their associated boundary conditions. However, directly solving Maxwell's equations is usually difficult, and exact analytical solutions can be found only for a limited number of simple structures, such as step-index slab waveguides, step-index fibers, coaxial lines, rectangular waveguides and circular waveguides. Numerical solutions may be possible for more complex problems. In this chapter, transverse electromagnetic (TEM) wave, transverse electric (TE) wave and transverse magnetic (TM) wave equations are derived directly from Maxwell's equations. Transmission lines such as microstrip, coupled microstrip, coplanar waveguide and coaxial line can support TEM waves. Planar optical waveguides and rectangular waveguides can support TE and TM waves.

2.2 GENERAL WAVE EQUATIONS

Maxwell's equations in their general form are written as:

$$\nabla \times \bar{E} = -\frac{\partial \bar{B}}{\partial t} \tag{2-1a}$$

$$\nabla \times \bar{H} = \frac{\partial \bar{D}}{\partial t} + \bar{J} \tag{2-1b}$$

$$\nabla \cdot \bar{D} = -\rho \tag{2-1c}$$

$$\nabla \cdot \bar{B} = 0 \tag{2-1d}$$

and the constitutive relations are:

$$\bar{D} = \varepsilon \bar{E} \tag{2-2a}$$

$$\bar{B} = \mu \bar{H} \tag{2-2b}$$

We assume source free and time harmonic fields with a $e^{j\omega t}$ dependence, from Equations (2-1) and (2-2), we obtain:

$$\nabla \times \bar{\mathrm{E}} = j\omega\mu \bar{\mathrm{H}} \tag{2-3a}$$

$$\nabla \times \bar{\mathrm{H}} = -j\omega\varepsilon \bar{\mathrm{E}} \tag{2-3b}$$

$$\nabla \cdot \bar{\mathrm{E}} = 0 \tag{2-3c}$$

$$\nabla \cdot \bar{\mathrm{H}} = 0 \tag{2-3d}$$

Taking the curl of Equation (2-3a) and using Equation (2-3b) yields:

$$\nabla \times \left(\nabla \times \bar{\mathrm{E}}\right) = -j\omega\mu \nabla \times \bar{\mathrm{H}} = \omega^2 \mu\varepsilon \bar{\mathrm{E}} \tag{2-4}$$

Using the vector identity $\nabla \times \nabla \times \bar{A} = \nabla\left(\nabla \cdot \bar{A}\right) - \nabla^2 \bar{A}$, which is valid for the rectangular components of an arbitrary vector, and noting that $\nabla \cdot \bar{\mathrm{E}} = 0$, yields:

$$\nabla^2 \bar{\mathrm{E}} + \omega^2 \mu\varepsilon \bar{\mathrm{E}} = 0 \tag{2-5a}$$

or

$$\nabla^2\bar{E} + k^2\bar{E} = 0 \tag{2-5b}$$

where $k^2 = \omega^2\mu\varepsilon$. Equation (2-5) is referred to as the wave equation or Helmholtz equation for $\bar{E}$. The constant k is called the wave number, or propagation constant. In the same manner, an identical equation for $\bar{H}$ can be derived:

$$\nabla^2\bar{H} + \omega^2\mu\varepsilon\bar{H} = 0 \tag{2-6a}$$

or

$$\nabla^2\bar{H} + k^2\bar{H} = 0 \tag{2-6b}$$

2.3 GENERAL SOLUTIONS FOR TEM, TE, AND TM WAVES

The electric and magnetic fields for arbitrary microwave transmission lines and optical waveguides that are invariant along z and for propagation along the + z-axis, can be written as:

$$\bar{\mathrm{E}}(x,y,z) = [\bar{e}_t(x,y) + \hat{z}e_z(x,y)]e^{-j\gamma z} \tag{2-7a}$$

$$\bar{\mathrm{H}}(x,y,z) = [\bar{h}_t(x,y) + \hat{z}h_z(x,y)]e^{-j\gamma z} \tag{2-7b}$$

where $\bar{e}_t(x,y)$ and $\bar{h}_t(x,y)$ are the transverse electric and magnetic field components, $e_z(x,y)$ and $h_z(x,y)$ are the longitudinal electric and magnetic field components, and $\gamma = \beta - j\alpha$ is the propagation constant. From Equations (2-3a) and (2-3b) with a $e^{-j\gamma z}$ z-dependence, six component equations can be derived:

$$\frac{\partial E_z}{\partial y} + j\gamma E_y = -j\omega\mu H_x \tag{2-8a}$$

$$-j\gamma E_x - \frac{\partial E_z}{\partial x} = -j\omega\mu H_y \tag{2-8b}$$

$$\frac{\partial E_y}{\partial x} - \frac{\partial E_x}{\partial y} = -j\omega\mu H_z \tag{2-8c}$$

$$\frac{\partial H_z}{\partial y} + j\gamma H_y = j\omega\varepsilon E_x \tag{2-8d}$$

$$-j\gamma H_x - \frac{\partial H_z}{\partial x} = j\omega\varepsilon E_y \tag{2-8e}$$

$$\frac{\partial H_y}{\partial x} - \frac{\partial H_x}{\partial y} = j\omega\varepsilon E_z \tag{2-8f}$$

The Equations (2-8) can be solved for the four transverse field components in terms of E_z and H_z as follows:

$$H_x = \frac{j}{k_c^2}\left(\omega\varepsilon\frac{\partial E_z}{\partial y} - \gamma\frac{\partial H_z}{\partial x}\right) \tag{2-9a}$$

$$H_y = -\frac{j}{k_c^2}\left(\omega\varepsilon\frac{\partial E_z}{\partial x} + \gamma\frac{\partial H_z}{\partial y}\right) \tag{2-9b}$$

$$E_x = -\frac{j}{k_c^2}\left(\gamma\frac{\partial E_z}{\partial x} + \omega\mu\frac{\partial H_z}{\partial y}\right) \tag{2-9c}$$

$$E_y = \frac{j}{k_c^2}\left(-\gamma\frac{\partial E_z}{\partial y} + \omega\mu\frac{\partial H_z}{\partial x}\right) \tag{2-9d}$$

where

$$k_c^2 = k^2 - \gamma^2 \tag{2-10}$$

is the cutoff wavenumber and

$$k = \omega\sqrt{\mu\varepsilon} = \frac{2\pi}{\lambda} \tag{2-11}$$

is the wavenumber of the material filling the transmission line or waveguide region.

A large variety of waveguides of practical interest have mode fields where not all components are present. Specially, for transmission lines, the solution of interest is often a TEM wave with transverse fields only, that is $E_z = H_z = 0$, whereas for waveguides, solution with $E_z = 0$ or $H_z = 0$ are often possible.

2.4 TEM WAVES

For transverse electromagnetic (TEM) waves $E_z = H_z = 0$, from Equation (2-9) if $E_z = H_z = 0$, then the transverse fields are also zero, unless $k_c^2 = 0$ which means $k^2 = \gamma^2$. Applying the condition to Equations (2-8b) and (2-8d) and eliminating H_y yields:

$$\gamma^2 E_x = \omega^2 \mu \varepsilon E_x \tag{2-12a}$$

or

$$\gamma = \omega\sqrt{\mu\varepsilon} = k \tag{2-12b}$$

as noted earlier. The cutoff wavenumber, $k_c = \sqrt{k^2 - \gamma^2}$, is thus zero for TEM waves. From Equation (2-5), the Helmholtz equation for E_x component is:

$$\left(\frac{\partial^2}{\partial x^2} + \frac{\partial^2}{\partial y^2} + \frac{\partial^2}{\partial z^2} + k^2\right) E_x = 0 \tag{2-13}$$

but for e^{-jz} dependence and $\frac{\partial^2 E_x}{\partial z^2} = -\gamma^2 E_x = -k^2 E_x$, then Equation (2-13) can be reduced to a two-dimensional wave equation for E_x:

$$\left(\frac{\partial^2}{\partial x^2} + \frac{\partial^2}{\partial y^2}\right) E_x = 0 \tag{2-14}$$

A similar result also applies to E_y, then we have:

$$\left(\frac{\partial^2}{\partial x^2} + \frac{\partial^2}{\partial y^2}\right) \bar{E}_t = \nabla_t^2 \bar{E}_t = 0 \tag{2-15a}$$

or

$$\nabla_t^2 \bar{e}_t(x, y) = 0 \tag{2-15b}$$

where $\nabla_t^2 = \frac{\partial^2}{\partial x^2} + \frac{\partial^2}{\partial y^2}$ is the Laplacian operator in the two transverse dimensions.

Equation (2-15) shows that the transverse electric fields $\bar{e}_t(x,y)$, of a TEM wave satisfy Laplace's equation. Following the same procedure, it is easy to show that the transverse magnetic fields of a TEM wave also satisfy Laplace's equation:

$$\nabla_t^2 \bar{h}_t(x,y) = 0 \tag{2-16}$$

Substituting Equation (2-7) into (2-3) and noting $e_z = h_z = 0$ yields:

$$\nabla_t \times \bar{e}_t = 0 \tag{2-17a}$$

$$\nabla_t \times \bar{h}_t = 0 \tag{2-17b}$$

$$\nabla_t \cdot \bar{e}_t = 0 \tag{2-17c}$$

$$\nabla_t \cdot \bar{h}_t = 0 \tag{2-17d}$$

Equation (2-17a) is just the condition that permits $\bar{e}_t$ to be expressed as the gradient of a scalar potential. Hence let:

$$\bar{e}_t(x,y) = -\nabla_t \phi(x,y) \tag{2-18}$$

where $\nabla_t = \hat{x}\frac{\partial}{\partial x} + \hat{y}\frac{\partial}{\partial y}$, using Equation (2-17c), one can show that ϕ is a solution of the two dimensional Laplace's equation:

$$\nabla_t^2 \phi(x,y) = 0 \tag{2-19}$$

The electric field is thus given by:

$$\bar{E}_t(x,y,z) = -\nabla_t \phi(x,y) e^{-j\beta z} \tag{2-20}$$

But this field must also satisfy the Equation (2-15), substituting (2-20) into (2-15) and using (2-19) gives

$$\nabla_t^2 \bar{E}_t = -\nabla_t \left(\nabla_t^2 \phi \right) = 0 \tag{2-21}$$

Thus the field satisfies the Equation (2-15). The wave impedance of a TEM mode can be found as the ratio of the transverse electric and magnetic fields:

$$Z_{TEM} = \frac{E_x}{H_y} = -\frac{E_y}{H_x} = \frac{\omega\mu}{\gamma} = \sqrt{\frac{\mu}{\varepsilon}} = \eta \tag{2-22}$$

From Equation (2-22), the wave impedance of a TEM mode is dependent only on the material constants.

2.5 TE WAVES

For Transverse electric (TE) wave $E_z = 0$ and $H_z \neq 0$, then h_z plays the role of a potential function from which the rest of the field components may be obtained. From Equations (2-9), we obtain:

$$H_x = -\frac{j\gamma}{k_c^2}\frac{\partial H_z}{\partial x} \tag{2-23a}$$

$$H_y = -\frac{j\gamma}{k_c^2}\frac{\partial H_z}{\partial y} \tag{2-23b}$$

$$E_x = -\frac{j\omega\mu}{k_c^2}\frac{\partial H_z}{\partial y} \tag{2-23c}$$

$$E_y = \frac{j\omega\mu}{k_c^2}\frac{\partial H_z}{\partial x} \tag{2-24d}$$

where $k_c = \sqrt{k^2 - \gamma^2} \neq 0$. Unlike the case of TEM waves, γ^2 will not equal to k^2 for TE waves. Instead the propagation constant $\gamma = \sqrt{k^2 - k_c^2}$ is generally a function of frequency and the geometry of the transmission line or waveguide. From Equation (2-6), the Helmholtz equation for the H_z component is:

$$\left(\frac{\partial^2}{\partial x^2} + \frac{\partial^2}{\partial y^2} + \frac{\partial^2}{\partial z^2} + k^2\right) H_z = 0 \tag{2-25}$$

Since $H_z(x, y, z) = h_z(x, y)e^{-j\gamma z}$ and $\frac{\partial^2 H_z}{\partial z^2} = -\gamma^2 h_z(x, y)e^{-j\gamma z}$, then Equation (2-25) can be reduced to a two-dimensional wave equation for h_z:

$$\left(\frac{\partial^2}{\partial x^2} + \frac{\partial^2}{\partial y^2} + k_c^2\right) h_z = 0 \tag{2-26}$$

since $k_c^2 = k^2 - \gamma^2$. This equation (2-26) is solved subject to the appropriate boundary conditions and the eigenvalue k_c^2 will be found to be a function of the waveguide configuration. The TE wave impedance can be found as:

$$Z_{TE} = \frac{E_x}{H_y} = -\frac{E_y}{H_x} = \frac{\omega\mu}{\gamma} = \frac{k\eta}{\gamma} \tag{2-27}$$

which is frequency and transmission line or waveguide structure dependent.

2.6 TM WAVES

For Transverse electric (TM) wave $H_z = 0$ and $E_z \neq 0$, then e_z plays the role of a potential function from which the rest of the field components may be obtained. From Equations (2-9), we obtain:

$$H_x = \frac{j\omega\varepsilon}{k_c^2}\frac{\partial E_z}{\partial y} \tag{2-28a}$$

$$H_y = -\frac{j\omega\varepsilon}{k_c^2}\frac{\partial E_z}{\partial x} \tag{2-28b}$$

$$E_x = -\frac{j\gamma}{k_c^2}\frac{\partial E_z}{\partial x} \tag{2-28c}$$

$$E_y = -\frac{j\gamma}{k_c^2}\frac{\partial E_z}{\partial y} \tag{2-28d}$$

As in the TE case, $k_c = \sqrt{k^2 - \gamma^2} \neq 0$, and the propagation constant $\gamma = \sqrt{k^2 - k_c^2}$ is generally a function of frequency and the geometry of the transmission line or waveguide. E_z is found from the Helmholtz equation :

$$\left(\frac{\partial^2}{\partial x^2} + \frac{\partial^2}{\partial y^2} + \frac{\partial^2}{\partial z^2} + k^2\right)E_z = 0 \tag{2-29}$$

Since $E_z(x,y,z) = e_z(x,y)e^{-j\gamma z}$ and $\frac{\partial^2 E_z}{\partial z^2} = -\gamma^2 e_z(x,y)e^{-j\gamma z}$, then Equation (2-29) can be reduced to a two-dimensional wave equation for e_z:

$$\left(\frac{\partial^2}{\partial x^2} + \frac{\partial^2}{\partial y^2} + k_c^2\right)e_z = 0 \tag{2-30}$$

since $k_c^2 = k^2 - \gamma^2$. This equation (2-30) is solved subject to the appropriate boundary conditions, the eigenvalue k_c^2 will be found to be a function of the waveguide configuration

The TM wave impedance can be found as:

$$Z_{TM} = \frac{E_x}{H_y} = -\frac{E_y}{H_x} = \frac{\gamma}{\omega\varepsilon} = \frac{\gamma\eta}{k} \tag{2-31}$$

which is frequency and transmission line or waveguide structure dependent.

CHAPTER 3

EFFICIENT AND ACCURATE NUMERICAL ANALYSIS OF MULTILAYER PLANAR AND OPTICAL WAVEGUIDES

3.1 INTRODUCTION

Guided and leaky modes are fundamental concepts in optical waveguiding theory. A knowledge of mode propagation characteristics is essential to the design of numerous guided-wave optoelectronic devices, passive and active components such as semiconductor lasers, electro-absorption and electro-optic modulators, switches, photodetectors, filters and couplers. Numerical methods that can efficiently and accurately model planar optical waveguides are thus of obvious importance since they are used as a basic tool in the design process.

The transfer matrix method (TMM) can generate the dispersion equation of the TE and TM modes in a straightforward manner. In this chapter, new formulations of the transfer matrix and dispersion equation have been derived for the waveguides which can consist of any combination of lossless, lossy (dielectric, semiconductor, metallic), active and anisotropic layers. By solving the dispersion equation using Cauchy's integration method, the mode propagation constant is

obtained, and the electromagnetic field distribution is found for both guided and leaky modes of lossless, lossy and active waveguides.

The new features that we present in this chapter include: (i) the formulation of the multilayer problem for anisotropic media characterized by a diagonal permittivity tensor, (ii) the derivation and use of an analytical derivative for the dispersion equation, and (iii) the selection of a new integration contour used in conjunction with Cauchy's integration method for locating leaky modes. Using an analytical derivative improves the accuracy of the method and greatly reduces the CPU time required to find modes. Our new integration contour improves the efficiency of the adaptive integration calculation.

3.2 TRANSFER MATRIX METHOD

The transfer matrix method provides a straightforward formulation of the multilayer planar optical waveguide problem. A multilayer nonmagnetic anisotropic slab waveguide structure ($\mu = \mu_0$) is shown in Figure 3.1. The refractive index tensor, $\bar{\bar{n}}_i$, of the i-th layer can be in general complex, i.e., $\tilde{n}_i = n_i - jk_i$ where k_i is the extinction coefficient of the i-th layer and $i = 1, 2, \cdots, r$ is the layer number.

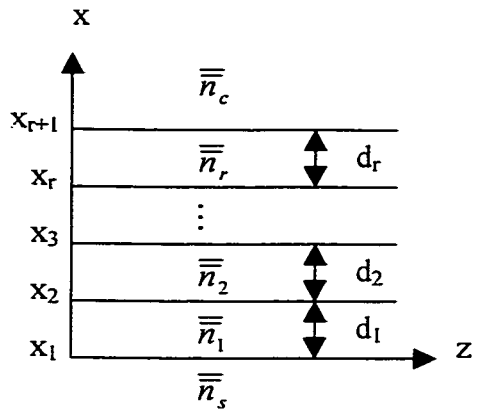

Figure 3.1. Structure of the multilayer planar optical waveguide

3.2.1 Maxwell's Equations and TE Field Solutions

Maxwell's curl equations [29] for source-free, time-harmonic fields in anisotropic media are:

$$\nabla \times \bar{E} = -j\omega\mu_0 \bar{H} \tag{3-1a}$$

$$\nabla \times \bar{H} = j\omega\varepsilon_0 \bar{\bar{\varepsilon}} \bar{E} \tag{3-1b}$$

where ε_0 is the free space permittivity, ω is the angular frequency, and $\bar{\bar{\varepsilon}}$ is a tensor of relative permittivity having the form:

$$\bar{\bar{\varepsilon}} = \begin{bmatrix} \tilde{\varepsilon}_{xx} & & \\ & \tilde{\varepsilon}_{yy} & \\ & & \tilde{\varepsilon}_{zz} \end{bmatrix} = \begin{bmatrix} \tilde{n}_{xx}^2 & & \\ & \tilde{n}_{yy}^2 & \\ & & \tilde{n}_{zz}^2 \end{bmatrix} \tag{3-2}$$

For a TE mode (E_x, E_z, $H_y=0$) propagating in the $+\hat{z}$ direction in the i-th layer, ($x_i \le x \le x_{i+1}$), the non-zero electric and magnetic field components are:

$$\bar{E}_i = \hat{y} E_{yi}(x) \exp(j\omega t - j\tilde{\gamma} z) \tag{3-3a}$$

$$\bar{H}_i = [\hat{x} H_{xi}(x) + \hat{z} H_{zi}(x)] \exp(j\omega t - j\tilde{\gamma} z) \tag{3-3b}$$

where $\hat{x}, \hat{y}, \hat{z}$ are the unit vectors in the x, y, z direction respectively, $\tilde{\gamma} = \beta - j\alpha = k_0(\bar{\beta} - j\bar{\alpha})$ is the complex propagation constant with β and α the phase and attenuation constants respectively and $k_0 = \omega/c = 2\pi/\lambda_0$, c is the speed of light in free space and λ_0 is the free space wavelength. From Equation (3-1) and (3-3), we can derive:

$$\frac{d^2 E_{yi}(x)}{dx} + \tilde{\kappa}_i^2 E_{yi}(x) = 0 \tag{3-4}$$

and

$$H_{zi}(x) = \frac{j}{\omega\mu_0} \frac{dE_{yi}(x)}{dx} \tag{3-5a}$$

$$H_{xi}(x) = -\frac{\tilde{\gamma}}{\omega\mu_0} E_{yi}(x) \tag{3-5b}$$

where $\tilde{\kappa}_i = \pm\sqrt{k_0^2 \tilde{n}_{yyi}^2 - \tilde{\gamma}^2}$. The tangential electric field and its derivative must satisfy Equation (3-4) and are related to the tangential magnetic fields through Equation (3-5) within the i-th layer. Solutions to Equation (3-4) are written as:

$$E_{yi}(x) = A_i \exp[-j\tilde{\kappa}_i(x - x_i)] + B_i \exp[+j\tilde{\kappa}_i(x - x_i)] \tag{3-6a}$$

$$\frac{dE_{yi}(x)}{dx} = -j\tilde{\kappa}_i A_i \exp[-j\tilde{\kappa}_i(x-x_i)] + j\tilde{\kappa}_i B_i \exp[+j\tilde{\kappa}_i(x-x_i)] \tag{3-6b}$$

or

$$E_{yi}(x) = \cos[\tilde{\kappa}_i(x-x_i)]E_{yi}(x_i) + \frac{1}{\tilde{\kappa}_i}\sin[\tilde{\kappa}_i(x-x_i)]\frac{dE_{yi}(x_i)}{dx} \tag{3-7a}$$

$$\frac{dE_{yi}(x)}{dx} = -\tilde{\kappa}_i \sin[\tilde{\kappa}_i(x-x_i)]E_{yi}(x_i) + \cos[\tilde{\kappa}_i(x-x_i)]\frac{dE_{yi}(x_i)}{dx} \tag{3-7b}$$

where x_i defines the boundary between the i-th and $(i+1)$-th layer. Equations (3-6) and (3-7) imply that any square root sign for $\tilde{\kappa}_i$ is acceptable.

3.2.2 Transfer Matrix and the Dispersion Equation for the TE Modes

Using Equations (3-7), the tangential electric field and its derivative at the bottom of the i-th layer, ($x=x_i$), can be expressed as a function of the field and its derivative within that layer as:

$$\begin{pmatrix} E_{yi}(x_i) \\ \dfrac{dE_{yi}(x_i)}{dx} \end{pmatrix} = \begin{pmatrix} \cos[\tilde{\kappa}_i(x-x_i)] & -\dfrac{1}{\tilde{\kappa}_i}\sin[\tilde{\kappa}_i(x-x_i)] \\ \tilde{\kappa}_i \sin[\tilde{\kappa}_i(x-x_i)] & \cos[\tilde{\kappa}_i(x-x_i)] \end{pmatrix} \begin{pmatrix} E_{yi}(x) \\ \dfrac{dE_{yi}(x)}{dx} \end{pmatrix} \tag{3-8}$$

Imposing the continuity of tangential fields at any layer interface in the multilayer structure, the fields tangential to the boundary at the top of the substrate layer (E_{ys}, $\frac{dE_{ys}}{dx}$) and at the boundary at the bottom of the cover layer (E_{yc}, $\frac{dE_{yc}}{dx}$) are related via the matrix product:

$$\begin{aligned} \begin{pmatrix} E_{ys} \\ \dfrac{dE_{ys}}{dx} \end{pmatrix} &= \prod_{i=1}^{r} M_i \begin{pmatrix} E_{yc} \\ \dfrac{dE_{yc}}{dx} \end{pmatrix} \\ &= \begin{pmatrix} m_{11} & m_{12} \\ m_{21} & m_{22} \end{pmatrix} \begin{pmatrix} E_{yc} \\ \dfrac{dE_{yc}}{dx} \end{pmatrix} \end{aligned} \tag{3-9}$$

where:

$$M_i = \begin{pmatrix} \cos(\tilde{\kappa}_i d_i) & -\frac{1}{\tilde{\kappa}_i}\sin(\tilde{\kappa}_i d_i) \\ \tilde{\kappa}_i \sin(\tilde{\kappa}_i d_i) & \cos(\tilde{\kappa}_i d_i) \end{pmatrix} \qquad for\ i = 1,2,\cdots,r \tag{3-10}$$

are the transfer matrices for all of the r layers of thickness d_i. For guided modes in an open structure, the tangential fields in the substrate and cover must be exponentially decaying:

$$\left.\begin{aligned} E_{ys}(x) &= A_s \exp(\tilde{\gamma}_s x) \\ \frac{dE_{ys}(x)}{dx} &= \tilde{\gamma}_s A_s \exp(\tilde{\gamma}_s x) \end{aligned}\right\} \quad for\ \ x \le 0 \tag{3-11}$$

$$\left.\begin{aligned} E_{yc}(x) &= B_c \exp[-\tilde{\gamma}_c (x - x_{r+1})] \\ \frac{dE_{yc}(x)}{dx} &= -\tilde{\gamma}_c B_c \exp[-\tilde{\gamma}_c (x - x_{r+1})] \end{aligned}\right\} \quad for\ \ x \ge x_{r+1} \tag{3-12}$$

where $\tilde{\gamma}_s = \pm\sqrt{\tilde{\gamma}^2 - k_0^2 \tilde{n}_{yys}^2}$, $\tilde{\gamma}_c = \pm\sqrt{\tilde{\gamma}^2 - k_0^2 \tilde{n}_{yyc}^2}$, and $\tilde{n}_{yys}$ *and* $\tilde{n}_{yyc}$ are the substrate and cover complex refractive indices along the y direction, respectively.

Equations (3-11) and (3-12) in conjunction with (3-9) yield the dispersion equation for the TE modes:

$$F(\tilde{\gamma}) = \tilde{\gamma}_s m_{11} + \tilde{\gamma}_c m_{22} - m_{21} - \tilde{\gamma}_s \tilde{\gamma}_c m_{12} = 0 \tag{3-13}$$

The zeros of which are the complex propagation constants $\tilde{\gamma}$.

3.2.3 Field Profiles in the Waveguide

Once the propagation constants are found, it is a simple matter to trace the field distributions [1] throughout the structure for each of the modes. We begin by inverting Equation (3-8), which yields:

$$\begin{pmatrix} E_{yi}(x) \\ \dfrac{dE_{yi}(x)}{dx} \end{pmatrix} = \begin{pmatrix} \cos[\tilde{\kappa}_i(x-x_i)] & \dfrac{1}{\tilde{\kappa}_i}\sin[\tilde{\kappa}_i(x-x_i)] \\ -\tilde{\kappa}_i \sin[\tilde{\kappa}_i(x-x_i)] & \cos[\tilde{\kappa}_i(x-x_i)] \end{pmatrix} \begin{pmatrix} E_{yi}(x_i) \\ \dfrac{dE_{yi}(x_i)}{dx} \end{pmatrix} \tag{3-14}$$

where $x_i \le x \le x_{i+1}$. The field amplitudes at a reference layer can be chosen arbitrarily. Choosing a value for E_{yi} in Equation (3-11), for example, sets the reference value for E_{ys} and $\dfrac{dE_{ys}}{dx}$ at the top of the substrate layer. Equation (3-14) is then employed to calculate the field amplitudes in other points of the structure in terms of this arbitrarily chosen amplitude. Applying the continuity of the tangential fields at any layer interface in the multilayer structure, the fields tangential to the boundaries at the top of the l-th layer (E_{yl} , $\dfrac{dE_{yl}}{dx}$) and at the top of the substrate layer (E_{ys} , $\dfrac{dE_{ys}}{dx}$) are related via a matrix product similar to Equation (3-9)

$$\begin{aligned} \begin{pmatrix} E_{yl} \\ \dfrac{dE_{yl}}{dx} \end{pmatrix} &= \prod_{i=1}^{l} \overline{M}_i \begin{pmatrix} E_{ys} \\ \dfrac{dE_{ys}}{dx} \end{pmatrix} \\ &= \begin{pmatrix} \overline{m}_{11} & \overline{m}_{12} \\ \overline{m}_{21} & \overline{m}_{22} \end{pmatrix} \begin{pmatrix} E_{ys} \\ \dfrac{dE_{ys}}{dx} \end{pmatrix} \end{aligned} \tag{3-15}$$

where:

$$\overline{M}_i = \begin{pmatrix} \cos(\tilde{\kappa}_i d_i) & \dfrac{1}{\tilde{\kappa}_i}\sin(\tilde{\kappa}_i d_i) \\ -\tilde{\kappa}_i \sin(\tilde{\kappa}_i d_i) & \cos(\tilde{\kappa}_i d_i) \end{pmatrix} \qquad for\ i = 1,2,\cdots,l \tag{3-16}$$

$E_{yi}(x)$ and $\dfrac{dE_{yi}(x)}{dx}$ are related to the amplitudes E_{yi} and $\dfrac{dE_{yi}}{dx}$ at the i-th interface by the Transfer Equation (3-14).

3.2.4 Power Equation for Guided Modes in Lossless Structures

The power of the i-layer in the propagation direction (z-direction) can be derived using Equation (3-3):

$$P_{zi} = -\frac{1}{2}\int_{x_i}^{x_{i+1}} E_y H_x dx = \frac{1}{2}\frac{\tilde{\gamma}}{\omega\mu_0}\int_{x_i}^{x_{i+1}} E_{yi}^2(x)dx = \frac{1}{2}\frac{\tilde{\gamma}}{k_0\eta_0}\int_{x_i}^{x_{i+1}} E_{yi}^2(x)dx \tag{3-17}$$

where $\tilde{\gamma}$ is the mode propagation constant and $\eta_0 = \sqrt{\frac{\mu_0}{\varepsilon_0}}$ is the free space wave impedance.

Substituting Equation (3-14) into Equation (3-17) and integrating, we obtain:

$$P_{zi} = \frac{\tilde{\gamma}}{4k_0\eta_0\tilde{\kappa}_i^2}\left[\left(\tilde{\kappa}_i E_{yi}^2(x_i) + \frac{1}{\tilde{\kappa}_i}\left(\frac{dE_{yi}(x)}{dx}\right)^2\right)\tilde{\kappa}_i d_i - \left(E_{yi+1}(x_{i+1})\frac{dE_{yi+1}(x_{i+1})}{dx} - E_{yi}(x_i)\frac{dE_{yi}(x_i)}{dx}\right)\right] \tag{3-18}$$

for $i = 1, 2, \cdots, r$

The power in the cover and substrate are given by:

$$P_{zc} = \frac{\tilde{\gamma}}{4k_0\eta_0\tilde{\gamma}_c}E_{yc}^2 \tag{3-19a}$$

$$P_{zs} = \frac{\tilde{\gamma}}{4k_0\eta_0\tilde{\gamma}_s}E_{ys}^2 \tag{3-19b}$$

3.2.5 Transfer Matrix and the Dispersion Equation for the TM Modes

For the TM modes (H_x, H_z, E_y=0) propagating in the $+\hat{z}$ direction in the i-th layer ($x_i \le x \le x_{i+1}$) the non-zero electric and magnetic field components are:

$$\bar{H}_i = \hat{y}H_{yi}(x)\exp(j\omega t - j\tilde{\gamma}z) \tag{3-20a}$$

$$\bar{E}_i = \left[\hat{x}E_{xi}(x) + \hat{z}E_{zi}(x)\right]\exp(j\omega t - j\tilde{\gamma}z) \tag{3-20b}$$

From Equations (3-1) and (3-20), we can derive:

$$\frac{d^2 H_{yi}(x)}{dx} + \tilde{\kappa}_i^2 H_{yi}(x) = 0 \tag{3-21}$$

and

$$E_{zi}(x) = -\frac{j}{\omega \varepsilon_0 \tilde{n}_{zzi}^2} \frac{dH_{yi}(x)}{dx} \tag{3-22a}$$

$$E_{xi}(x) = \frac{\tilde{\gamma}}{\omega \varepsilon_0 \tilde{n}_{xxi}^2} H_{yi}(x) \tag{3-22b}$$

where $\tilde{\kappa}_i = \pm \frac{\tilde{n}_{zzi}}{\tilde{n}_{xxi}} \sqrt{k_0^2 \tilde{n}_{xxi}^2 - \tilde{\gamma}^2}$.

The same procedure as in the case of TE modes is applied to derive the transfer matrix for the TM modes. The resulting layer transfer matrices M_i in (3-10) have the same form with the only difference being that $\tilde{\kappa}_i$ must be replaced by $\tilde{\kappa}_i / \tilde{n}_{zzi}^2$ in the coefficients of the sine terms, and in (3-13) $\tilde{\gamma}_s$ and $\tilde{\gamma}_c$ must be replaced by $\tilde{\gamma}_s / \tilde{n}_{zzs}^2$ and $\tilde{\gamma}_c / \tilde{n}_{zzc}^2$, because the tangential fields must be continuous at the boundary. So M_i and $F(\tilde{\gamma})$ become:

$$M_i = \begin{pmatrix} \cos(\tilde{\kappa}_i d_i) & -\frac{\tilde{n}_{zzi}^2}{\tilde{\kappa}_i} \sin(\tilde{\kappa}_i d_i) \\ \frac{\tilde{\kappa}_i}{\tilde{n}_{zzi}^2} \sin(\tilde{\kappa}_i d_i) & \cos(\tilde{\kappa}_i d_i) \end{pmatrix} \qquad \text{for } i = 1, 2, \cdots, r \tag{3-23}$$

and

$$F(\tilde{\gamma}) = \frac{\tilde{\gamma}_s}{\tilde{n}_{zzs}^2} m_{11} + \frac{\tilde{\gamma}_c}{\tilde{n}_{zzc}^2} m_{22} - m_{21} - \frac{\tilde{\gamma}_s \tilde{\gamma}_c}{\tilde{n}_{zzs}^2 \tilde{n}_{zzc}^2} m_{12} = 0 \tag{3-24}$$

The field transfer matrix $\overline{M}_i$ is the inverse of Equation (3-23):

$$\overline{M}_i = \begin{pmatrix} \cos(\tilde{\kappa}_i d_i) & \frac{\tilde{n}_{=i}^2}{\tilde{\kappa}_i}\sin(\tilde{\kappa}_i d_i) \\ -\frac{\tilde{\kappa}_i}{\tilde{n}_{=i}^2}\sin(\tilde{\kappa}_i d_i) & \cos(\tilde{\kappa}_i d_i) \end{pmatrix} \qquad for\ i = 1, 2, \cdots, r \tag{3-25}$$

and the power equation for individual layers is given by:

$$P_{zi} = \frac{\eta_0 \tilde{\gamma}}{4k_0 \tilde{\kappa}_i^2}\frac{\tilde{n}_{=i}^2}{\tilde{n}_{xxi}^2}\left[\left(\frac{\tilde{\kappa}_i}{\tilde{n}_{=i}^2}H_{yi}^2(x_i) + \frac{\tilde{n}_{=i}^2}{\tilde{\kappa}_i}\left(\frac{dH_{yi}(x_i)}{dx}\right)^2\right)\tilde{\kappa}_i d_i - \left(H_{yi+1}(x_{i+1})\frac{dH_{yi+1}(x_{i+1})}{dx} - H_{yi}(x_i)\frac{dH_{yi}(x_i)}{dx}\right)\right] \tag{3-26}$$

$$for\ \ i = 1, 2, \cdots, r$$

$$P_{zc} = \frac{\eta_0 \tilde{\gamma}}{4k_0 \tilde{n}_{xxc}^2 \tilde{\gamma}_c} H_{yc}^2 \tag{3-27a}$$

$$P_{zs} = \frac{\eta_0 \tilde{\gamma}}{4k_0 \tilde{n}_{xxs}^2 \tilde{\gamma}_s} H_{ys}^2 \tag{3-27b}$$

3.3 CAUCHY'S INTEGRAL METHOD

3.3.1 Cauchy's Integral Method

Cauchy's integral method [5] is based on the argument principle [30] and the residue theorem of complex analysis. If the function *f(z)* is analytic and does not go to zero over a closed integral contour, then the argument principle has the form:

$$S_0 = \frac{1}{j2\pi}\oint_C \frac{f'(z)}{f(z)}dz = N_z - N_p \tag{3-28}$$

where N_z is the number of zeros and N_p is number of poles inside the region enclosed by the

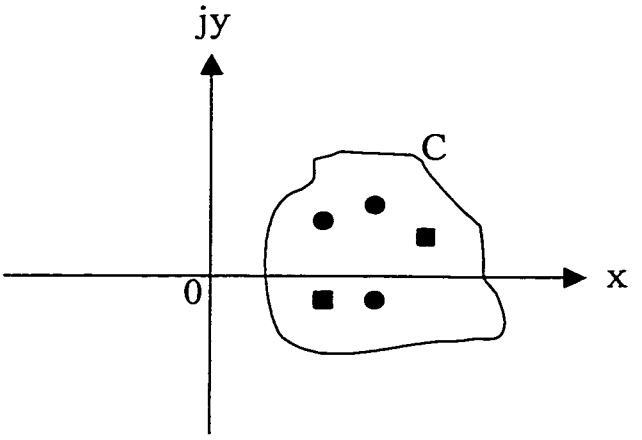

Figure 3.2 The arbitrary integral contour in the complex plane. The ' ■ 's correspond to the poles, and the ' ● 's correspond to the roots

contour *C*. If there are no poles in the region enclosed by the integral contour *C*, then S_0 is the number of zeros, and from the residue theorem we have:

$$S_m = \frac{1}{j2\pi}\oint_C z^m \frac{f'(z)}{f(z)}dz = \sum_{i=1}^{S_0} z_i^m \qquad for\ m = 1,2,\cdots,S_0 \tag{3-29}$$

where z_i, $i=1,2, \ldots, S_0$, are the roots of $f(z)$ inside C and S_m is the sum of z_i^m with $m=1,2, \ldots, S_0$. Equation (3-29) leads to a system of equations that can be used to evaluate the coefficients of a polynomial $p(z)$ of degree S_0, which has the same roots, $z_1, \cdots, z_{S_0}$, as the function $f(z)$ inside C. The approximation polynomial, $p(z)$, can be written as:

$$p(z) = \prod_{i=1}^{S_0} (z - z_i) = \sum_{k=0}^{S_0} C_k z^k \tag{3-30}$$

with $C_{S_0} = 1$. The coefficients C_k are given via Newton's recursive formula:

$$C_k = \frac{1}{(k - S_0)} \sum_{j=1}^{S_0 - k} S_j C_{k+j} \qquad \text{for } k = S_0 - 1, \cdots, 0 \tag{3-31}$$

The polynomial $p(z)$ can be solved by standard techniques such as Laguerre's method [31]. Following the above procedure, the initial difficult problem of finding the zeros of an arbitrary function $f(z)$ is transformed to the problem of finding the zeros of the polynomial $p(z)$, for which a variety of reliable numerical methods exist.

3.3.2 Integration Contour

Cauchy's integral method can be used to solve the dispersion equation of the multilayer planar optical waveguide in a straightforward manner. Once the poles have been identified, which are at $\bar{\beta} = \tilde{n}_c$, and at $\bar{\beta} = \tilde{n}_s$ shown in Figure 2.2(a) and 2.2(b), the rectangular integral contour C_1 is selected for the guided modes. The area between the minimum and the maximum real parts of all the refractive indices is enclosed by the contour C_1. The integral contour C_2 is selected for leaky modes. These contours do not enclose any of the poles.

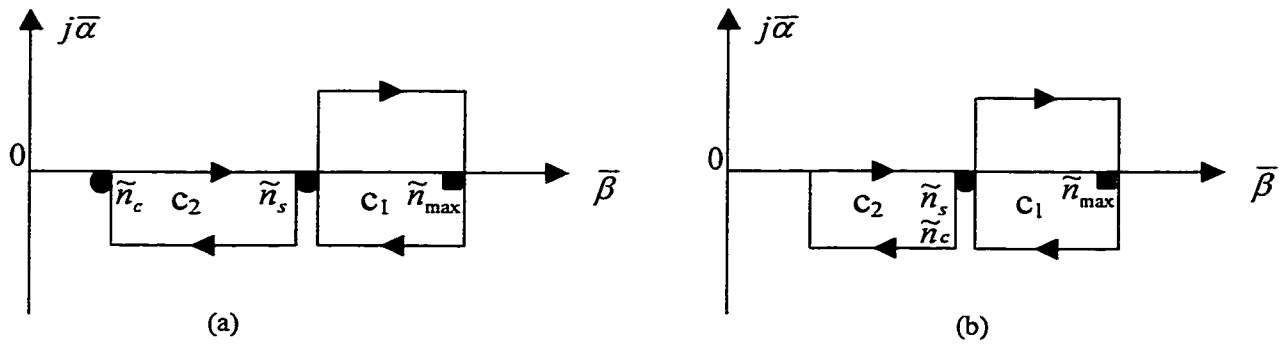

Figure 3.3 The integral contours in the complex plane. The ' ● 's correspond to the poles, $\tilde{n}_{\max}$ is the complex refractive index with the maximum real part and is enclosed by C_1. For TE modes in anisotropic media: $\tilde{n}_{\max} = \tilde{n}_{yy\max}$, $\tilde{n}_s = \tilde{n}_{yys}$, $\tilde{n}_c = \tilde{n}_{yyc}$; for TM modes in anisotropic media: $\tilde{n}_{\max} = \tilde{n}_{xx\max}$, $\tilde{n}_s = \tilde{n}_{xxs}$, $\tilde{n}_c = \tilde{n}_{xxc}$. (a) $\tilde{n}_c < \tilde{n}_s$, (b) $\tilde{n}_c = \tilde{n}_s$

3.3.3 Numerical Derivative

To solve Equation (3-28) and (3-29) we need the value of the derivative of the dispersion equation. If the derivative of the function cannot be obtained analytically, we can use the numerical derivative based on Cauchy's theorem [30]. The first derivative of a function *f(z)* at the point $z=z_0$ is given by:

$$f'(z_0) = \frac{1}{j2\pi} \oint_D \frac{f(z)}{(z-z_0)^2} dz \tag{3-32}$$

where *D* is any closed path which encloses the point z_0 and *f(z)* is analytic inside and on *D*. For the numerical calculation of the derivative $f'(z_0)$ Equation (3-32) was transformed with the variable transformation $z = z_0 + R\, e^{j2\pi t}$ to

$$f'(z_0) = \int_{t=0}^{1} \frac{f(z_0 + \mathrm{Re}^{j2\pi t})}{\mathrm{Re}^{j2\pi t}} dt \tag{3-33}$$

The variable R represents the radius of the circle with center z_0, over which the function $f(z)$ is evaluated. The radius can be set, in principle, arbitrarily small provided the corresponding circle does not include singularities. The above integral is periodic with period 1. Using the trapezoidal rule of quadrature scheme

$$f'(z_0) \approx \frac{1}{mR} \sum_{k}^{m} \frac{f(z_0 + \mathrm{Re}^{j2\pi k/m})}{e^{j2\pi k/m}} \tag{3-34}$$

With a simple termination criterion that two consecutive integration differences must be less than a small arbitrary number δ. If $[f'(z_0)]^m$ is the integration result via and m-point trapezoidal rule, the termination criterion is

$$\left| \left[f'(z_0) \right]^{2m} - \left[f'(z_0) \right]^{m} \right| < \delta \tag{3-35}$$

From Equations (3-34) and (3-35), It is clear that the computation of the numerical derivative is the most intensive computational task in Cauchy's integral method, which needs several $f(z)$ evaluations, and it is needed on each node, x_i, over the contour C. When a zero z is very close to the contour C, the numerical derivative converges very slowly and inaccurately. In multilayer planar optical waveguides, the derivative of the dispersion equation can be derived analytically. Reference [8] gives an analytical derivative in exponential form. We obtained the analytical derivatives of the transfer matrices and the dispersion equations; they are given and discussed in section 3.4.

3.3.4 Numerical Integration

To calculate the values of Equations (3-28) and (3-29), the numerical integration method and the adaptive integration method [32] were selected which are similar to those in reference [7]. The integration (quadrature) of function *F(z)* is represented by the summation:

$$\int_a^b F(z) = \sum_{i=1}^{K} W_i F(z_i) \tag{3-36}$$

where W_i are the weights and $a \leq z_i \leq b$ are the integration nodes. A 7-point Gaussian rule $G_7 f$ and 15-point Kronrod [33] rule $K_{15} f$ are used to estimate integration on the straight complex line interval [a, b]. The local quadrature estimate is taken as $K_{15} f$ since the Kronrod rule is more accurate than the Gaussian rule. If the local quadrature error estimate $| K_{15} f - G_7 f | / | K_{15} f |$ is less than a pre-specified tolerance, the local quadrature estimate is accepted as the actual integration result for the specific interval. Otherwise this interval is bisected and the same procedure is applied to the two new subintervals. In the same integration routine the calculation of the products $z_i^m f'(z_i) / f(z_i)$ for $m = 1, \cdots, S_0$, can be incorporated such that $f(z_i)$ and $f'(z_i)$ are evaluated only once for the specific node z_i for all the summations $S_1, \cdots, S_{S_0}$.

3.3.5 Laguerre's Method

The polynomial *p(z)* can be solved by Laguerre's method [31]. Laguerre's method is complex methods. It requires complex arithmetic, even while converging to real roots. To motivate the Laguerre formulas we can note the following relations between the polynomial and its roots and derivatives

$$p(z)=\prod_{i=1}^{n}(z-z_i)=(z-z_1)(z-z_2)\cdots(z-z_n) \tag{3-37}$$

$$\ln|p(z)|=\ln|z-z_1|+\ln|z-z_2|+\cdots+\ln|z-z_n| \tag{3-38}$$

$$\frac{d\ln|p(z)|}{dz}=\frac{1}{z-z_1}+\frac{1}{z-z_2}+\cdots+\frac{1}{z-z_n}=\frac{p'(z)}{p(z)}\equiv G \tag{3-39}$$

$$-\frac{d^2\ln|p(z)|}{dz^2}=\frac{1}{(z-z_1)^2}+\frac{1}{(z-z_2)^2}+\cdots+\frac{1}{(z-z_n)^2}=\left[\frac{p'(z)}{p(z)}\right]^2-\frac{p''(z)}{p(z)}\equiv H \tag{3-40}$$

From these relations, the root z_1 that we seek is assumed to be located some distance a from our current guess x, while all other roots are assumed to be located at a distance b

$$z-z_1=a \tag{3-41a}$$

$$z-z_i=b \qquad i=2,3,\cdots,n \tag{3-41b}$$

Then Equations (3-39) and (3-40) become

$$\frac{1}{a}+\frac{n-1}{b}=G \tag{3-42}$$

$$\frac{1}{a^2}+\frac{n-1}{b^2}=H \tag{3-43}$$

which yield as the solution for a

$$a=\frac{n}{G\pm\sqrt{(n-1)(nH-G^2)}} \tag{3-44}$$

where the sign should be taken to yield the largest magnitude for the denominator. The method operates iteratively: For a trial value x, a is calculated by Equation (3-44). Then $x-a$ becomes the next trial value. This continues until a is sufficiently small.

3.3.6 Muler's Method

The roots of polynomial *p(z)* and *f(z)* do not coincide due to the integration errors introduced by Equation (3-36). First S_0 should be confined to $S_0 \leq 4$. Then, after the roots of the polynomial *p(z)* are obtained. A further refinement must be performed to find the roots of *f(z)* by applying Muller's Method [31] with the initial guess being the roots of *p(z)*.

Muller's method uses quadratic interpolation among three points. Solving for the zeros of the quadratic allows the method to find complex pairs of roots. Given three previous guesses for the root z_{i-2}, z_{i-1}, z_i and the values of the function *f(z)* at those points, the next approximation z_{i+1} is produced by following formulas,

$$q \equiv \frac{z_i - z_{i-1}}{z_{i-1} - z_{i-2}} \tag{3-46a}$$

$$A \equiv qf(z_i) - q(1+q)f(z_{i-1}) + q^2 f(z_{i-2}) \tag{3-46b}$$

$$B \equiv (2q+1)f(z_i) - (1+q)^2 f(z_{i-1}) + q^2 f(z_{i-2}) \tag{3-46c}$$

$$C \equiv (1+q)f(z_i) \tag{3-46d}$$

followed by

$$z_{i+1} = z_i - (z_i - z_{i-1})\left[\frac{2C}{B \pm \sqrt{B^2 - 4AC}}\right] \tag{3-47}$$

where the sign in the denominator of Equation (3-47) is chosen to make its absolute value or modulus as large as possible. Starting the iterations with z_i which is the root of $p(z)$, and three values have equally spaced values on the real axis. This continues until $|z_{i+1} - z_i|$ is sufficiently small, then the root of $f(z)$ can be obtained as accurate as you wanted.

3.4 DERIVATIVE OF THE TRANSFER MATRICES AND DISPERSION EQUATIONS

3.4.1 Derivative of the Transfer Matrix and Dispersion Equation for the TE Modes

For the TE modes, let $\tilde{\gamma} = k_0 \tilde{u}$, $\tilde{\kappa}_i = \pm k_0 \sqrt{\tilde{n}_{yyi}^2 - \tilde{u}^2}$, $\frac{d\tilde{\kappa}_i}{d\tilde{u}} = -\frac{k_0^2}{\tilde{\kappa}_i}\tilde{u}$ and $\frac{d}{d\tilde{u}}(\frac{1}{\tilde{\kappa}_i}) = \frac{k_0^2}{\tilde{\kappa}_i^3}\tilde{u}$. Then from Equation (3-10) we derive:

$$\frac{dM_i}{d\tilde{u}} = \tilde{u}\begin{pmatrix} \frac{k_0^2 d_i}{\tilde{\kappa}_i}\sin(\tilde{\kappa}_i d_i) & \frac{k_0^2 d_i}{\tilde{\kappa}_i^2}\cos(\tilde{\kappa}_i d_i) - \frac{k_0}{\tilde{\kappa}_i^3}\sin(\tilde{\kappa}_i d_i) \\ -\frac{k_0^2}{\tilde{\kappa}_i}\sin(\tilde{\kappa}_i d_i) - k_0^2 d_i \cos(\tilde{\kappa}_i d_i) & \frac{k_0^2 d_i}{\tilde{\kappa}_i}\sin(\tilde{\kappa}_i d_i) \end{pmatrix} \quad for\ i = 1, \cdots, r \tag{3-34}$$

The derivative of the Transfer Matrix is then:

$$\frac{dM}{d\tilde{u}} = \sum_{j=1}^{r}\prod_{\substack{i=1 \\ i\neq j}}^{r} M_i \frac{dM_j}{d\tilde{u}} = \begin{pmatrix} \frac{dm_{11}}{d\tilde{u}} & \frac{dm_{12}}{d\tilde{u}} \\ \frac{dm_{21}}{d\tilde{u}} & \frac{dm_{22}}{d\tilde{u}} \end{pmatrix} \tag{3-35}$$

The derivative of $\tilde{\gamma}_s$ *and* $\tilde{\gamma}_c$ with respect to $\tilde{u}$ is $\frac{d\tilde{\gamma}_s}{d\tilde{u}} = \frac{k_0^2\tilde{u}}{\tilde{\gamma}_s}$ *and* $\frac{d\tilde{\gamma}_c}{d\tilde{u}} = \frac{k_0^2\tilde{u}}{\tilde{\gamma}_c}$, and from Equation (3-13) we obtain the derivative of the dispersion equation as:

$$\begin{aligned} \frac{dF(\tilde{u})}{d\tilde{u}} = {} & \frac{k_0^2\tilde{u}}{\tilde{\gamma}_s}m_{11} + \frac{k_0^2\tilde{u}}{\tilde{\gamma}_c}m_{22} + \tilde{\gamma}_s\frac{dm_{11}}{d\tilde{u}} + \tilde{\gamma}_c\frac{dm_{22}}{d\tilde{u}} - \frac{dm_{21}}{d\tilde{u}} \\ & - \frac{k_0^2\tilde{u}\tilde{\gamma}_c}{\tilde{\gamma}_s}m_{12} - \frac{k_0^2\tilde{u}\tilde{\gamma}_s}{\tilde{\gamma}_c}m_{12} - \tilde{\gamma}_s\tilde{\gamma}_c\frac{dm_{12}}{d\tilde{u}} \end{aligned} \tag{3-36}$$

3.4.2 Derivative of the Transfer Matrix and Dispersion Equation for the TM Modes

For the TM modes, $\tilde{\kappa}_i = \pm\frac{\tilde{n}_{zzi}}{\tilde{n}_{xxi}} k_0 \sqrt{\tilde{n}_{xxi}^2 - \tilde{u}^2} = \pm k\sqrt{\tilde{n}_{xxi}^2 - \tilde{u}^2}$, where $k = \frac{\tilde{n}_{zzi}}{\tilde{n}_{xxi}} k_0$; then

$\frac{d\tilde{\kappa}_i}{d\tilde{u}} = -\frac{k^2}{\tilde{\kappa}_i}\tilde{u}$ and $\frac{d}{d\tilde{u}}(\frac{1}{\tilde{\kappa}_i}) = \frac{k^2}{\tilde{\kappa}_i^3}\tilde{u}$, and from Equation (3-23) we derive:

$$\frac{dM_i}{d\tilde{u}} = \tilde{u}\begin{pmatrix} \frac{k^2 d_i}{\tilde{\kappa}_i}\sin(\tilde{\kappa}_i d_i) & \frac{k^2\tilde{n}_{zzi}^2 d_i}{\tilde{\kappa}_i^2}\cos(\tilde{\kappa}_i d_i) - \frac{k^2\tilde{n}_{zzi}^2}{\tilde{\kappa}_i^3}\sin(\tilde{\kappa}_i d_i) \\ -\frac{k^2}{\tilde{\kappa}_i\tilde{n}_{zzi}^2}\sin(\tilde{\kappa}_i d_i) - \frac{k^2 d_i}{\tilde{n}_{zzi}^2}\cos(\tilde{\kappa}_i d_i) & \frac{k^2 d_i}{\tilde{\kappa}_i}\sin(\tilde{\kappa}_i d_i) \end{pmatrix} \quad for\ i = 1,\cdots,r \tag{3-37}$$

The derivative of the dispersion equation in this case is:

$$\begin{aligned} \frac{dF(\tilde{u})}{d\tilde{u}} = {} & \frac{k_0^2\tilde{u}}{\tilde{\gamma}_s\tilde{n}_{xxs}^2} m_{11} + \frac{k_0^2\tilde{u}}{\tilde{\gamma}_c\tilde{n}_{xxc}^2} m_{22} + \frac{\tilde{\gamma}_s}{\tilde{n}_{zzs}^2}\frac{dm_{11}}{d\tilde{u}} + \frac{\tilde{\gamma}_c}{\tilde{n}_{zzc}^2}\frac{dm_{22}}{d\tilde{u}} - \frac{dm_{21}}{d\tilde{u}} \\ & - \frac{\tilde{\gamma}_s\tilde{\gamma}_c}{\tilde{n}_{zzs}^2\tilde{n}_{zzc}^2}\frac{dm_{12}}{d\tilde{u}} - \frac{k_0^2\tilde{u}\tilde{\gamma}_c}{\tilde{n}_{xxs}^2\tilde{n}_{zzc}^2\tilde{\gamma}_s} m_{12} - \frac{k_0^2\tilde{u}\tilde{\gamma}_s}{\tilde{n}_{xxc}^2\tilde{n}_{zzs}^2\tilde{\gamma}_c} m_{12} \end{aligned} \tag{3-38}$$

3.5 NUMERICAL RESULTS AND DISCUSSION

3.5.1 Guided Modes in Lossless Waveguides

Cauchy's integral method was applied to the 4-layer waveguide [1] defined in Table 3.1. The integral contour used is C_1 as shown in Figure 3.3. The results are in excellent agreement with those reported in reference [1] as is shown in Table 3.1. The field distributions of E_y for TE modes and H_y for TM modes are shown in Figures 3.4 and 3.5 respectively

Table 3.1. Guided Modes in a 4-layer Lossless Waveguide and the Relative Percentage Power In Each Layer

4-layer Lossless Waveguide: n_s=1.5, n_1=1.66, n_2=1.60, n_3=1.53, n_4=1.66, n_c=1.0, $d_1=d_2=d_3=d_4$=0.5μm, λ_0=0.6328μm								
	Effective	**Percentage Relative Power**						
Mode	**Index**	**Substrate**	**Layer 1**	**Layer 2**	**Layer 3**	**Layer 4**	**cover**	
TE_0	1.622728682	3.933	76.342	19.268	0.396	0.061	0.0	this method
	1.622729	3.9	76.3	19.3	0.4	0.1	0.0	reference [1]
TE_1	1.605275698	0.018	0.199	0.185	11.442	87.125	1.031	
	1.605276	0.0	0.2	0.2	11.4	87.1	1.0	
TE_2	1.557136152	6.561	20.741	59.009	12.296	1.353	0.040	
	1.557136	6.6	20.7	59.0	12.3	1.4	0.0	
TE_3	1.503587112	32.126	18.577	14.740	27.969	6.268	0.320	
	1.503587	32.1	18.6	14.7	28.0	6.3	0.3	
TM_0	1.620031318	3.807	74.335	21.351	0.465	0.041	0.000	
	1.620031	3.8	74.3	21.4	0.5	0.0	0.0	
TM_1	1.594788478	0.032	0.285	0.429	15.357	83.377	0.520	
	1.594788	0.0	0.3	0.4	15.4	83.4	0.5	
TM_2	1.554980690	7.258	21.260	57.315	11.969	0.217	0.028	
	1.554981	7.3	21.3	57.3	12.0	0.2	0.0	
TM_3	1.501817805	44.996	15.093	12.970	22.664	4.166	0.111	
	1.501818	45.0	15.1	13.0	22.7	4.2	0.1	

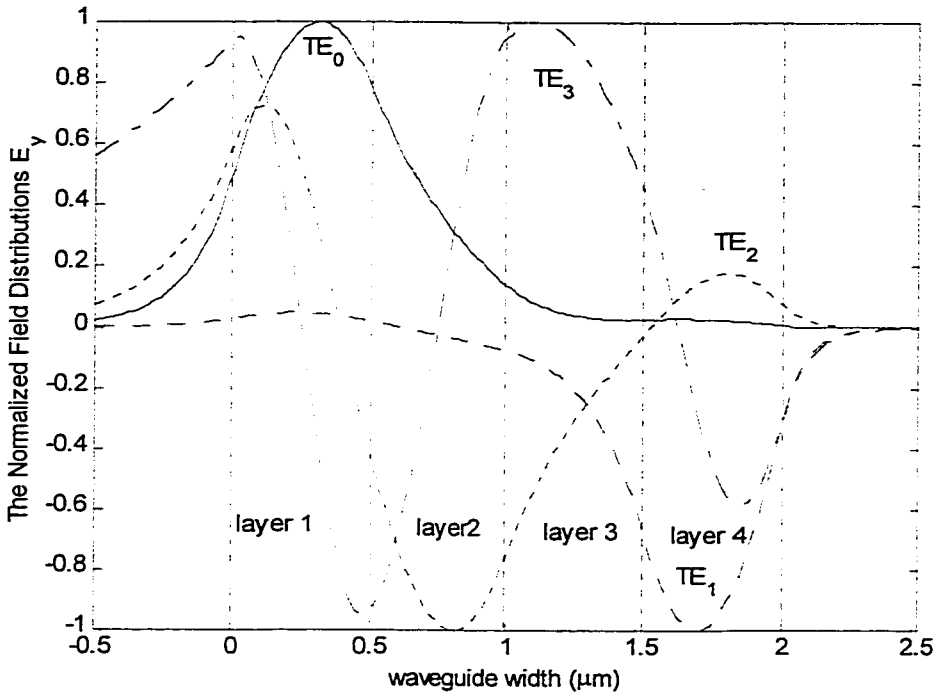

Figure 3.4 Field distributions E_y for TE guided modes

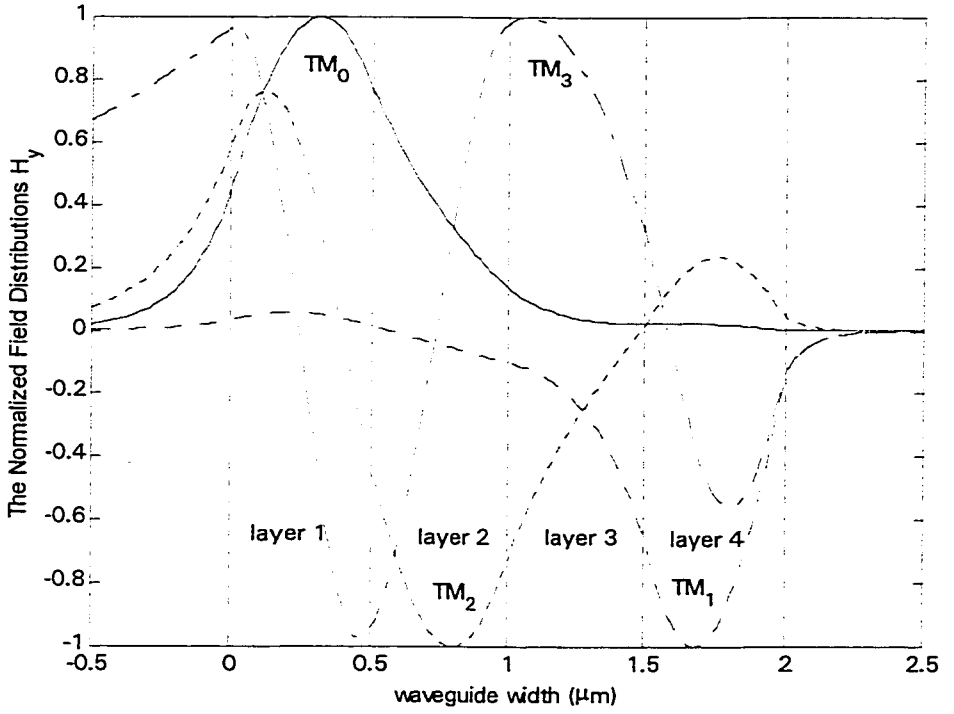

Figure 3.5 Field distributions H_y for TM guided modes

3.5.2 Guided Modes in Lossy Waveguides

Cauchy's integral method was applied to the 6-layer lossy waveguide [34] defined in Table 3.2. For the guided modes of lossy waveguides, the integral contour C_I can be selected as in the lossless case. Due to the losses, the imaginary part of the mode propagation constants will be less than zero, so the top part of the integral contour can be taken along the $\overline{\beta}$ axis. The reference paper did not give the mode propagation constants of TE modes, but for the TM modes, the results are perfect agreement with those reported [34].

Table 3.2. Guided Modes in a 6-layer Lossy Waveguide

6-layer Lossy Waveguide: n_s=3.172951, n_1=3.16455, n_2=3.22534, n_3=3.39583, $\tilde{n}_4$ =3.5321-j0.08817, n_5=3.39614, n_6=3.38327, n_c=1.0, d_1=0.6μm, d_2=1.6μm,d_3=0.518μm, d_4=0.6μm, d_5=0.2μm, d_6=0.1μm, λ_0=1.523μm				
	Present Method		***Reference [34]***	
	Effective Index		**Effective Index**	
Mode	$\overline{\beta}$	$\overline{\alpha} \times 10^{-3}$	$\overline{\beta}$	$\overline{\alpha} \times 10^{-3}$
TE_0	3.460829694	72.66334292		
TE_1	3.316707802	23.27581759		
TE_2	3.208555428	12.78206799		
TE_3	3.195490593	12.58595565		
TM_0	3.455331605	70.59384419	3.4553	70.60
TM_1	3.310634936	23.38856648	3.3106	23.39
TM_2	3.208026621	6.48375244	3.2080	6.484
TM_3	3.181898028	15.79829719	3.1819	15.80

3.5.3 Guided Modes in Active Waveguides

We have applied our method to the analysis of a 4-layer semiconductor amplifier [35] as defined in Table 3.3. It consists of an InP substrate, an *n*-doped InP layer, and InGaAsP active layer a *p*-doped InP layer and a thin gold contact layer deposited on top of the structure. For the guided

modes of active waveguides, the integral contour C_I should be selected as in the lossless case. The results obtained are perfect agreement with those of the reference [35]. The field distributions for the TM modes are shown in figure 3.6. From Figure 3.6, it is clearly to see that the TM_0 mode is a guided mode and the field is located in layer 2. Whereas for the plasmon mode, the field is mainly located in the layer 4 surface (metal).

Table 3.3. Guided Modes in a 4-layer Active Waveguide

4-layer Active Waveguide: n_s=3.16, $\tilde{n}_1$=3.16-j0.0001, $\tilde{n}_2$=3.6+j0.002, $\tilde{n}_3$=3.16-j0.0001, $\tilde{n}_4$=0.18-j10.2, n_c=1.0, d_1=3.0μm, d_2=0.15μm, d_3=1.0μm, d_4=0.04μm, λ_0=1.30μm				
	Present Method		***Reference [35]***	
	Effective Index		**Effective Index**	
Mode	$\overline{\beta}$	$\overline{\alpha} \times 10^{-4}$	$\overline{\beta}$	$\overline{\alpha} \times 10^{-4}$
TE_0	3.280880013	-9.139181909	3.2808	- 9.139
TM	3.334498481	75.18872326 (plasmon mode)		
TM_0	3.248098484	-5.463070134	3.2480	-5.463

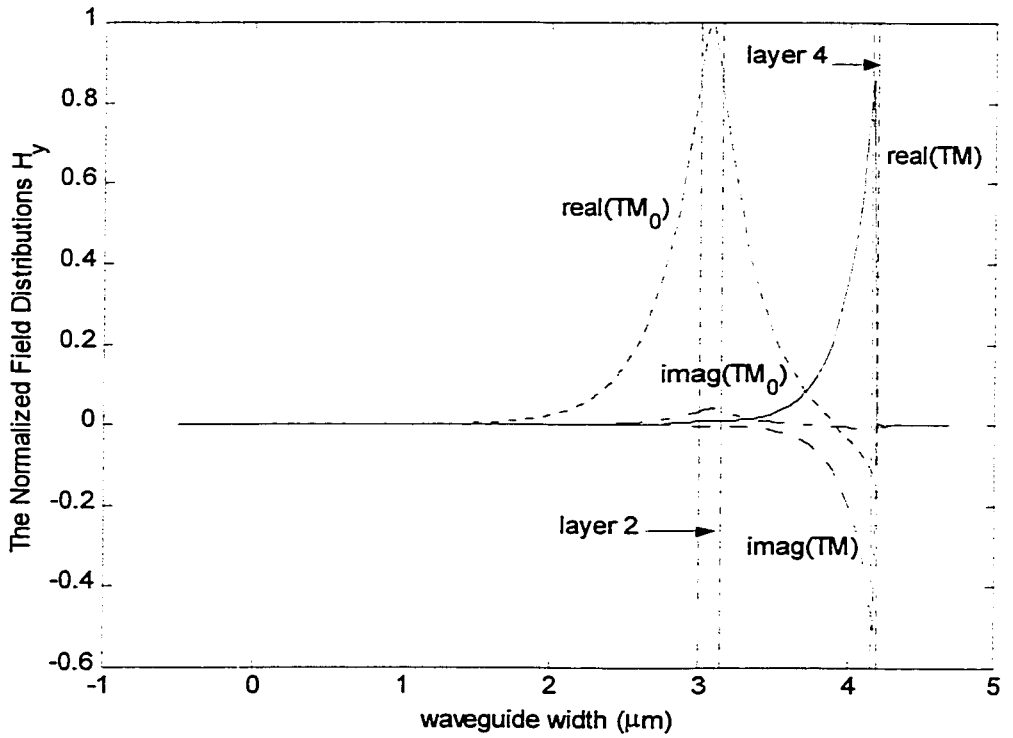

Figure 3.6 Field distributions H_y for TM plasmon mode and TM guided modes

3.5.4 Guided Modes in Quantum Well Active Waveguides

Quantum well layers used in active photonic devices are in fact anisotropic media since their optical response is different for electric field of light parallel and perpendicular to the direction of growth. This is the uniaxial anisotropy, which appears even though quantum wells are made up from the cubic semiconductor materials and can be essential in the real life active waveguides of modeling. We applied our method to a typical structure of the InP-based SCH QW laser emitting in 1.55μm as defined in Table 3.4. The second layer is the anisotropic quantum well active layer. The results are shown in Table 3.4.

Table 3.4. Guided Modes in a 6-layer Quantum Well Active Waveguide

6-layer Anisotropic Active Waveguide: $\tilde{n}_s$=3.13575-j6.2264×10^{-5}, $\tilde{n}_1$=3.16404-j1.0005×10^{-5}, $\tilde{n}_{xx2}=\tilde{n}_{yy2}$=3.393856+j0.0069093, $\tilde{n}_{zz2}$=3.395891+j0.0032438, $\tilde{n}_3$=3.16987-j1.3991×10^{-4}, $\tilde{n}_4$=3.38838-j2.7498×10^{-4}, $\tilde{n}_5$=3.17034-j2.829×10^{-4}, $\tilde{n}_6$=3.46930-j0.083828, $\tilde{n}_c$=0.59-j12.63, d_1=1.5μm, d_2=0.2μm, d_3=0.2μm, d_4=0.01μm, d_5=1.3μm, d_6=0.2μm, λ_0=1.55μm		
Present Method		
	Effective Index	
Mode	$\overline{\beta}$	$\overline{\alpha} \times 10^{-3}$
TE_0	3.211912271	-2.295751586
TE_1	3.146335751	1.833386157
TE_2	3.137997320	2.519718051
TM_0	3.204193956	-1.750073292
TM_1	3.144266723	0.155723815

3.5.5 Leaky Modes in Lossless Waveguides

Cauchy's integral method can be used to find leaky modes. The leaky mode propagation constants satisfy the same dispersion equation as the guided modes, but the appropriate sign of

$\tilde{\gamma}_s$ and $\tilde{\gamma}_c$ must be chosen [1]. If we assume $\tilde{\gamma}_s = \gamma_s^r + j\gamma_s^i$ *and* $\tilde{\gamma}_c = \gamma_c^r + j\gamma_c^i$, for $\overline{\beta} < n_s$ ($\overline{\beta} < n_c$), we should choose $\gamma_s^r < 0 \, and \, \gamma_s^i > 0$ ($\gamma_c^r < 0 \, and \, \gamma_c^i > 0$). The integral contour is selected as C_2, as shown in Figure 3.2(a) for $n_s > n_c$. The reason for selecting the top part of the integral contour along the $\overline{\beta}$ axis is that the imaginary part of the leaky mode propagation constants is negative. The integral contour above the $\overline{\beta}$ axis will lead to large integration errors and generate the roots for the polynomial *p(z)* far away from the roots of the dispersion equation. For the waveguide structure defined in Table 3.1, our results are complete agreement with those reported in reference [1], as shown in Table 3.5.

Table 3.5. Leaky Modes in a 4-layer Lossless Waveguide

4-layer Lossless Waveguide: n_s=1.5, n_1=1.66, n_2=1.60, n_3=1.53, n_4=1.66, n_c=1.0, d_1=d_2=d_3=d_4=0.5μm, λ_0=0.6328μm				
	Present Method		***Reference [1]***	
	Effective Index		**Effective Index**	
Mode	$\overline{\beta}$	$\overline{\alpha}$	$\overline{\beta}$	$\overline{\alpha}$
TE_4	1.461856641	0.007155871	1.46186	0.00716
TE_5	1.382489223	0.018165877	1.38250	0.01817
TE_6	1.281364436	0.035877392	1.28136	0.03588
TE_7	1.142314462	0.052876075	1.14231	0.05288
TE_8	1.003037019	0.070770941	1.00304	0.07077
TM_4	1.451534978	0.011923599		
TM_5	1.370664375	0.030142063		
TM_6	1.273737061	0.056791773		
TM_7	1.157312853	0.087578491		
TM_8	1.036950265	0.103078083		

3.5.6 ARROW Waveguides

ARROW (AntiResonant Reflecting Optical Waveguide) waveguides [10], [16] are based on Fabry-Perot reflection instead of total internal reflection. Cauchy's integral method can also be used to obtain mode propagation constants in ARROW waveguides. A 9-layer ARROW can be used as a directional coupler [37]; the structure of interest is defined in Table 3.6. The first 6 TE and TM ARROW modes are given in Table 3.6. Figure 3.7 and 3.8 show the spatial distribution of the H_y field component related to the first two TM ARROW modes. These figures show that the structure supports a pair of symmetric and asymmetric modes with most of the mode power located in layers 3 and 7, which implies that the structure could be used as a directional coupler. The figures also show that leakage directed into the substrate occurs for these two modes.

Table 3.6. ARROW Modes in a 9-layer ARROW Waveguide

9-layer ARROW Waveguide: n_s=3.5, n_1=1.46, n_2=1.50, n_3=1.46, n_4=1.50, n_5=1.46, n_6=1.50, n_7=1.46, n_8=1.50, n_9=1.46, n_c=1.0, d_1=2.0μm, d_2=0.448μm d_3=4.0μm, d_4=0.448μm, d_5=2.0μm, d_6=0.448μm d_7=4.0μm, d_8=0.448μm, d_9=2.0μm, λ_0=0.6328μm		
	Present Method	
Mode	**Effective Index**	
(First 6)	$\bar{\beta}$	$\bar{\alpha} \times 10^{-4}$
TE_1	1.457920191	0.007106242
TE_2	1.457791244	0.009053396
TE_3	1.453780369	0.114698816
TE_4	1.453045406	0.420121480
TE_5	1.451864807	0.693651857
TE_6	1.450269491	0.732515869
TM_1	1.457925423	0.045880488
TM_2	1.457782773	0.057163274
TM_3	1.453795449	0.645756672
TM_4	1.452928430	2.555862981
TM_5	1.451781628	4.567101184
TM_6	1.450247659	4.357488809

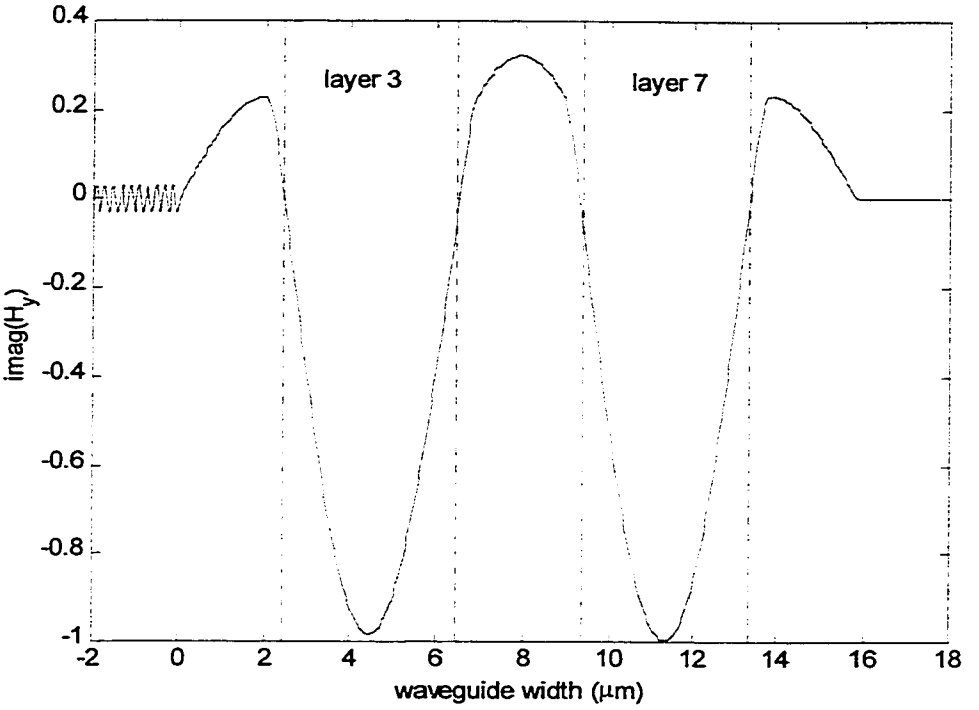

Figure 3.7 Field distribution for the symmetric TM mode (Effective index=1.457925423-j4.588048807×10^{-6})

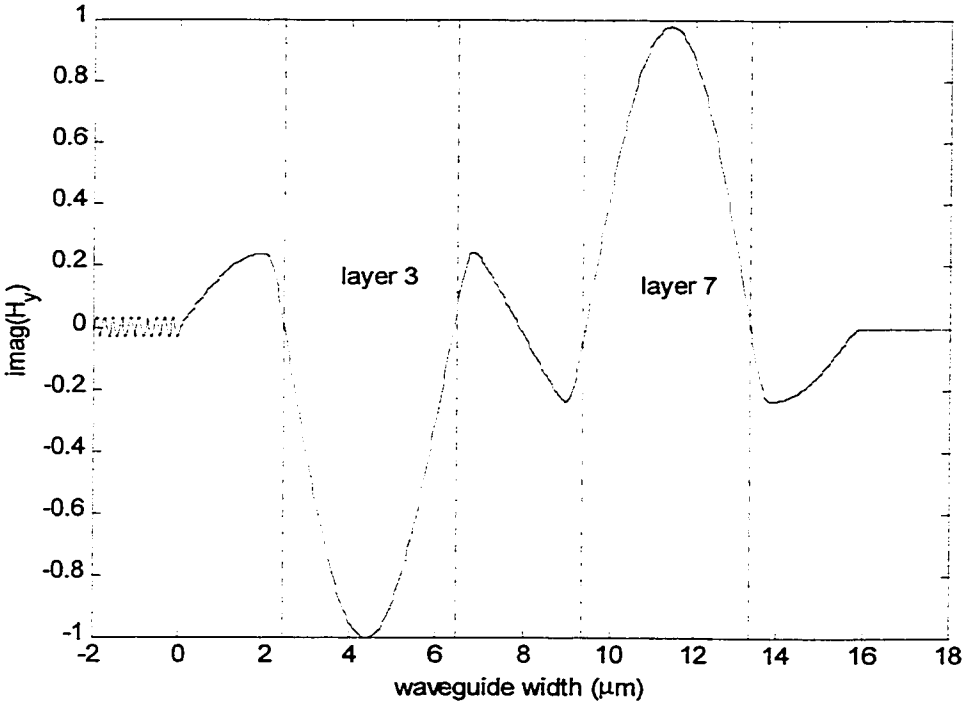

Figure 3.8 Field distribution for the anti-symmetric TM mode (Effective index=1.457782773-j5.716327355×10^{-6})

An 11-layer ARROW waveguide with a center layer thickness comparable with fiber core can be used as a directional coupler[38], the structure of interest is defined in Table 3.7. The integral contour was selected as shown in figure 3.3(b). Table 3.7 gives first 17 modes. There are many more modes. The figure 3.9 and 3.10 shown the mode fields distributions for last two modes.

Table 3.7. Modes in a 11-layer ARROW Waveguide

11-layer ARROW Waveguide: n_s=1.490755, n_1=1.590030, n_2=1.490755, n_3=1.590030, n_4=1.490755, n_5=1.590030, n_6=1.490755, n_7=1.590030, n_8=1.490755, n_9=1.590030, n_{10}=1.490755, n_{11}=1.590030, n_c=1.490755, d_1=0.305μm, d_2=3.000μm d_3=0.305μm, d_4=6.0μm, d_5=0.305μm, d_6=93.000μm d_7=0.305μm, d_8=6.0μm, d_9=0.305μm d_{10}=3.0μm, d_{11}=0.305μm, λ_0=0.6328μm				
	Present Method		***Reference***	
	Effective Index		**Effective Index**	
Mode	$\overline{\beta}$	$\overline{\alpha} \times 10^{-8}$	$\overline{\beta}$	$\overline{\alpha} \times 10^{-8}$
TM_0	1.490751120	0.000000139		
TM_1	1.490739481	0.000001172		
TM_2	1.490720083	0.000004316		
TM_3	1.490692928	0.000011583		
TM_4	1.490658015	0.000026630		
TM_5	1.490615348	0.000056476		
TM_6	1.490564930	0.000115238		
TM_7	1.490506765	0.000232783		
TM_8	1.490440859	0.000476397		
TM_9	1.490367228	0.001010578		
TM_{10}	1.490285894	0.002284523		
TM_{11}	1.490196907	0.005736103		
TM_{12}	1.490100403	0.017268474		
TM_{13}	1.489996875	0.075023038		
TM_{14}	1.489890569	0.909540543		
TM_{15}	1.489840332	6.891975394	1.489840	6.8286
TM_{16}	1.489828288	6.690569597	1.489828	6.6640

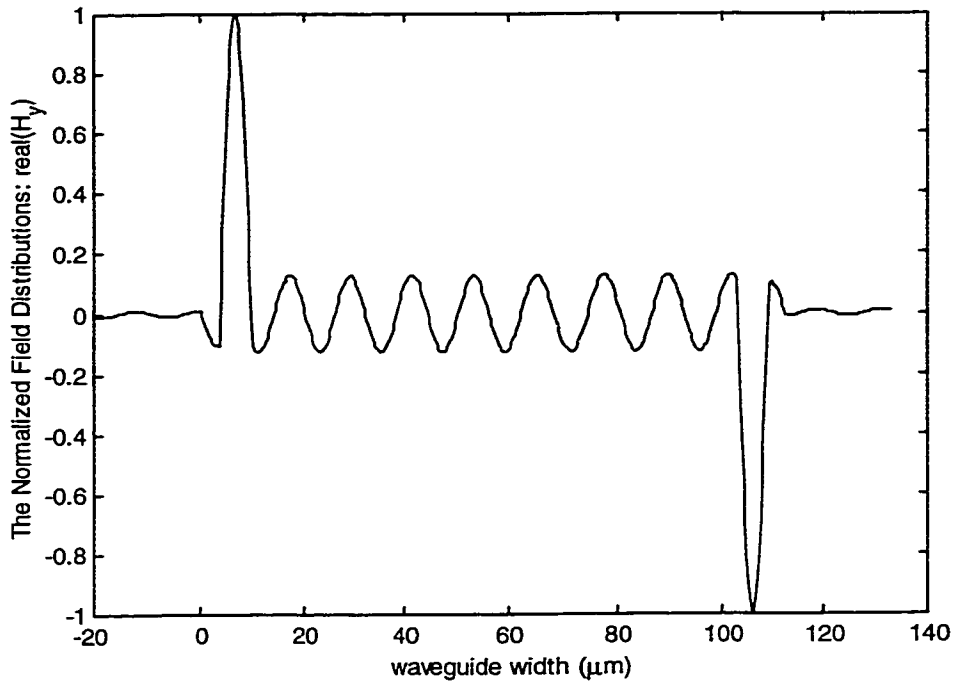

Figure 3.9 Field distribution for the anti-symmetric TM supermode (Effective index=1.489840332-j6.891975394×10^{-8})

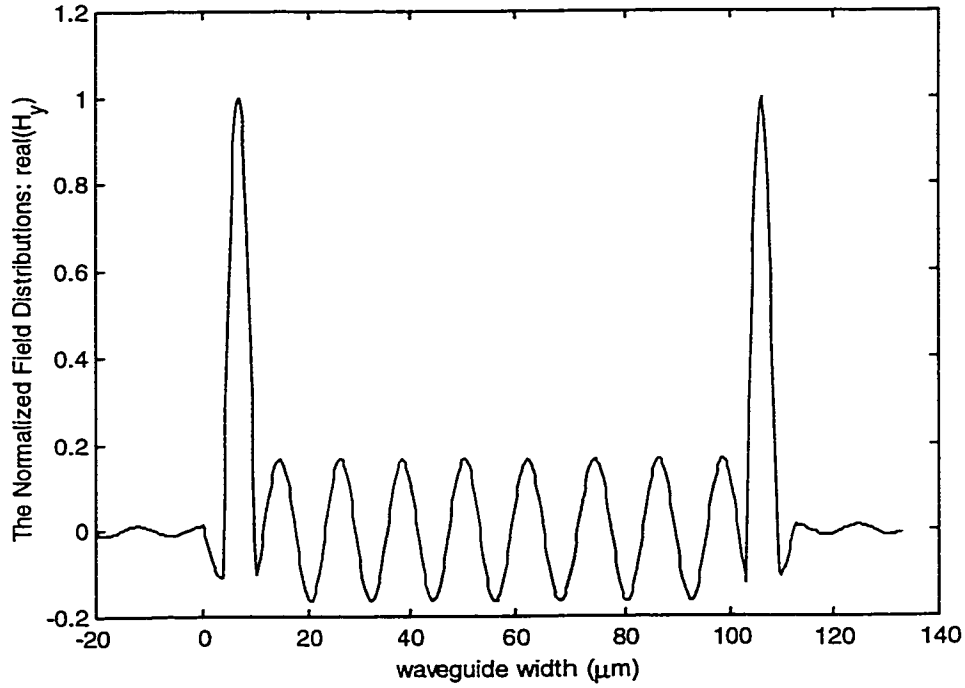

Figure 3.10 Field distribution for the symmetricTM supermode (Effective index=1.489828288-j6.690569597×10^{-8})

3.5.7 Anisotropic ARROW Waveguides

Many anisotropic materials have desirable properties at optical wavelengths, including low losses, and large electro-optic or photo-elastic effects. In addition, anisotropy may be introduced during material growth or device processing. It is thus important for a mutilayer waveguide modeling tool to be able to handle effectively such materials.

We have applied our method to obtain the propagation constant of modes supported by an anisotropic ARROW waveguide [39]; the structure of interest is defined in Table VII. The first 4 modes for the isotropic (*AR=1*) and anisotropic cases ($AR = n_{xxi}/n_{zzi} = 1.03$), are given in Table 3.7.

Table 3.8 RROW Modes in a 3-layer Anisotropic ARROW Waveguide

3-layer Anisotropic ARROW Waveguide: n_s=3.85, n_{zz1}=1.46, n_{zz2}=2.3, n_{zz3}=1.46, n_c=1, d_1=2μm, d_2=0.08862μm, d_3=4μm, λ_0=0.633μm, $n_{xxi}=n_{yyi}$, $AR=n_{xxi}/n_{zzi}$, i=1, 2, 3				
	AR=1		***AR=1.03***	
Mode	**Effective Index**		**Effective Index**	
(first 4)	$\overline{\beta}$	$\overline{\alpha} \times 10^{-3}$	$\overline{\beta}$	$\overline{\alpha} \times 10^{-3}$
TE_1	1.457952154	0.000053466	1.501809523	0.000049401
TE_2	1.451960454	0.051917452	1.495985306	0.052781073
TE_3	1.451218176	0.191225065	1.495298322	0.183569017
TE_4	1.441470497	0.004315053	1.485794492	0.003987602
TM_1	1.457900218	0.002423250	1.501634713	0.002515956
TM_2	1.451794241	0.541505227	1.495329277	0.563194729
TM_3	1.451328712	1.155123065	1.494879648	1.193653747
TM_4	1.441003286	0.188415226	1.484210720	0.195573469

3.6 SUMMARY

In this chapter, a numerical method based on Cauchy's integration in the complex plane has been developed to characterize the modes supported by multilayer planar optical waveguides constructed from lossy anisotropic media. The analytical derivative of the dispersion equation was obtained and the integral contour to be used for finding leaky modes was discussed. The method reported has several important advantages over other methods for finding modes of planar waveguides. An advantage is the ability to find the total number of modes in a region of interest in the complex plane. Another advantage is that the method can be used to characterize lossless, lossy, active and ARROW waveguides in anisotropic media. The method can generate guided modes as well as leaky modes. The combination of high accuracy, low computation time and the broad range of applicability makes the method very attractive for integration into commercial computer-aided design and modeling tools for integrated optics.

CHAPTER 4

THE METHOD OF LINES FOR THE ELECTROSTATIC ANALYSIS OF MULTI-CONDUCTOR TRANSMISSION LINES

4.1 INTRODUCTION

The quasi-TEM analysis of multi-conductor transmission lines such as (coupled) microstrip lines and (coupled) coplanar waveguides is of significant practical importance to the design of monolithic microwave integrated circuits (MMIC's) and high-speed optoelectronic devices such as traveling-wave photodetectors and modulators. The need for accurate and fast computer-aided design (CAD) tools that can model the quasi-TEM performance of multi-conductor transmission lines having a finite metallization thickness and embedded in inhomogeneous anisotropic media is manifest. It is desirable that a numerical technique forming the basis of such a CAD tool be robust and operates with limited computing resources while rapidly providing accurate solutions to a wide range of transmission line problems.

Numerous methods have been proposed for the quasi-TEM analysis of transmission lines. Commonly encountered methods include the boundary element method [11], [12]; the finite

element method [13], [14]; the mode matching method [15]-[18]; the spectral domain method [19], [20]; the conformal mapping method [21]; the finite difference method [22]; the moment method [23], [24]; and the method of lines [25], [26]. Of the methods listed above, only the finite element and finite difference methods can perform the quasi-TEM analysis of transmission lines comprised of conductors of finite thickness embedded in inhomogeneous anisotropic dielectric media. However, both of these methods suffer from the same well-known drawbacks stemming from the fact that they are based on a full domain discretization.

The method of lines (MoL), formulated for the full-wave analysis of microwave and optical waveguides, is well-developed [27], [28], and is well-known for its numerical performance, that is, its high accuracy, rapid speed of computation and minimal memory requirements. In a 2-D problem, the numerical performance of the MoL is due mainly to the fact that only one of the dimensions of the computational domain is discretized while generalized analytical solutions are introduced along the remaining dimension as part of the solution process. The MoL however has not been widely used for the quasi-TEM analysis of transmission lines, perhaps due to the fact that a formulation that can handle finite thickness conductors embedded in inhomogeneous anisotropic dielectric media is unavailable.

When a transmission line is used at frequencies where geometrical dispersion can be neglected, that is when the quasi-TEM approximation holds, then an expensive full-wave analysis of the structure may be wasteful. Furthermore, a quasi-TEM numerical method can be much more robust and numerically efficient compared to its full-wave counterpart and thus more suitable for introduction into commercial CAD packages. The main advantage of the quasi-TEM MoL, compared to the full-wave MoL, is that in the end a small inhomogeneous matrix problem is

generated and solved directly via matrix inversion or using an efficient matrix solver. In the full-wave MoL, a homogeneous matrix problem is generated and solved by locating a zero of the determinant of the matrix, a procedure difficult to automate in a robust manner if the method is to be incorporated into a CAD package.

4.2 FORMULATION

4.2.1 Electric Potential and Field Equations

The generic multi-conductor transmission line structure considered is shown in Figure 4.1. A rectangular conducting box encloses a structure consisting of several inner conductors embedded in an inhomogeneous anisotropic dielectric material described by the diagonal permittivity tensor:

$$\bar{\varepsilon} = \begin{bmatrix} \varepsilon_{xx}(x) & \\ & \varepsilon_{yy}(x) \end{bmatrix} \tag{4-1}$$

Any dependency along y in the permittivity profile is handled by layering such that each layer only has an x dependency. The structure is assumed invariant along the z direction.

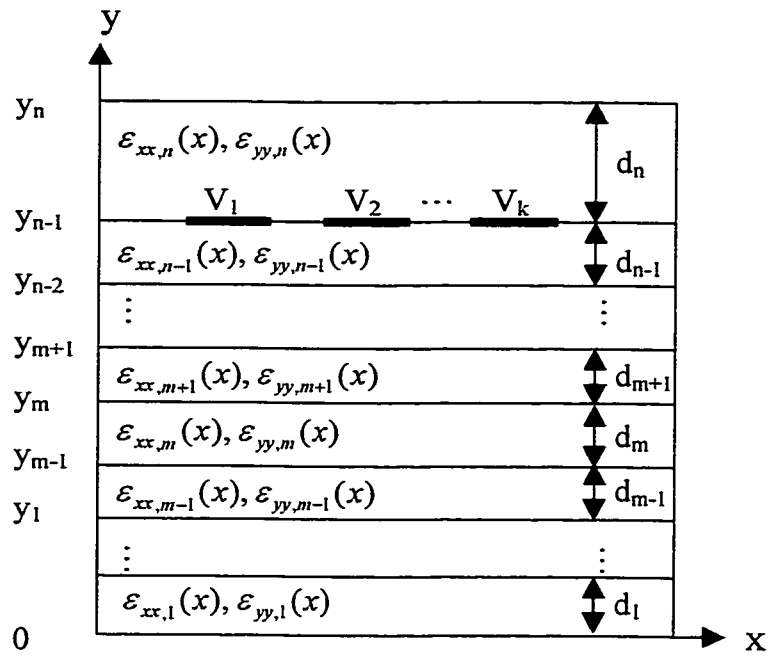

Figure 4.1 Generic multi-conductor transmission line structure

The TEM approximation means that the longitudinal fields of a mode are neglected and that the spatial distributions of the transverse fields are assumed invariant with frequency (geometrical and material dispersion are neglected). The electrostatic field for a mode of interest is then generated by appropriately setting the voltages on each metal conductor. The electrostatic field must then satisfy Gauss' law over the *x-y* plane:

$$\nabla \cdot \bar{D} = \nabla \cdot (\bar{\varepsilon} \cdot \bar{E}) = \begin{cases} \rho_v & \textit{in metals} \\ 0 & \textit{in dielectrics} \end{cases} \tag{4-2}$$

where $\bar{E}$ and $\bar{D}$ are the electric field intensity and displacement vectors respectively. The electric potential $\phi(x, y)$ is then defined such that:

$$\bar{E}(x, y) = -\nabla \phi(x, y) = -\hat{x} \frac{\partial \phi(x, y)}{\partial x} - \hat{y} \frac{\partial \phi(x, y)}{\partial y} \tag{4-3}$$

Substituting Equation (4-3) into Equation (4-2) yields Poisson's equation for inhomogeneous anisotropic media:

$$\frac{\partial}{\partial x}\left(\varepsilon_{xx}(x) \frac{\partial \phi(x, y)}{\partial x} \right) + \frac{\partial}{\partial y}\left(\varepsilon_{yy}(x) \frac{\partial \phi(x, y)}{\partial y} \right) = -\rho_v \tag{4-4}$$

Simplifying the above for dielectric media ($\rho_v = 0$) yields Laplace's equation:

$$\frac{1}{\varepsilon_{yy}(x)} \frac{\partial}{\partial x}\left(\varepsilon_{xx}(x) \frac{\partial \phi(x, y)}{\partial x} \right) + \frac{\partial^2 \phi(x, y)}{\partial y^2} = 0 \tag{4-5}$$

If a dielectric is homogeneous then the above simplifies to:

$$\frac{\varepsilon_{xx}}{\varepsilon_{yy}} \frac{\partial^2 \phi(x, y)}{\partial x^2} + \frac{\partial^2 \phi(x, y)}{\partial y^2} = 0 \tag{4-6}$$

On all metal surfaces, the potential is set to:

$$\phi(x, y) = \begin{cases} V_j & \textit{on the inner conductors} \quad j = 1, 2, \cdots, k \\ 0 & \textit{on the outer conductor} \end{cases} \tag{4-7}$$

4.2.2 Application of Method of Lines

In a manner consistent with the full-wave MoL [27], the differential equation to be solved is discretized along one dimension and the remaining dimension is treated analytically. If the transverse dimension is discretized as shown in Figure 4.2, then the potential ϕ, and the relative

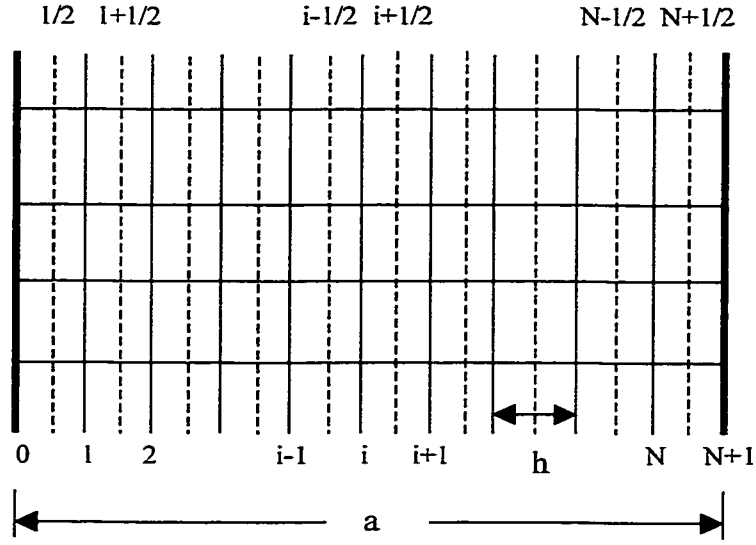

Figure 4.2 Equidistant line system used to discretize the transverse dimension

Permittivities ε_{rxx} and ε_{ryy} are discretized along x and expressed as a vector and diagonal matrices:

$$\bar{\phi} = [\phi_0 \ \phi_1 \cdots \phi_N \ \phi_{N+1}]^T \tag{4-8a}$$

$$[\varepsilon_{rxx}]_{diag} = \begin{bmatrix} \varepsilon_{rxx,1/2} & & & \\ & \varepsilon_{rxx,1+1/2} & & \\ & & \ddots & \\ & & & \varepsilon_{rxx,N+1/2} \end{bmatrix} \tag{4-8b}$$

$$[\varepsilon_{ryy}]_{diag} = \begin{bmatrix} \varepsilon_{ryy,1} & & & \\ & \varepsilon_{ryy,2} & & \\ & & \ddots & \\ & & & \varepsilon_{ryy,N} \end{bmatrix} \tag{4-8c}$$

The components ϕ_i of the vector (4-8a) are known on the solid lines and are functions of y. The components of the relative permittivity tensor must be discretized such that Equation (4-5) can be readily expressed in discrete form. This is achieved by discretizing ε_{rxx} on the dashed lines, which are positioned at the midpoint between solid lines, and discretizing ε_{ryy} on the solid lines.

Applying an $O(h^2)$ central difference formula on lines $i-\frac{1}{2}$ and $i+\frac{1}{2}$ we approximate the first derivative with respect to x of the potential as:

$$\frac{\partial \phi_{i-1/2}}{\partial x} \approx \frac{\phi_i - \phi_{i-1}}{h} \tag{4-9a}$$

and

$$\frac{\partial \phi_{i+1/2}}{\partial x} \approx \frac{\phi_{i+1} - \phi_i}{h} \tag{4-9b}$$

Then on any line i, the term in the second derivative with respect to x of the potential in Equation (4-5) is approximated as:

$$\begin{aligned} \left(\frac{1}{\varepsilon_{ryy}}\frac{\partial}{\partial x}\left(\varepsilon_{rxx}\frac{\partial \phi}{\partial x}\right)\right)_i &\approx \frac{1}{\varepsilon_{ryy,i}} \frac{\varepsilon_{rxx,i+1/2}\dfrac{\partial \phi_{i+1/2}}{\partial x} - \varepsilon_{rxx,i-1/2}\dfrac{\partial \phi_{i-1/2}}{\partial x}}{h} \\ &= \frac{1}{h^2}\left(\frac{\varepsilon_{rxx,i-1/2}}{\varepsilon_{ryy,i}}\phi_{i-1} - \frac{\varepsilon_{rxx,i-1/2}+\varepsilon_{rxx,i+1/2}}{\varepsilon_{ryy,i}}\phi_i + \frac{\varepsilon_{rxx,i+1/2}}{\varepsilon_{ryy,i}}\phi_{i+1}\right) \end{aligned} \tag{4-10a}$$

or:

$$\left(\frac{1}{\varepsilon_{ryy}}\frac{\partial}{\partial x}\left(\varepsilon_{rxx}\frac{\partial \phi}{\partial x}\right)\right)_i \approx -\frac{1}{h^2}\left(a_i\phi_{i-1} - b_i\phi_i + c_i\phi_{i+1}\right) \tag{4-10b}$$

where:

$$a_i = \frac{\varepsilon_{rxx,j-1/2}}{\varepsilon_{ryy,j}},\ b_i = \frac{\varepsilon_{rxx,j-1/2} + \varepsilon_{rxx,j+1/2}}{\varepsilon_{ryy,j}} \text{ and } c_i = \frac{\varepsilon_{rxx,j+1/2}}{\varepsilon_{ryy,j}} \tag{4-10c}$$

Applying (4-10b) on all lines from 1 through N yields:

$$\begin{bmatrix} \frac{1}{\varepsilon_{ryy,1}} \frac{\partial}{\partial x}\left(\varepsilon_{rxx} \frac{\partial \phi}{\partial x}\right)_1 \\ \frac{1}{\varepsilon_{ryy,2}} \frac{\partial}{\partial x}\left(\varepsilon_{rxx} \frac{\partial \phi}{\partial x}\right)_2 \\ \vdots \\ \frac{1}{\varepsilon_{ryy,N}} \frac{\partial}{\partial x}\left(\varepsilon_{rxx} \frac{\partial \phi}{\partial x}\right)_N \end{bmatrix} = -\frac{1}{h^2} \begin{bmatrix} -a_1 & b_1 & -c_1 & & \\ & -a_2 & b_2 & -c_2 & \\ & & \ddots & & \\ & & -a_N & b_N & -c_N \end{bmatrix} \begin{bmatrix} \phi_0 \\ \phi_1 \\ \phi_2 \\ \vdots \\ \phi_N \\ \phi_{N+1} \end{bmatrix} \tag{4-11}$$

Lateral boundary conditions must now be applied on lines 0 and N+1. For a Dirichlet (D) boundary condition $\phi = 0$ must be enforced, and for a Newmann (N) boundary condition $\frac{\partial}{\partial x}\phi = 0$ must be enforced. Application of lateral boundary conditions to the above yields:

$$\begin{bmatrix} \frac{1}{\varepsilon_{ryy,1}} \frac{\partial}{\partial x}\left(\varepsilon_{rxx} \frac{\partial \phi}{\partial x}\right)_1 \\ \frac{1}{\varepsilon_{ryy,2}} \frac{\partial}{\partial x}\left(\varepsilon_{rxx} \frac{\partial \phi}{\partial x}\right)_2 \\ \vdots \\ \frac{1}{\varepsilon_{ryy,N}} \frac{\partial}{\partial x}\left(\varepsilon_{rxx} \frac{\partial \phi}{\partial x}\right)_N \end{bmatrix} = -\frac{1}{h^2} \begin{bmatrix} d_l & -e_l & & \\ -a_2 & b_2 & -c_2 & \\ & \ddots & & \\ & & -e_r & d_r \end{bmatrix} \begin{bmatrix} \phi_1 \\ \phi_2 \\ \vdots \\ \phi_N \end{bmatrix} = -\frac{1}{h^2} P \begin{bmatrix} \phi_1 \\ \phi_2 \\ \vdots \\ \phi_N \end{bmatrix} = -\frac{1}{h^2} P \bar{\phi} \tag{4-12}$$

where $d_l = b_1$, $e_l = c_1$, $e_r = a_N$ and $d_r = b_N$ if Dirichlet boundary conditions are applied to both the left and right boundaries, respectively. If Newmann boundary conditions are applied to both boundaries then $d_l = e_l = c_1$ and $e_r = d_r = a_N$. The four possible combinations of lateral boundary conditions generate from the above, four possible $N \times N$ matrices: P_{DD}, P_{DN}, P_{ND} and P_{NN}.

Substituting (4-12) and (4-8) into (4-5), yields:

$$\frac{d^2\bar{\phi}}{dy^2} - \frac{1}{h^2} P\bar{\phi} = 0 \tag{4-13}$$

A transformation matrix T is now introduced, thus defining the potential in the transform domain $\tilde{\phi}$:

$$\bar{\phi} = T\tilde{\phi} \tag{4-14}$$

Substituting the above into (4-13) and simplifying yields:

$$\frac{d^2\tilde{\phi}}{dy^2} - \frac{1}{h^2} T^{-1} PT\tilde{\phi} = 0 \tag{4-15}$$

The matrix T is selected such that P is diagonalized:

$$\frac{d^2\tilde{\phi}}{dy^2} - \frac{1}{h^2}[\lambda^2]_{diag}\tilde{\phi} = 0 \tag{4-16}$$

Thus λ^2 and T are the eigenvalues and eigenmatrix, respectively, of P. For an inhomogeneous layer λ^2 and T are obtained numerically, but for a homogeneous layer λ^2 and T are known analytically [27] and $T^{-1} = T^t$.

Equation (4-16) describes an $N \times N$ system of uncoupled second order ordinary differential equations along y. On line i and within the m^{th} layer, as defined in Figure 4.1, Equation (4-16) yields the component equation:

$$\frac{d^2\tilde{\phi}_i}{dy^2} - \frac{1}{h^2}\lambda^2_{m,i}\tilde{\phi}_i = 0 \tag{4-17}$$

which has the following analytical solution [27]:

$$\tilde{\phi}_i(y) = \cosh\left[\frac{\lambda_{m,i}}{h}(y - y_{m-1})\right]\tilde{\phi}_i(y_{m-1}) + \frac{h}{\lambda_{m,i}}\sinh\left[\frac{\lambda_{m,i}}{h}(y - y_{m-1})\right]\frac{d\tilde{\phi}_i(y_{m-1})}{dy} \tag{4-18a}$$

$$\frac{d\tilde{\phi}_i(y)}{dy} = \frac{\lambda_{m,i}}{h}\sinh\left[\frac{\lambda_{m,i}}{h}(y - y_{m-1})\right]\tilde{\phi}_i(y_{m-1}) + \cosh\left[\frac{\lambda_{m,i}}{h}(y - y_{m-1})\right]\frac{d\tilde{\phi}_i(y_{m-1})}{dy} \tag{4-18b}$$

The system equation operating on the potentials at $y = y_{n-1}$ is now derived. Within the bottom layer, the boundary condition applicable at $y = 0$ is $\bar{\phi}(0) = 0$, which yields $\tilde{\phi}(0) = 0$ in the transform domain. Substituting the latter into (4-18a) and rearranging yields a relationship between the transformed potential and its normal derivative, just below the interface between the first and second layers:

$$\tilde{\phi}(y_1^-) = A_1 \frac{d\tilde{\phi}(y_1^-)}{dy} \tag{4-19}$$

where:

$$A_1 = \left[\frac{h}{\lambda_{1,i}}\tanh\left(\frac{\lambda_{1,i}}{h}d_1\right)\right]_{diag} \tag{4-20}$$

The boundary conditions applicable on the potentials at an interface between dielectric layers are deduced by enforcing the continuity of tangential $\bar{E}$ and normal $\bar{D}$ over the interface:

$$\bar{\phi}(y_m^-) = \bar{\phi}(y_m^+) \tag{4-21a}$$

$$[\varepsilon_{ryy,m+1}]\frac{d\bar{\phi}(y_m^+)}{dy} - [\varepsilon_{ryy,m}]\frac{d\bar{\phi}(y_m^-)}{dy} = 0 \tag{4-21b}$$

Applying (4-21), (4-18) and (4-14) successively at $y = y_1$, $y = y_2$ ... $y = y_m$ yields the following general recursive relationship between the transformed potential and its normal derivative at any interface $2 \le m \le n-1$:

$$\tilde{\phi}(y_m^-) = A_m \frac{d\tilde{\phi}(y_m^-)}{dy} \tag{4-22}$$

where:

$$A_m = \left\{ B_m + \left[\frac{h}{\lambda_{m,i}} \tanh\left(\frac{\lambda_{m,i}}{h} d_m \right) \right]_{diag} \right\} \left\{ \left[\frac{h}{\lambda_{m,i}} \tanh\left(\frac{\lambda_{m,i}}{h} d_m \right) \right]_{diag} B_m + 1 \right\}^{-1} \tag{4-23a}$$

and:

$$B_m = T_m^{-1} (T_{m-1} A_{m-1} T_{m-1}^{-1} [\varepsilon_{ryy,m-1}]^{-1}) [\varepsilon_{ry,m}] T_m \tag{4-23b}$$

with A_1 given by (4-20).

Similarly, within the top layer, the boundary condition applicable at $y = y_n$ is $\bar{\phi}(y_n) = 0$, which yields $\tilde{\phi}(y_n) = 0$ in the transform domain. Substituting the latter into (4-18a) and rearranging yields a relationship between the transformed potential and its normal derivative at y_{n-1}^+:

$$\tilde{\phi}(y_{n-1}^+) = A_n \frac{d\tilde{\phi}(y_{n-1}^+)}{dy} \tag{4-24}$$

where:

$$A_n = -\left[\frac{h}{\lambda_{n,i}} \tanh\left(\frac{\lambda_{n,i}}{h} d_n \right) \right]_{diag} \tag{4-25}$$

Applying (4-14) to (4-22) and (4-24), yields:

$$\frac{d\bar{\phi}(y_{n-1}^+)}{dy} = T_n A_n^{-1} T_n^{-1} \bar{\phi}(y_{n-1}^+) \tag{4-26a}$$

and

$$\frac{d\bar{\phi}(y_{n-1}^-)}{dy} = T_{n-1} A_{n-1}^{-1} T_{n-1}^{-1} \bar{\phi}(y_{n-1}^-) \tag{4-26b}$$

The boundary conditions applicable at $y = y_{n-1}$ are:

$$\bar{\phi}(y_{n-1}^{-}) = \bar{\phi}(y_{n-1}^{+}) \tag{4-27a}$$

$$[\varepsilon_{ryy,n}]\frac{d\bar{\phi}(y_{n-1}^{+})}{dy} - [\varepsilon_{ryy,n-1}]\frac{d\bar{\phi}(y_{n-1}^{-})}{dy} = -\frac{\bar{\rho}_s}{\varepsilon_0} \tag{4-27b}$$

Substituting (4-26) into (4-27) defines the system equation:

$$G\bar{\phi}(y_{n-1}) = \frac{\bar{\rho}_s}{\varepsilon_0} \tag{4-28}$$

where the system matrix G is given by:

$$G = [\varepsilon_{ryy,n-1}]T_{n-1}A_{n-1}^{-1}T_{n-1}^{-1} - [\varepsilon_{ryy,n}]T_nA_n^{-1}T_n^{-1} \tag{4-29}$$

Solving (4-28), yields the potential distribution and charge density on the metals at $y = y_{n-1}$.

To solve Equation (4-28) for the multi-conductor transmission line structure shown in Figure 4.1, the potential and charge density vectors are first partitioned into sub-vectors on the conductor and dielectric portions of the interface, and known potential and charge densities are applied. The charge density must be null on the dielectric portions of the interface and the potential on the conductors must be set equal to the voltages applied:

$$\bar{\phi}(y_{n-1}) = \left[\bar{\phi}_1\ \bar{V}_1\ \bar{\phi}_2 \cdots \bar{V}_k\ \bar{\phi}_{k+1}\right]^T \tag{4-30a}$$

$$\bar{\rho}_s(y_{n-1}) = \left[0\ \bar{\rho}_{s1}\ 0 \cdots \bar{\rho}_{sk}\ 0\right]^T \tag{4-30b}$$

Where k is the number of conductors, and $\bar{V}_1$, $\bar{V}_2 \cdots \bar{V}_k$ and $\bar{\rho}_{s1}, \bar{\rho}_{s2} \cdots \bar{\rho}_{sk}$ are the voltage and charge density sub-vectors on metals 1, 2, 3... k, respectively. Letting $G^I = G^{-1}$ and substituting (4-30) into (4-28) and partitioning G^I accordingly yield:

$$\begin{bmatrix} G^I_{1,1} & G^I_{1,2} & \cdots & G^I_{1,2k+1} \\ G^I_{2,1} & G^I_{2,2} & \cdots & G^I_{2,2k+1} \\ \vdots & & \ddots & \vdots \\ G^I_{2k+1,1} & G^I_{2k+1,2} & \cdots & G^I_{2k+1,2k+1} \end{bmatrix} \begin{bmatrix} 0 \\ \bar{\rho}_{s1} \\ 0 \\ \vdots \\ \bar{\rho}_{sk} \\ 0 \end{bmatrix} = \varepsilon_0 \begin{bmatrix} \bar{\phi}_1 \\ \bar{V}_1 \\ \bar{\phi}_2 \\ \vdots \\ \bar{V}_k \\ \bar{\phi}_{k+1} \end{bmatrix} \tag{4-31}$$

The above can be used to form two matrix equations:

$$\begin{bmatrix} G^I_{2,2} & G^I_{2,4} & \cdots & G^I_{2,2k} \\ G^I_{4,2} & G^I_{4,4} & \cdots & G^I_{4,2k} \\ \vdots & & \ddots & \vdots \\ G^I_{2k,2} & G^I_{2k,4} & \cdots & G^I_{2k,2k} \end{bmatrix} \begin{bmatrix} \bar{\rho}_{s1} \\ \bar{\rho}_{s2} \\ \vdots \\ \bar{\rho}_{sk} \end{bmatrix} = \varepsilon_0 \begin{bmatrix} \bar{V}_1 \\ \bar{V}_2 \\ \vdots \\ \bar{V}_k \end{bmatrix} \tag{4-32}$$

and

$$\begin{bmatrix} \bar{\phi}_1 \\ \bar{\phi}_2 \\ \vdots \\ \bar{\phi}_{k+1} \end{bmatrix} = \frac{1}{\varepsilon_0} \begin{bmatrix} G^I_{1,2} & G^I_{1,4} & \cdots & G^I_{1,2k} \\ G^I_{3,2} & G^I_{3,4} & \cdots & G^I_{3,2k} \\ \vdots & & \ddots & \vdots \\ G^I_{2k+1,2} & G^I_{2k+1,4} & \cdots & G^I_{2k+1,2k} \end{bmatrix} \begin{bmatrix} \bar{\rho}_{s1} \\ \bar{\rho}_{s2} \\ \vdots \\ \bar{\rho}_{sk} \end{bmatrix} \tag{4-33}$$

which can be solved directly for the unknown charge densities and potentials, respectively. Once the charge density has been computed, the capacitance of the transmission line can be obtained followed by the effective dielectric constant and the characteristic impedance [40]:

$$C = \frac{1}{V} \int \rho_s(x) dx \tag{4-34a}$$

$$\varepsilon_{r,eff} = \frac{C}{C_a} \tag{4-34b}$$

$$Z_0 = \frac{1}{c_0 \sqrt{C C_a}} \tag{4-34c}$$

where c_0 is the speed of light in vacuum and C_a is the capacitance when all dielectrics are replaced by vacuum.

Once the potential at $y = y_{n-1}$ has been obtained, the potential at all layer interfaces located at $y = y_1$, $y = y_2$ ... $y = y_{n-2}$ can be computed via:

$$\bar{\phi}(y_{m-1}) = T_m \left\{ \left[\cosh\left(\frac{\lambda_{m,i}}{h} d_m \right) \right]_{diag} - \left[\frac{h}{\lambda_{m,i}} \sinh\left(\frac{\lambda_{m,i}}{h} d_m \right) \right]_{diag} A_m^{-1} \right\} T_m^{-1} \bar{\phi}(y_m) \tag{4-35}$$

The potential at any point $y \le y_1$ located within the bottom layer is computed using:

$$\bar{\phi}(y) = T_1 \left[\frac{\sinh\left(\frac{\lambda_{1,i}}{h} y \right)}{\sinh\left(\frac{\lambda_{1,i}}{h} d_1 \right)} \right]_{diag} T_1^{-1} \bar{\phi}(y_1) \tag{4-36a}$$

The potential at a point $y_{m-1} \le y \le y_m$ located within any layer $2 \le m \le n-1$ is computed using:

$$\bar{\phi}(y) = T_m \left\{ \left[\cosh\left(\frac{\lambda_{m,i}}{h} (y_m - y) \right) \right]_{diag} - \left[\frac{h}{\lambda_{m,i}} \sinh\left(\frac{\lambda_{m,i}}{h} (y_m - y) \right) \right]_{diag} A_m^{-1} \right\} T_m^{-1} \bar{\phi}(y_m) \tag{4-36b}$$

The potential at a point $y_{n-1} \le y \le y_n$ located within the top layer is computed using:

$$\bar{\phi}(y) = T_n \left[\frac{\sinh\left(\frac{\lambda_{n,i}}{h} (y_n - y) \right)}{\sinh\left(\frac{\lambda_{n,i}}{h} d_n \right)} \right]_{diag} T_n^{-1} \bar{\phi}(y_{n-1}) \tag{4-36c}$$

Once the potential distribution has been obtained everywhere inside the structure, the electric and magnetic field distributions can also be computed. Knowledge of the electric fields is of

importance to the design of numerous components, such as electro-optic modulators and switches.

The E_y field component from equation (4-3) is given by

$$\bar{E}_y(y) = -\frac{d\bar{\phi}(y)}{dy} \tag{4-37}$$

so this component will be known at the same location as the potential (on the solid lines). The following set of relationships can be used to generate this field component in the structure:

$$\bar{E}_y(y) = -T_1 \left[\frac{\cosh\left(\frac{\lambda_{1,i}}{h} y\right)}{\frac{h}{\lambda_{1,i}} \sinh\left(\frac{\lambda_{1,i}}{h} d_1\right)} \right]_{diag} T_1^{-1} \bar{\phi}(y_1) \quad for \quad 0 \le y \le y_1 \tag{4-38a}$$

$$\bar{E}_y(y) = -T_m \left\{ \left[\frac{h}{\lambda_{m,i}} \sinh\left(\frac{\lambda_{m,i}}{h}(y_m - y)\right) \right]_{diag} + \left[\cosh\left(\frac{\lambda_{m,i}}{h}(y_m - y)\right) \right]_{diag} A_m^{-1} \right\} T_m^{-1} \bar{\phi}(y_m) \tag{4-38b}$$

$$for \quad y_{m-1} \le y \le y_m$$

$$\bar{E}_y(y) = T_n \left[\frac{\cosh\left(\frac{\lambda_{n,i}}{h}(y_n - y)\right)}{\frac{h}{\lambda_{n,i}} \sinh\left(\frac{\lambda_{n,i}}{h} d_n\right)} \right]_{diag} T_n^{-1} \bar{\phi}(y_{n-1}) \quad for \quad y_{n-1} \le y \le y_n \tag{4-38c}$$

The E_x field component from Equation (4-3) is given by:

$$\bar{E}_x(y) = -\frac{d\bar{\phi}(y)}{dx} \tag{4-39}$$

from which it is evident that the first derivative of the potential must be taken across the lines. Using an $O(h^2)$ central difference approximation for this derivative yields:

$$\begin{bmatrix} E_{x,1/2} \\ E_{x,1+1/2} \\ \vdots \\ E_{x,N+1/2} \end{bmatrix} = -\frac{1}{h}\begin{bmatrix} -1 & 1 & & \\ & -1 & 1 & \\ & & \ddots & \\ & & -1 & 1 \end{bmatrix}\begin{bmatrix} \phi_0 \\ \phi_1 \\ \phi_2 \\ \vdots \\ \phi_N \\ \phi_{N+1} \end{bmatrix} \tag{4-40}$$

The E_x field component will thus be known between the potential lines (on the dashed lines). Applying the relevant boundary condition to lines 0 and N+1 generates from the above one of the four possible $N \times N$ matrices: D_{DD}, D_{DN}, D_{ND} and D_{NN}. The E_x field component can then be obtained at any location y from the potential vector using:

$$\bar{E}_x(y) = -\frac{1}{h} D\bar{\phi}(y) \tag{4-41}$$

The magnetic field distributions can be obtained from the electric fields via:

$$\bar{H}_x(y) = -\sqrt{\frac{\varepsilon_{eff}}{\mu_0}}\bar{E}_y(y) \tag{4-42a}$$

$$\bar{H}_y(y) = \sqrt{\frac{\varepsilon_{eff}}{\mu_0}}\bar{E}_x(y) \tag{4-42b}$$

4.3 EXTENSION FOR CONDUCTORS OF FINITE THICKNESS

It is well-known that the finite thickness of the conductors in a transmission line can have an important effect on the propagation characteristics and field distribution of the quasi-TEM mode. In the full-wave MoL the extension to handle the finite thickness of the conductors [12], [41] is straightforward relative to the electrostatic case, since in the electrostatic case non-zero Dirichlet boundary conditions must be applied.

A multi-layer microstrip structure having a finite metallization thickness d_m is shown in Figure 4.3. Other structures such as coupled lines and coplanar waveguides can be handled in a similar manner. Following [27], the layer containing the conductors is partitioned into regions comprised of dielectric portions and metal portions as shown in Figure 4.3. It is assumed for simplicity that

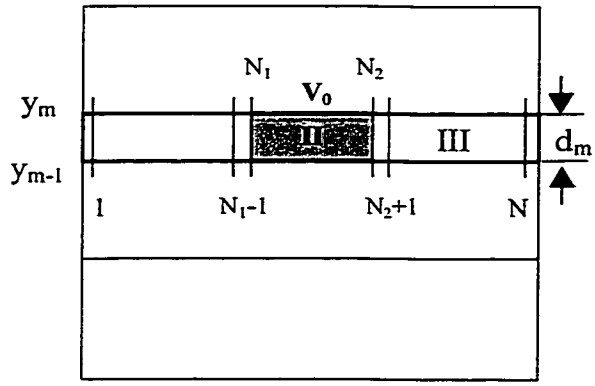

Figure 4.3 Multi-layer microstrip structure with finite conductor thickness d_m, the conductor corresponds to region II

the dielectric portions are isotropic and homogeneous having a relative permittivity $\varepsilon_{r,m}$ though the development can easily be modified to handle the anisotropic inhomogeneous case as well. In

region I, the second derivative of the potential is approximated using the central difference formula:

$$\frac{\partial^2 \phi_i}{\partial x^2} \approx \frac{\phi_{i-1} - 2\phi_i + \phi_{i+1}}{h^2} \tag{4-43}$$

Substituting the above into Equation (4-6), simplified for isotropic media, yields:

$$-\frac{1}{h^2}\begin{bmatrix} -1 & 2 & -1 & & \\ & -1 & 2 & -1 & \\ & & \ddots & & \\ & & -1 & 2 & -1 \end{bmatrix}\begin{bmatrix} \phi_0 \\ \phi_1 \\ \phi_2 \\ \vdots \\ \phi_{N_1} \end{bmatrix} + \frac{d^2\vec{\phi}}{dy^2} = 0 \tag{4-44}$$

Applying boundary conditions to the above yields:

$$\frac{d^2\vec{\phi}}{dy^2} - \frac{1}{h^2} P_{DD}\vec{\phi} + \frac{\vec{V}}{h^2} = 0 \tag{4-45}$$

Equation (4-45) is in general form and holds in all dielectric sub-regions with only the vector $\vec{V}$ and the dimension of the system changing from one region to the other. The applicable boundary conditions in region I are: $\phi_0 = 0$ and $\phi_{N_1} = V_0$ while the boundary conditions applicable in region III are: $\phi_{N_2} = V_0$ and $\phi_{N+1} = 0$. The voltage vector $\vec{V}$ in regions I and III is thus: $\vec{V} = \vec{V}_I$ and $\vec{V} = \vec{V}_{III}$, respectively, where:

$$\vec{V}_I = [0\ 0 \cdots V_0]^T_{(N_1-1)} \tag{4-46a}$$

and:

$$\vec{V}_{III} = [V_0\ 0 \cdots 0]^T_{(N-N_2)} \tag{4-46b}$$

Equation (4-45) can be solved in each sub-region by applying the transformation defined by Equation (4-14) $\bar{\phi} = T_{I,III}\tilde{\phi}$ and multiplying through by $T_{I,III}^{-1}$:

$$\frac{d^2\tilde{\phi}}{dy^2} - \frac{1}{h^2}T_{I,III}^{-1}P_{DD}T_{I,III}\tilde{\phi} + \frac{1}{h^2}T_{I,III}^{-1}\bar{V}_{I,III} = 0 \tag{4-47}$$

The transformation matrices $T_{I,III}$ are then selected such that P_{DD} is diagonalized in each sub-region. The above thus describes a system of uncoupled second-order differential equations. On line i and within the m^{th} layer, as defined in Figure 4.3, Equation (4-47) yields the component equation:

$$\frac{d^2\tilde{\phi}_i}{dy^2} - \frac{1}{h^2}\lambda_{m,i}^2\tilde{\phi}_i + \frac{1}{h^2}\left[T_{I,III}^{-1}\bar{V}_{I,III}\right]_i = 0 \tag{4-48}$$

which has the following general solution within the dielectric sub-regions I and III of layer m:

$$\begin{aligned}\tilde{\phi}_i(y) = \cosh\left[\frac{\lambda_{m,i}}{h}(y-y_{m-1})\right]\left(\tilde{\phi}_i(y_{m-1}) - \frac{\left[T_{I,III}^{-1}\bar{V}_{I,III}\right]_i}{\lambda_{m,i}^2}\right) \\ + \frac{h}{\lambda_{m,i}}\sinh\left[\frac{\lambda_{m,i}}{h}(y-y_{m-1})\right]\frac{d\tilde{\phi}_i(y_{m-1})}{dy} + \frac{\left[T_{I,III}^{-1}\bar{V}_{I,III}\right]_i}{\lambda_{m,i}^2}\end{aligned} \tag{4-49a}$$

$$\begin{aligned}\frac{d\tilde{\phi}_i(y)}{dy} = \frac{\lambda_{m,i}}{h}\sinh\left[\frac{\lambda_{m,i}}{h}(y-y_{m-1})\right]\left(\tilde{\phi}_i(y_{m-1}) - \frac{\left[T_{I,III}^{-1}\bar{V}_{I,III}\right]_i}{\lambda_{m,i}^2}\right) \\ + \cosh\left[\frac{\lambda_{m,i}}{h}(y-y_{m-1})\right]\frac{d\tilde{\phi}_i(y_{m-1})}{dy}\end{aligned} \tag{4-49b}$$

It is implied in the above that the set of eigenvalues $\lambda_{m,i}$ are associated with either T_I or T_{III} and thus belong either to region I or III. Evaluating (4-49) at $y = y_m^-$ and $y_{m-1} = y_{m-1}^+$, transforming back to the spatial domain, and manipulating such that the normal derivatives are given in terms of the potentials, yields:

$$\frac{d\bar{\phi}(y_{m-1}^{+})}{dy} = -T_{I,III}\left[\frac{\lambda_{m,i}}{h}\coth\left(\frac{\lambda_{m,i}}{h}d_m\right)\right]_{diag} T_{I,III}^{-1}\bar{\phi}(y_{m-1}) + T_{I,III}\left[\frac{\lambda_{m,i}}{h}\coth\left(\frac{\lambda_{m,i}}{h}d_m\right)\right]_{diag} T_{I,III}^{-1}\bar{\phi}(y_m) + T_{I,III}\left[\frac{1}{h\lambda_{m,i}}\left(\coth\left(\frac{\lambda_{m,i}}{h}d_m\right) - \operatorname{csch}\left(\frac{\lambda_{m,i}}{h}d_m\right)\right)\right]_{diag} T_{I,III}^{-1}\bar{V}_{I,III} \quad (4\text{-}50a)$$

$$\frac{d\bar{\phi}(y_{m}^{-})}{dy} = -T_{I,III}\left[\frac{\lambda_{m,i}}{h}\operatorname{csch}\left(\frac{\lambda_{m,i}}{h}d_m\right)\right]_{diag} T_{I,III}^{-1}\bar{\phi}(y_{m-1}) + T_{I,III}\left[\frac{\lambda_{m,i}}{h}\coth\left(\frac{\lambda_{m,i}}{h}d_m\right)\right]_{diag} T_{I,III}^{-1}\bar{\phi}(y_m) - T_{I,III}\left[\frac{1}{h\lambda_{m,i}}\left(\coth\left(\frac{\lambda_{m,i}}{h}d_m\right) - \operatorname{csch}\left(\frac{\lambda_{m,i}}{h}d_m\right)\right)\right]_{diag} T_{I,III}^{-1}\bar{V}_{I,III} \quad (4\text{-}50b)$$

Within region II, the following must hold since the potential is invariant everywhere inside the metal:

$$\frac{d\bar{\phi}(y_{m-1}^{+})}{dy} = \frac{d\bar{\phi}(y_{m}^{-})}{dy} = 0 \quad (4\text{-}51)$$

Collating (4-50) and (4-51), forms the following equations for the normal derivative of the potential across regions I, II and III at the positions y_{m-1}^{+} and y_{m}^{-}:

$$\frac{d\bar{\phi}(y_{m-1}^{+})}{dy} = -TBT^{-1}\bar{\phi}(y_{m-1}) + TCT^{-1}\bar{\phi}(y_m) + TDT^{-1}\bar{V}_t \quad (4\text{-}52a)$$

$$\frac{d\bar{\phi}(y_{m}^{-})}{dy} = -TCT^{-1}\bar{\phi}(y_{m-1}) + TBT^{-1}\bar{\phi}(y_m) - TDT^{-1}\bar{V}_t \quad (4\text{-}52b)$$

where:

$$T = \begin{bmatrix} T_I & & \\ & 0 & \\ & & T_{III} \end{bmatrix} \qquad T^{-1} = \begin{bmatrix} T_I^{-1} & & \\ & 0 & \\ & & T_{III}^{-1} \end{bmatrix} \quad (4\text{-}53a)$$

$$B=\begin{bmatrix} B_I & & \\ & 0 & \\ & & B_{III} \end{bmatrix} \qquad B_{I,III}=\left[\frac{\lambda_{m,i}}{h}\coth\left(\frac{\lambda_{m,i}}{h}d_m\right)\right]_{diag} \tag{4-53b}$$

$$C=\begin{bmatrix} C_I & & \\ & 0 & \\ & & C_{III} \end{bmatrix} \qquad C_{I,III}=\left[\frac{\lambda_{m,i}}{h}\operatorname{csch}\left(\frac{\lambda_{m,i}}{h}d_m\right)\right]_{diag} \tag{4-53c}$$

$$D=\begin{bmatrix} D_I & & \\ & 0 & \\ & & D_{III} \end{bmatrix} \qquad D_{I,III}=\left[\frac{1}{h\lambda_{m,i}}\left(\coth\left(\frac{\lambda_{m,i}}{h}d_m\right)-\operatorname{csch}\left(\frac{\lambda_{m,i}}{h}d_m\right)\right)\right]_{diag} \tag{4-53d}$$

and

$$\bar{V}_t=\left[\bar{V}_I \;\; 0 \;\; \bar{V}_{III}\right]^T_{(N)} \tag{4-53e}$$

Equations (4-26a) and (4-26b) can be written at y_m^+ and y_{m-1}^-, respectively, to take into account the dielectric layers above and below the conductors:

$$\frac{d\bar{\phi}(y_m^+)}{dy}=T_{m+1}A_{m+1}^{-1}T_{m+1}^{-1}\bar{\phi}(y_m^+) \tag{4-54a}$$

$$\frac{d\bar{\phi}(y_{m-1}^-)}{dy}=T_{m-1}A_{m-1}^{-1}T_{m-1}^{-1}\bar{\phi}(y_{m-1}^-) \tag{4-54b}$$

Combining Equations (4-52) and (4-54) to satisfy the boundary conditions given by Equation (4-27) and written for the interfaces at y_{m-1} and y_m, yields the following system equation:

$$\begin{bmatrix} y_{11} & y_{12} \\ y_{21} & y_{22} \end{bmatrix}\begin{bmatrix} \bar{\phi}(y_{m-1}) \\ \bar{\phi}(y_m) \end{bmatrix}+\begin{bmatrix} z_{11} & \\ & z_{22} \end{bmatrix}\begin{bmatrix} \bar{V}_t \\ \bar{V}_t \end{bmatrix}=\frac{1}{\varepsilon_0}\begin{bmatrix} \bar{\rho}_{st} \\ \bar{\rho}_{sb} \end{bmatrix} \tag{4-55}$$

where:

$$y_{11}=-\varepsilon_{r,m}TCT^{-1} \tag{4-56a}$$

$$y_{12}=-[\varepsilon_{ryy,m+1}]T_{m+1}A_{m+1}^{-1}T_{m+1}^{-1}+\varepsilon_{r,m}TBT^{-1} \tag{4-56b}$$

$$y_{21} = [\varepsilon_{ryy,m-1}] T_{m-1} A_{m-1}^{-1} T_{m-1}^{-1} + \varepsilon_{r,m} TBT^{-1} \tag{4-56c}$$

$$y_{22} = -\varepsilon_{r,m} TCT^{-1} \tag{4-56d}$$

$$z_{11} = -\varepsilon_{r,m} TDT^{-1} \tag{4-56e}$$

$$z_{22} = -\varepsilon_{r,m} TDT^{-1} \tag{4-56f}$$

Partitioning (4-55) in a manner similar to Equation (4-28) and solving the ensuing reduced systems yields the potential distributions $\bar{\phi}(y_{m-1})$, $\bar{\phi}(y_m)$ and charge distributions $\bar{\rho}_{sb}$, $\bar{\rho}_{st}$ at $y = y_{m-1}$ and $y = y_m$, respectively.

The charge distribution on the left and right edges of the metal conductor can be obtained by evaluating the appropriate boundary conditions. On the left edge the following boundary condition must hold:

$$\frac{d\phi_{N_1}^{+}(y)}{dx} - \varepsilon_{r,m} \frac{d\phi_{N_1}^{-}(y)}{dx} = -\frac{\rho_{sl}(y)}{\varepsilon_0} \tag{4-57}$$

which simplifies to:

$$\frac{d\phi_{N_1}^{-}(y)}{dx} = \frac{\rho_{sl}(y)}{\varepsilon_{r,m}\varepsilon_0} \tag{4-58}$$

since $\frac{d\phi_{N_1}^{+}(y)}{dx} = 0$ due to the fact that the potential inside the conductor is invariant. Equation (4-58) can be evaluated at any position y by applying the analytical solution for the potential in region I and using an $O(h)$ or $O(h^2)$ backward difference formula to approximate the derivative along x of $\phi_{N_1}^{-}(y)$ since the latter must be taken across the lines. The charge distribution on the right edge $\rho_{sr}(y)$ can be evaluated in a similar manner.

Once the charge distributions on all edges have been obtained, the capacitances, effective permittivity and characteristic impedance of the line can then be computed using Equations (4-34).

4.4 ABRUPT DISCONTINUITY IN THE DIELECTRIC CONSTANT ALONG THE TRANSVERSE DIMENSION

It is best to put the interface where the dielectric constant has an abrupt transition at the midpoint between solid lines (on an ε_{rxx} dashed line) or to choose the discretization in such a way that this condition is satisfied, as shown in Figure 4.4. The boundary condition to be enforced at this interface is:

$$\varepsilon_{rxx}^{A} \frac{\partial \phi_{i+1/2}^{A}}{\partial x} = \varepsilon_{rxx}^{B} \frac{\partial \phi_{i+1/2}^{B}}{\partial x} \tag{4-59}$$

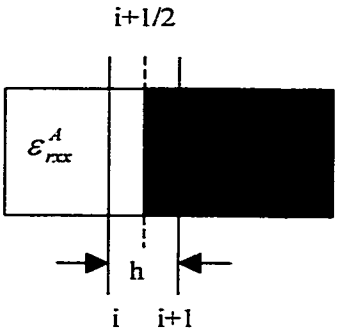

Figure 4.4 Abrupt discontinuity in dielectric constant along the transverse dimension

The derivatives along x are approximated using backward and forward $O(h)$ finite difference formulas:

$$\frac{\partial \phi_{i+1/2}^{A}}{\partial x} \approx \frac{\phi_{i+1/2} - \phi_i}{h/2} \tag{4-60a}$$

and

$$\frac{\partial \phi_{i+1/2}^{B}}{\partial x} \approx \frac{\phi_{i+1} - \phi_{i+1/2}}{h/2} \tag{4-60b}$$

Substituting the above into Equation (4-59) yields:

$$\phi_{i+1/2} = \frac{\varepsilon_{rxx}^{A}\phi_i + \varepsilon_{rxx}^{B}\phi_{i+1}}{\varepsilon_{rxx}^{A} + \varepsilon_{rxx}^{B}} \tag{4-61}$$

Using (4-61) with (4-59) and (4-60) yields:

$$\varepsilon_{rxx}^{A}\frac{\partial\phi_{i+1/2}^{A}}{\partial x} = \varepsilon_{rxx}^{B}\frac{\partial\phi_{i+1/2}^{B}}{\partial x} \approx \left(\frac{2\varepsilon_{rxx}^{A}\varepsilon_{rxx}^{B}}{\varepsilon_{rxx}^{A} + \varepsilon_{rxx}^{B}}\right)\left(\frac{\phi_{i+1} - \phi_i}{h}\right) \tag{4-62}$$

from which it is clear that selecting the equivalent dielectric constant at the interface on line i+1/2 as:

$$\varepsilon_{rxx,i+1/2} = \frac{2\varepsilon_{rxx}^{A}\varepsilon_{rxx}^{B}}{\varepsilon_{rxx}^{A} + \varepsilon_{rxx}^{B}} \tag{4-63}$$

satisfies the applicable boundary condition. Numerical investigations have confirmed this result. Note that the equivalent dielectric constant (4-63) is given by a formula that resembles that used to compute the equivalent impedance of a series combination of capacitors.

4.5 NON-EQUIDISTANT DISCRETIZATION

In the case of extreme differences in the width of the conductors and the intermediate gaps, the number of lines that must be used to adequately represent the features of the structure increases, and as a consequence, so does the computing time. The non-equidistant discretization scheme allows the line spacing to be reduced near small structure features and increased in regions where the fields do not vary rapidly with the transverse dimension thus keeping the computational costs low [27].

The non-equidistant discretization scheme is shown in Figure 4.5. The transverse derivatives can be approximated using central difference formulae:

$$\frac{\partial \phi_{i-1/2}}{\partial x} \approx \frac{\phi_i - \phi_{i-1}}{h_i} \tag{4-64a}$$

and

$$\frac{\partial \phi_{i+1/2}}{\partial x} \approx \frac{\phi_{i+1} - \phi_i}{h_{i+1}} \tag{4-64b}$$

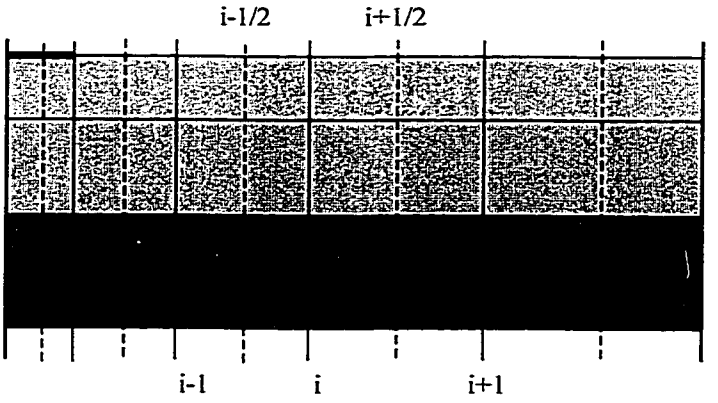

Figure 4.5 Nonequidistant discretization scheme

Then for any line i, the second derivative of the potential is approximated as:

$$\left(\frac{1}{\varepsilon_{ryy}}\frac{\partial}{\partial x}\left(\varepsilon_{rxx}\frac{\partial\phi}{\partial x}\right)\right)_i \approx \frac{1}{\varepsilon_{ryy,i}}\left(\frac{\varepsilon_{rxx,i+1/2}\dfrac{\partial\phi_{i+1/2}}{\partial x}-\varepsilon_{rxx,i-1/2}\dfrac{\partial\phi_{i-1/2}}{\partial x}}{\dfrac{h_i}{2}+\dfrac{h_{i+1}}{2}}\right) \tag{4-65}$$

$$=\frac{2}{h_i h_{i+1}(h_i+h_{i+1})}\left(\frac{\varepsilon_{rxx,i-1/2}}{\varepsilon_{ryy,i}}h_{i+1}\phi_{i-1}-\frac{\varepsilon_{rxx,i-1/2}h_{i+1}+\varepsilon_{rxx,i+1/2}h_i}{\varepsilon_{ryy,i}}\phi_i+\frac{\varepsilon_{rxx,i+1/2}h_i}{\varepsilon_{ryy,i}}\phi_{i+1}\right)$$

Letting $h_i=\alpha_i h$ and $h_{i+1}=\alpha_{i+1}h$, and substituting into the above yields:

$$\left(\frac{1}{\varepsilon_{ryy}}\frac{\partial}{\partial x}\left(\varepsilon_{rxx}\frac{\partial\phi}{\partial x}\right)\right)_i \approx \frac{2}{h^2(\alpha_i+\alpha_{i+1})}\left[\frac{\varepsilon_{rxx,i-1/2}}{\varepsilon_{ryy,i}}\frac{1}{\alpha_i}\phi_{i-1}-\left(\frac{\varepsilon_{rxx,i-1/2}}{\varepsilon_{ryy,i}}\frac{1}{\alpha_i}+\frac{\varepsilon_{rxx,i+1/2}}{\varepsilon_{ryy,i}}\frac{1}{\alpha_{i+1}}\right)\phi_i+\frac{\varepsilon_{rxx,i-1/2}}{\varepsilon_{ryy,i}}\frac{1}{\alpha_{i+1}}\phi_{i+1}\right] \tag{4-66}$$

$$=-\frac{1}{h^2}\left(-a_i\phi_{i-1}+b_i\phi_i-c_i\phi_{i+1}\right)$$

where h is the smallest line spacing and the coefficients a_i, b_i and c_i are observed directly from the equation. The expansion coefficients α_i are normally selected such that the lines are spaced in a geometrical progression.

4.6 OPEN STRUCTURE ALONG VERTICAL DIMENSIONS

Structures that are open along the vertical dimensions have outlines similar to that shown in Figure 4.1 except that $d_1 \to \infty$ and $d_n \to \infty$. From Equations (4-19) and (4-24), we have:

$$A_1 = \left[\frac{h}{\lambda_{1,i}}\tanh(\frac{\lambda_{1,i}}{h}d_1)\right]_{diag} \tag{4-67a}$$

$$A_n = -\left[\frac{h}{\lambda_{n,i}}\tanh(\frac{\lambda_{n,i}}{h}d_n)\right]_{diag} \tag{4-67b}$$

In an open structure, $\tanh(\frac{\lambda_{1,i}}{h}d_1) \to 1$ and $\tanh(\frac{\lambda_{n,i}}{h}d_n) \to 1$, so the above simplifies to:

$$A_1 = \left[\frac{h}{\lambda_{1,i}}\right]_{diag} \tag{4-68a}$$

$$A_n = -\left[\frac{h}{\lambda_{n,i}}\right]_{diag} \tag{4-68b}$$

As $d_1 \to \infty$ and $d_n \to \infty$, from (4-34), the electric potential distribution in layer 1 can be obtained using:

$$\bar{\phi}(y) = T_1\left[e^{(\frac{\lambda_{1,i}}{h}y)}\right]_{diag} T_1^{-1}\bar{\phi}(y_1) \qquad y \le y_1 \tag{4-69a}$$

and in all other layers using:

$$\bar{\phi}(y) = T_m\left(\left[\cosh[\frac{\lambda_{m,i}}{h}(y_m - y)]\right]_{diag} - \left[\frac{h}{\lambda_{m,i}}\sinh[\frac{\lambda_{m,i}}{h}(y_m - y)]\right]_{diag} A_m^{-1}\right)T_m^{-1}\bar{\phi}(y_m) \tag{4-69b}$$

where $y_{m-1} \le y \le y_m$, and $2 \le m \le n-1$

$$\bar{\phi}(y) = T_n \left[e^{-\frac{\lambda_{n,i}}{h}(y-y_{n-1})} \right]_{diag} T_n^{-1} \bar{\phi}(y_{n-1}) \qquad y \geq y_{n-1} \tag{4-69c}$$

The electric field distribution in layer 1 can be obtained using:

$$\bar{E}_y(y) = -T_1 \left[\frac{\lambda_{1,i}}{h} e^{(\frac{\lambda_{1,i}}{h} y)} \right]_{diag} T_1^{-1} \bar{\phi}(y_1) \qquad y \leq y_1 \tag{4-70a}$$

and in all other layers using:

$$\bar{E}_y(y) = -T_m \left(\left[\frac{h}{\lambda_{m,i}} \sinh[\frac{\lambda_{m,i}}{h}(y_m - y)] \right]_{diag} + \left[\cosh[\frac{\lambda_{m,i}}{h}(y_m - y)] \right]_{diag} A_m^{-1} \right) T_m^{-1} \bar{\phi}(y_m) \tag{4-70b}$$

where $y_{m-1} \leq y \leq y_m$, and $2 \leq m \leq n-1$

$$\bar{E}_y(y) = T_n \left[\frac{\lambda_{n,i}}{h} e^{-\frac{\lambda_{n,i}}{h}(y-y_{n-1})} \right]_{diag} T_n^{-1} \bar{\phi}(y_{n-1}) \qquad y \geq y_{n-1} \tag{4-70c}$$

4.7 NUMERICAL RESULTS

4.7.1 Microstrip on an Anisotropic Multi-Layer Substrate

To validate the proposed formulation, the convergence behavior of our method is examined for a microstrip line on isotropic and anisotropic multi-layer media. The structure of interest is shown in Figure 4.6(a). The parameters computed are the effective dielectric constant $\varepsilon_{r,eff}$ and

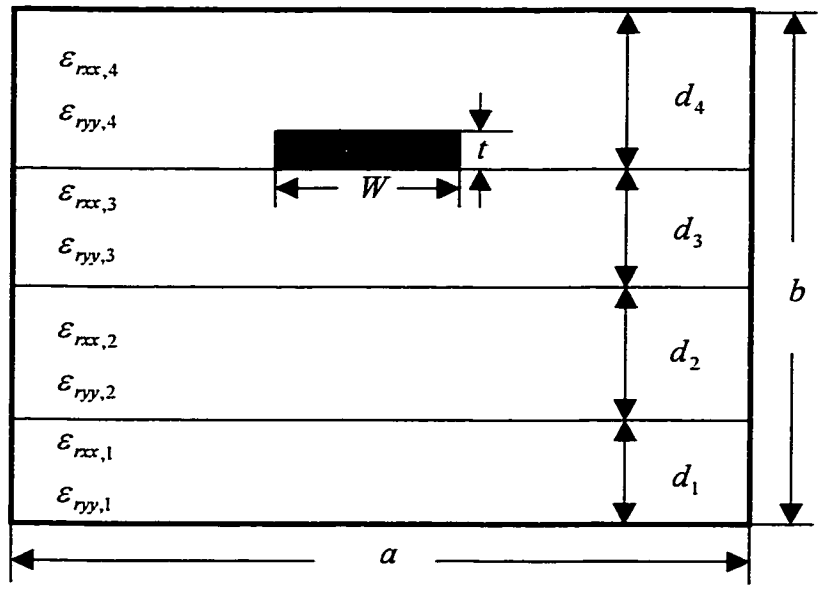

Figure 4.6(a) Microstrip line of width W and thickness t on a multi-layer anisotropic substrate. The physical parameters in arbitrary units are: a=3.0, b=2.0, $d_1=d_2=d_3=0.4$, $d_4=0.8$ and W=0.6. The material parameters for the isotropic case are: $\varepsilon_{rxx,1}=\varepsilon_{ryy,1}=1$, $\varepsilon_{rxx,2}=\varepsilon_{ryy,2}=6$, $\varepsilon_{rxx,3}=\varepsilon_{ryy,3}=10$, $\varepsilon_{rxx,4}=\varepsilon_{ryy,4}=1$, and for the anisotropic case: $\varepsilon_{rxx,1}=3$, $\varepsilon_{ryy,1}=6$, $\varepsilon_{rxx,2}=6$, $\varepsilon_{ryy,2}=10$, $\varepsilon_{rxx,3}=43$, $\varepsilon_{ryy,3}=28$, $\varepsilon_{rxx,4}=\varepsilon_{ryy,4}=1$.

characteristic impedance Z_0 for different values of equidistant line spacing h. Richardson's extrapolation is then used to estimate $\varepsilon_{r,eff}$ and Z_0 for $h=0$ thus providing reference values for the calculation of *anticipated* errors which are computed as:

$$Error(\varepsilon_{r,eff}) = \frac{\varepsilon_{r,eff}^{ref} - \varepsilon_{r,eff}}{\varepsilon_{r,eff}^{ref}} \qquad (4\text{-}71a)$$

and:

$$Error(Z_0) = \frac{Z_0^{ref} - Z_0}{Z_0^{ref}} \tag{4-71b}$$

The convergence results are shown in Figure 4.6(b) for isotropic and anisotropic media considering metallization thicknesses of t=0 and t=0.2. From Figure 4.6(b), it is clear that the

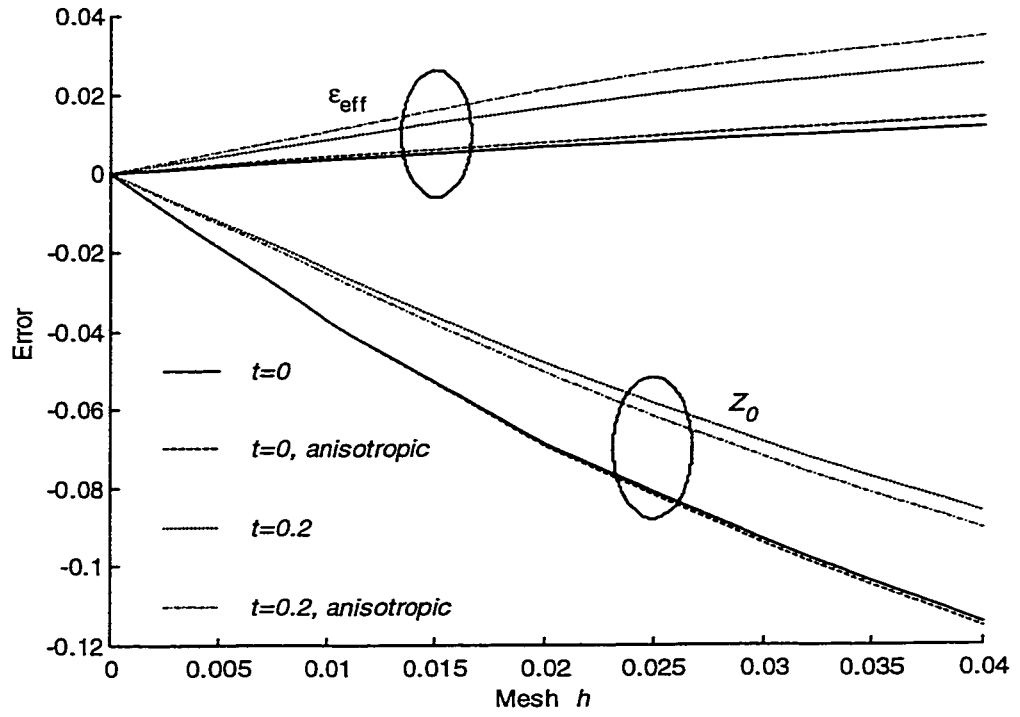

Figure 4.6(b) Convergence of the effective dielectric constant and characteristic impedance of the structure for the isotropic and anisotropic cases. Two conductor thicknesses are considered: t=0 and t=0.2.

convergence is monotonic. It is also apparent that the error in the characteristic impedance is larger than the error in the effective dielectric constant for the same line spacing. The effective dielectric constant and characteristic impedance as a function of the metallization thickness are shown in Figures 4.6(c) and 4.6(d), for the isotropic and anisotropic case respectively. A line spacing of h=0.02 was used to carry out these computations.

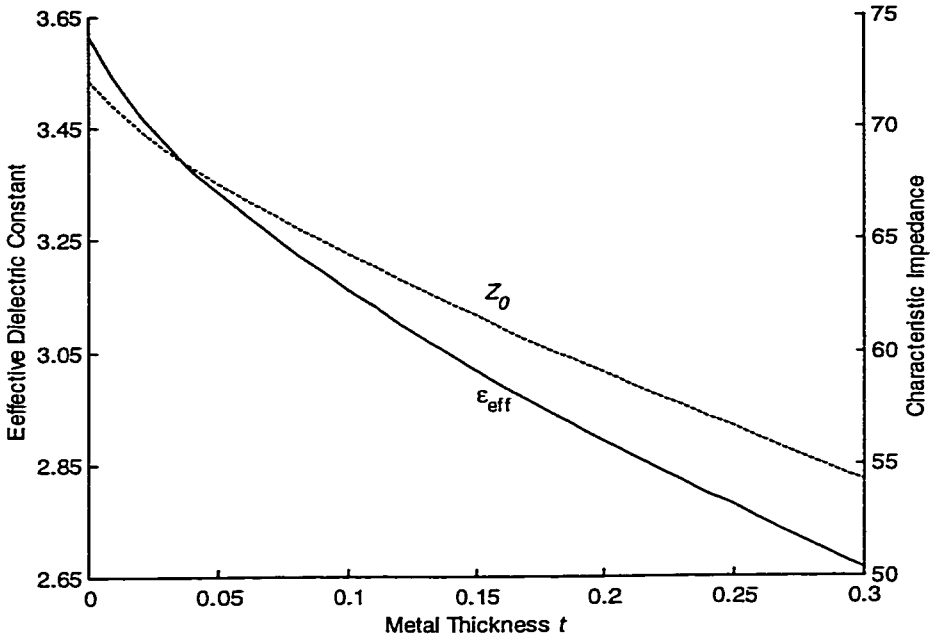

Figure 4.6(c) Effective dielectric constant and characteristic impedance as a function of the conductor thickness for the isotropic case.

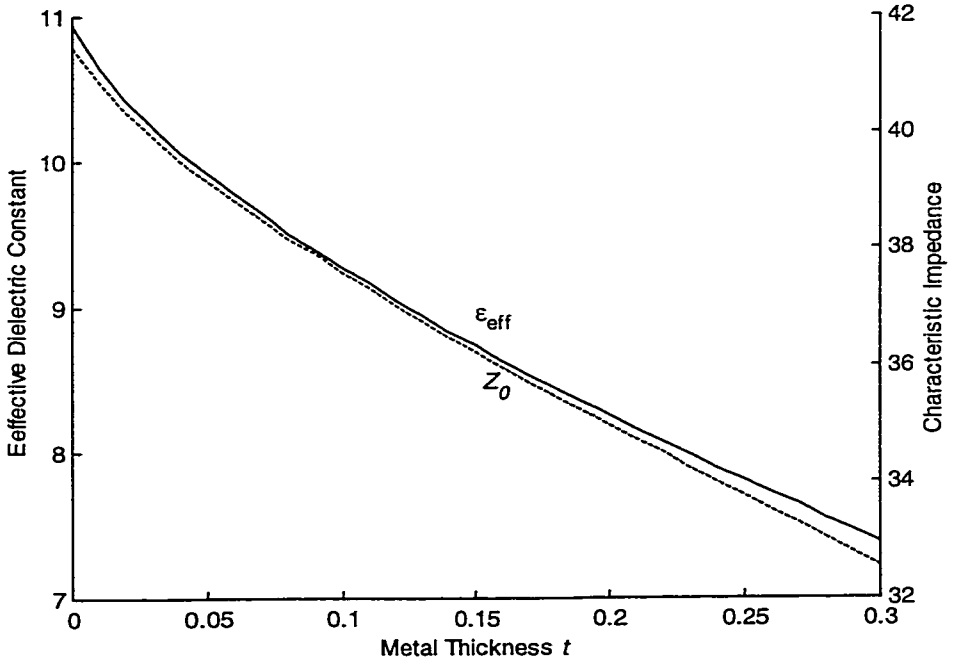

Figure 4.6(d) Effective dielectric constant and characteristic impedance as a function of the conductor thickness for the anisotropic case.

4.7.2 Microstrip on a Inhomogeneous Anisotropic Multi-Layer Substrate

A microstrip line on an inhomogeneous anisotropic multi-layer substrate is shown as in Figure 4.8(a) [22]. The physical parameters are the same as in Figure 4.6(a) except for the third layer, which has a limited width. Abrupt changes in the dielectric constant along the transverse direction are thus present in this layer. An equivalent dielectric constant applicable on such vertical interfaces must be found such that the boundary condition stating that normal $\bar{D}$'s must be continuous over the interface is enforced. The value of the dielectric constant that satisfies this condition has been determined as in section 4.4.

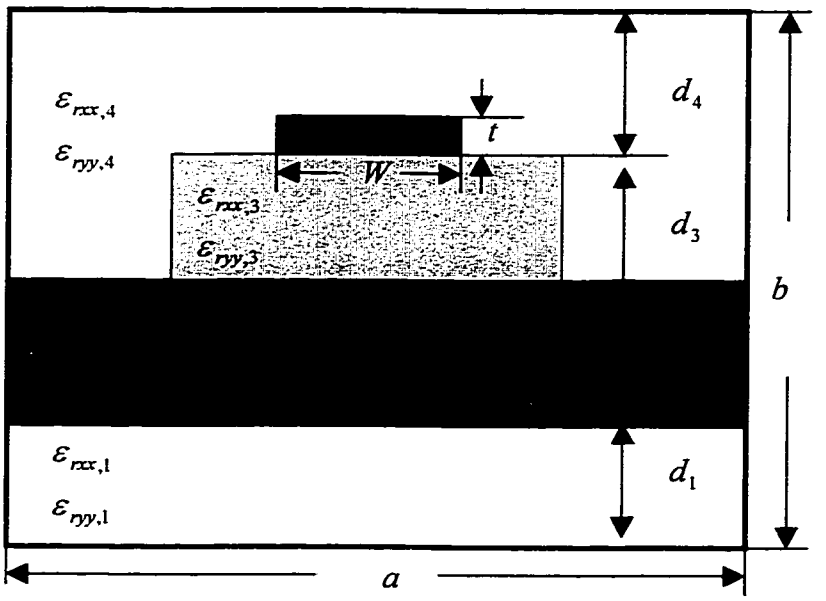

Figure 4.7(a) A microstrip line of width W and thickness t on a multi-layer inhomogeneous anisotropic substrate. The physical parameters are the same as those in Figure 4.6(a) except that the width of the third layer in arbitrary units is: L=1.4.

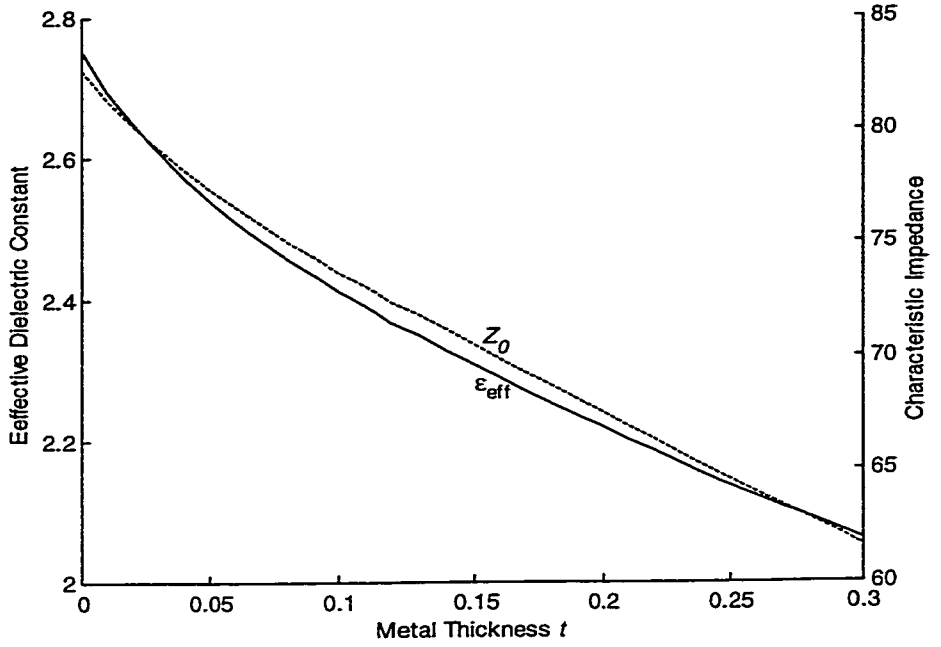

Figure 4.7(b) Effective dielectric constant and characteristic impedance as a function of the conductor thickness for the isotropic case.

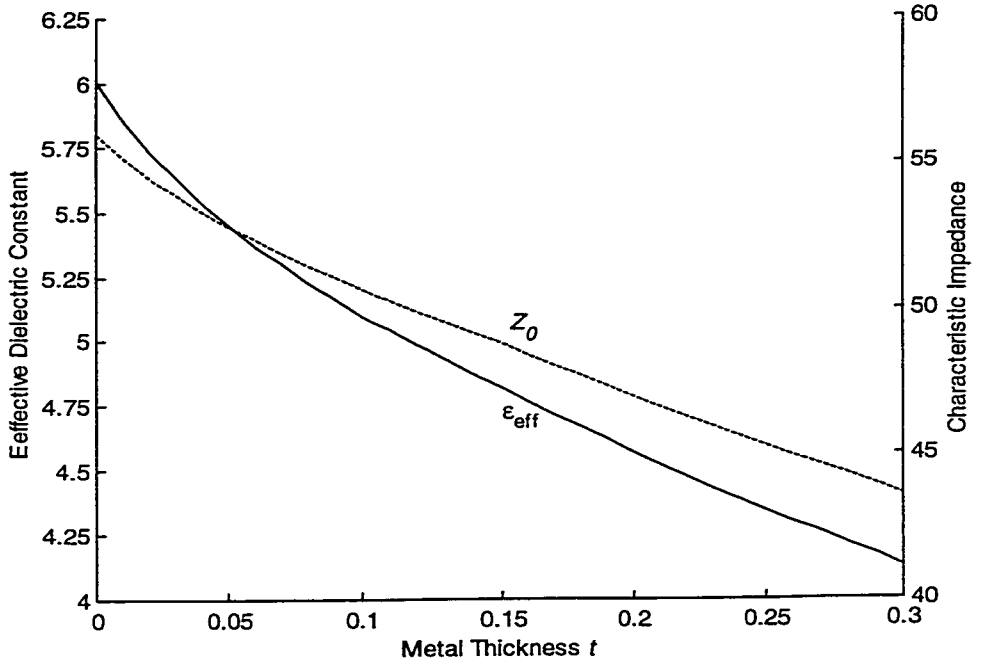

Figure 4.7(c) Effective dielectric constant and characteristic impedance as a function of the conductor thickness for the anisotropic case.

The effective dielectric constant and characteristic impedance as a function of conductor thickness are shown in Figures 4.7(b) and 4.7(c) for the isotropic and anisotropic cases, respectively. An equidistant line spacing of h=0.02 was used. The effective dielectric constants calculated by the MoL for a conductor thickness of t=0 are shown in Table 4.1. The difference between the results calculated by this method and those reported in reference [22] is less than 1%.

Table 4.1 Effective dielectric constant for a microstrip of zero conductor thickness on an inhomogeneous multi-layer substrate.

	This method	Reference[12]	Difference
Isotropic	2.7538	2.7517	0.076%
Anisotropic	6.0044	6.0619	0.949%

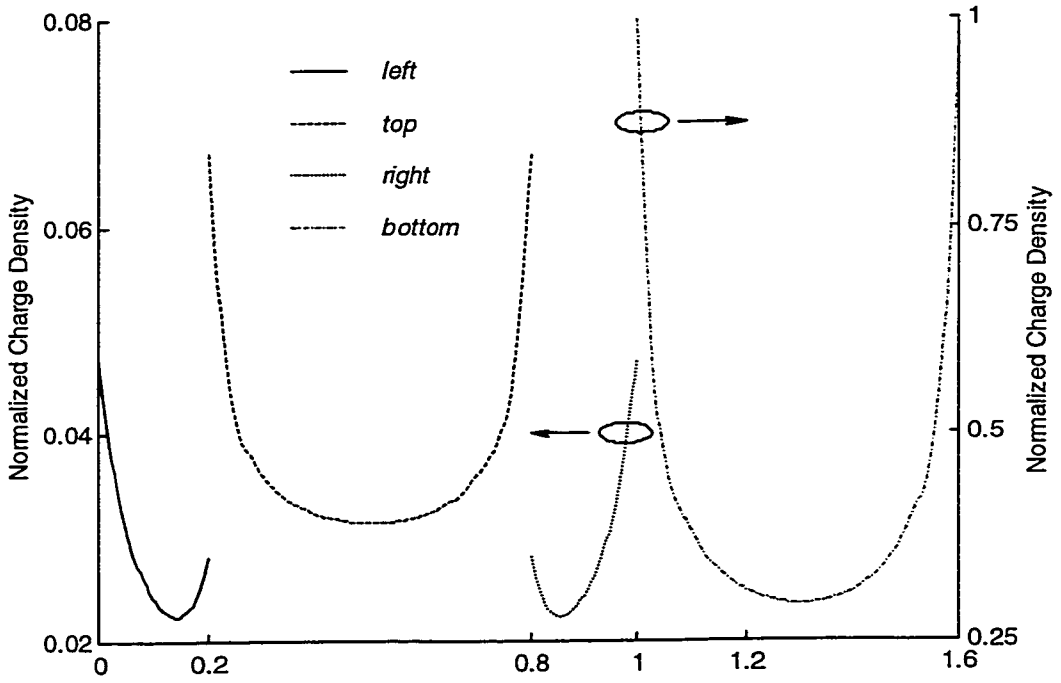

Figure 4.7(d) Charge distribution on all conductor edges for the anisotropic case and t=0.2. A line spacing of h=0.04 was used and the charge distribution is normalized such that the maximum value is unity; the relative magnitude on all edges is conserved.

Other static quantities of interest can be calculated using the method. The charge distribution over all metal edges, and the potential distribution are shown in Figures 4.7(d) and 4.7(e) for the anisotropic case and a metallization thickness of t=0.2. A line spacing of h=0.04 was used and a voltage of 1V applied to the microstrip. Figure 4.7(e) reveals that all boundary conditions applicable to the potential are indeed respected. The electric fields distributions for E_x and E_y are shown in Figures 4.7(f) and 4.7(g) respectively.

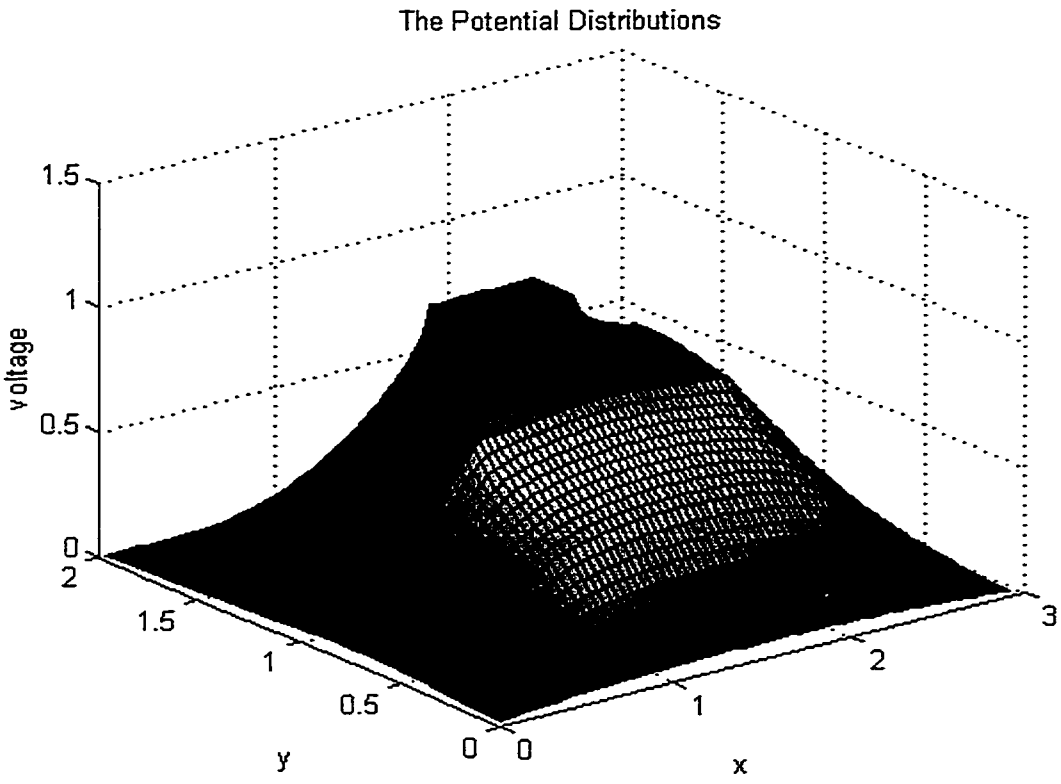

Figure 4.7(e) Potential distribution over the cross-section of the structure for the anisotropic case and t=0.2. A line spacing of h=0.04 was used and a voltage of 1V was applied to the microstrip.

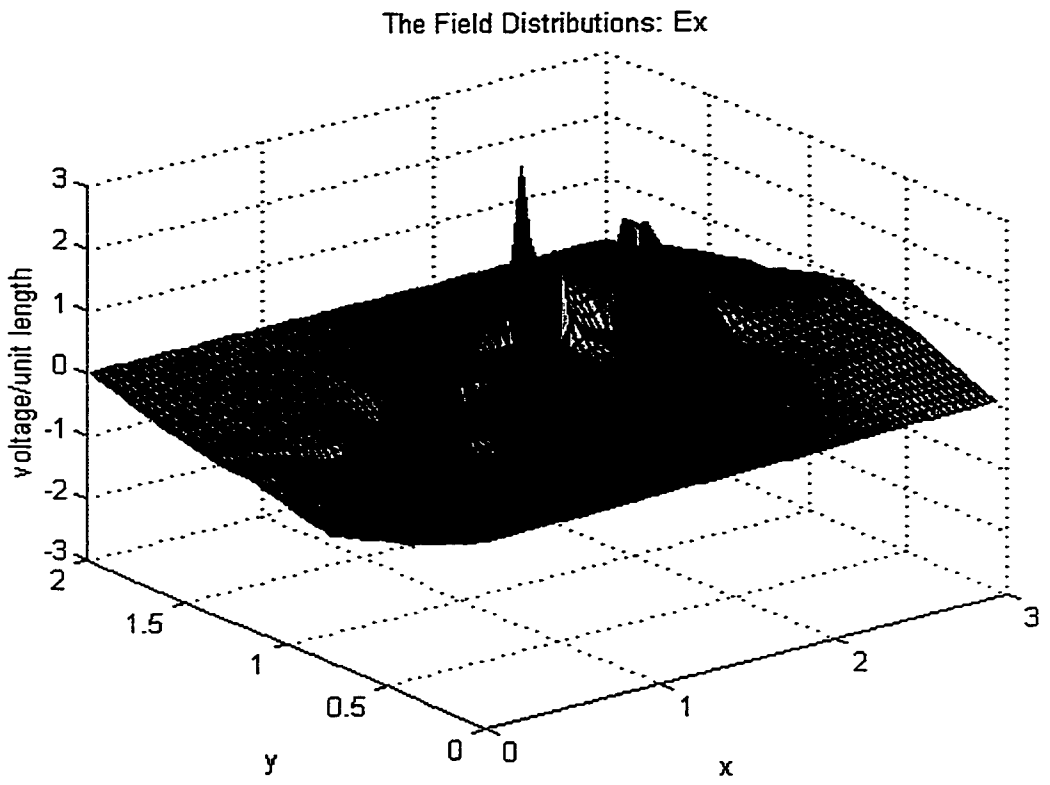

Figure 4.7(f) Electric distribution E_x over the cross-section of the structure for the anisotropic case and t=0.2. A line spacing of h=0.04 was used and a voltage of 1V was applied to the microstrip.

Structures such as those shown in the Figure 4.7(a) often require a non-equidistant discretization so that all lateral dimensions and boundary conditions are respected. A non-equidistant discretization scheme applicable to this formulation is presented in section 4.5 and results computed using this scheme for the structure shown as in Figure 4.7(a) are in good agreement with those computed using an equidistant line spacing.

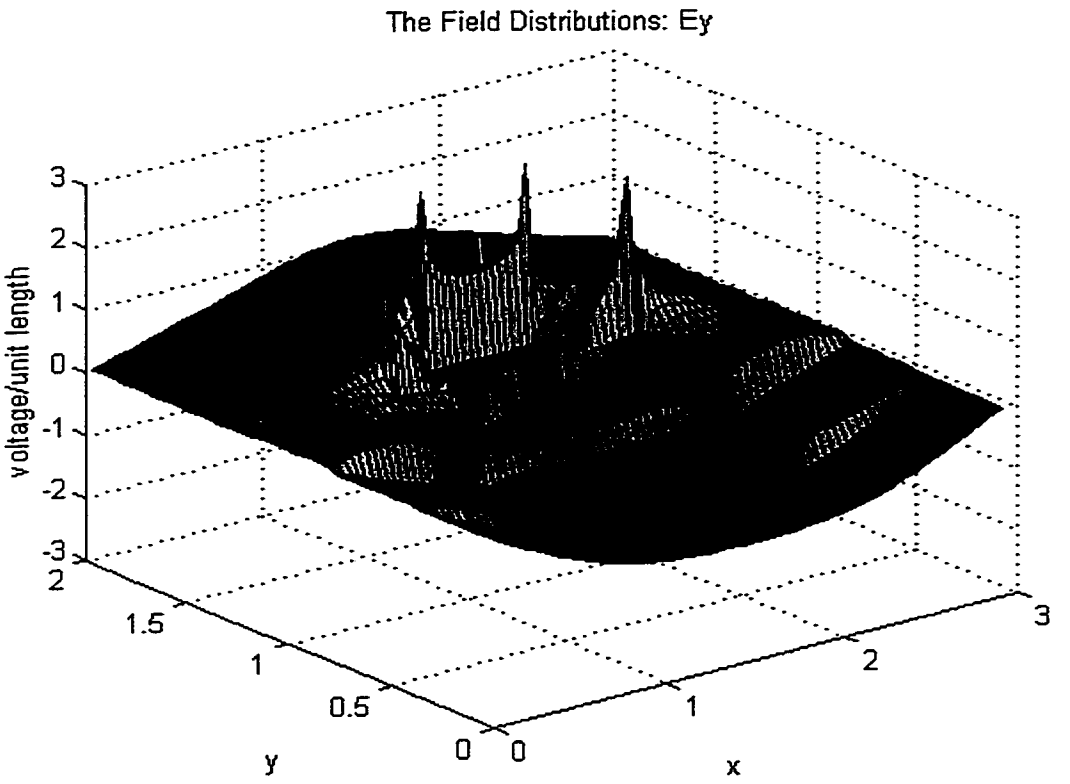

Figure 4.7(g) Electric distribution E_y over the cross-section of the structure for the anisotropic case and t=0.2. A line spacing of h=0.04 was used and a voltage of 1V was applied to the microstrip.

4.7.3 Microstrip on an Anisotropic Substrate Having a 2-D Gaussian Permittivity Profile

A microstrip on an inhomogeneous anisotropic substrate having a continuously variable permittivity can also be handled by the method. The structure is shown in Figure 4.8(a).

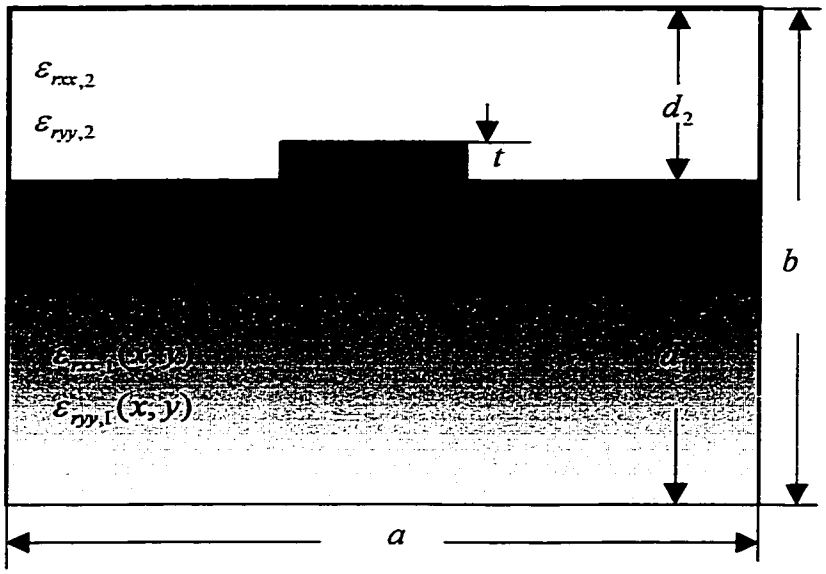

Figure 4.8 (a) A microstrip of width W and thickness t on an inhomogeneous anisotropic substrate is shown as the inset. The physical parameters in arbitrary units are: a=3.0, b=2.0, d_1=1.2, d_2=0.8 and W=0.6. The substrate permittivity tensor is described by the two-dimensional Gaussian distributions given by Equation (4-72).

The relative permittivity tensor of the substrate has the following spatial dependency:

$$\varepsilon_{rxx,1} = 1 + \Delta\varepsilon_{rxx,1} e^{-[(x-p)/p]^2} e^{-[(y-q)/q]^2} \tag{4-72a}$$

and

$$\varepsilon_{ryy,1} = 1 + \Delta\varepsilon_{ryy,1} e^{-[(x-p)/p]^2} e^{-[(y-q)/q]^2} \tag{4-72b}$$

where $p = a/2$ and $q = d_1$. Two cases are considered: the isotropic case where $\Delta\varepsilon_{rxx,1} = \Delta\varepsilon_{ryy,1} = 6$, $\varepsilon_{rxx,2} = \varepsilon_{ryyx,2} = 1$ and the anisotropic case where $\Delta\varepsilon_{rxx,1} = 43$, $\Delta\varepsilon_{ryy,1} = 28$, $\varepsilon_{rxx,2} = \varepsilon_{ryyx,2} = 1$.

The permittivity of the substrate varies in a continuous fashion along the vertical direction so the substrate is divided into thin layers where the permittivity in each layer is assumed constant along the vertical direction. The effective dielectric constant and characteristic impedance were computed as a function of conductor thickness and the results are shown in Figure 4.8(b) for the anisotropic case. A line spacing of h=0.02 and a substrate layering thickness of d=0.02 were found to be adequate to compute the results to a reasonable accuracy. The effective dielectric

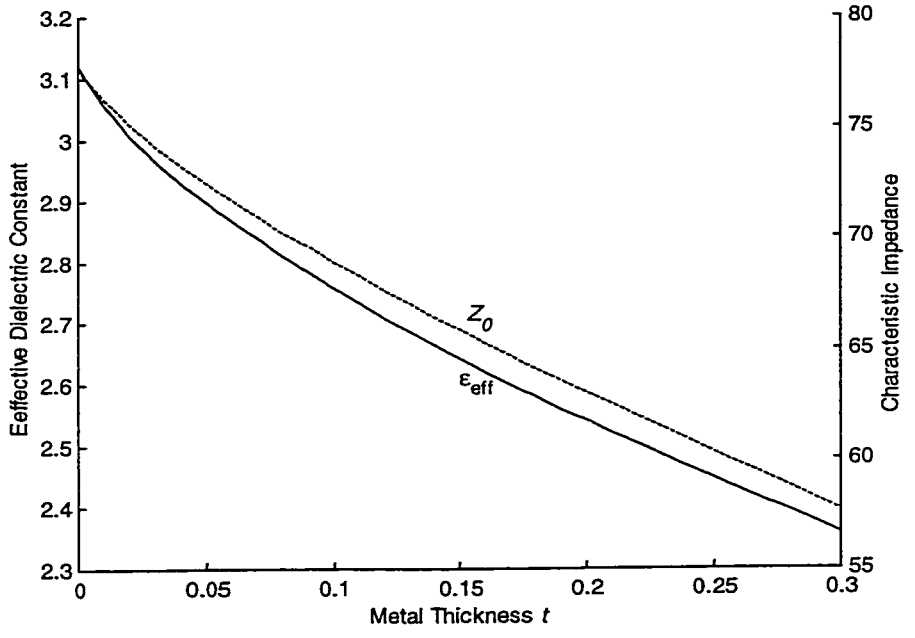

Figure 4.8 (b) Effective dielectric constant and characteristic impedance are plotted as a function of the conductor thickness for the isotropic case.

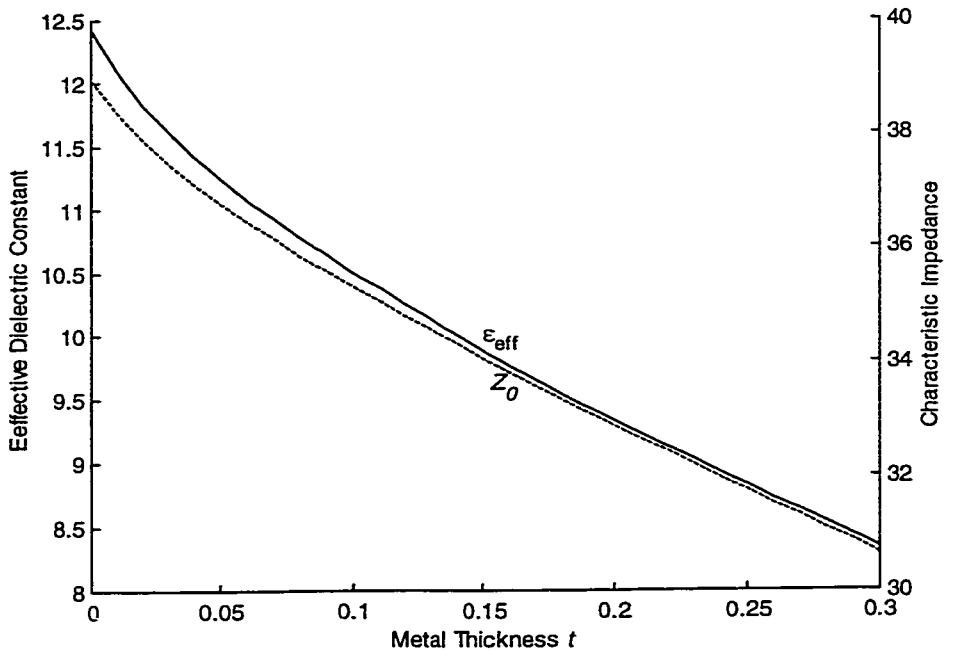

Figure 4.8 (c) Effective dielectric constant and characteristic impedance are plotted as a function of the conductor thickness for the anisotropic case.

constant calculated using the MoL for a metallization thickness of t=0 are shown in Table 4.2. The difference between the results calculated by the MoL and those reported in [22] is less than 0.05%.

Table 4.2 Effective dielectric constant for a microstrip of zero conductor thickness on an inhomogeneous substrate having a 2-D Gaussian permittivity profile.

.	This method	Reference[12]	Difference
Isotropic	3.1198	3.1213	0.048%
Anisotropic	12.4154	12.4150	0.003%

4.7.4 Rectangular Coaxial Air Lines

In order to further validate the method, symmetric rectangular coaxial lines in air were analyzed [11], [17], [18]. The dimensions of the structures considered are: a=b=1mm, $d_2=d_3=0$, $d_1+d_4=1$mm and the permittivities of the dielectric layers are: $\varepsilon_{rxx,1}=\varepsilon_{ryy,1}=\varepsilon_{rxx,4}=\varepsilon_{ryy,4}=1$, where all quantities are given with respect to Figure 4.6(a). The dimensions d_1 and d_4 are selected such that the center conductor is centered along the vertical axis; this conductor is also centered along the horizontal axis. Various center conductor widths W and thicknesses t were considered. Table 4.3 shows the convergence with line spacing h of the characteristic impedance for various center conductor dimensions. The value of characteristic impedance at h=0 is obtained by using Richardson's extrapolation formula. Table 4.4 shows that the characteristic impedance obtained using the MoL is in very good agreement with the results reported in the literature for all center conductor dimensions considered.

Table 4.3 Convergence with line spacing h of the characteristic impedance of rectangular coaxial air lines having various center conductor widths and thicknesses. The characteristic impedance at h=0 is obtained using Richardson's extrapolation formula.

W (mm)	t (mm)	Z_0 (Ω) h=0.05 (mm)	Z_0 (Ω) h=0.025 (mm)	Z_0 (Ω) h=0.0125 (mm)	Z_0 (Ω) h=0.00625 (mm)	Z_0 (Ω) h=0
0.2	0.1	145.899	128.544	120.077	115.485	110.497
0.2	0.2	115.701	104.308	98.614	95.525	92.182
0.4	0.1	98.103	90.153	85.876	83.460	80.782
0.4	0.2	80.112	74.562	71.556	69.863	67.993
0.6	0.2	54.656	52.952	51.820	51.092	50.221

Table 4.4 Characteristic impedance of rectangular coaxial air lines. Comparison of results computed using this method with results published in the literature

W (mm)	t (mm)	Z_0 (Ω) Reference [11]	Z_0 (Ω) Reference [17]	Z_0 (Ω) Reference [18]	Z_0 (Ω) This Method
0.2	0.1	108.96	108.07	109.32	110.50
0.2	0.2	92.44	91.04	90.19	92.18
0.4	0.1	80.92	79.18	80.20	80.78
0.4	0.2	67.62	66.84	66.82	67.99
0.6	0.2	50.54	49.42	49.65	50.22

4.7.5 Coplanar Waveguide (CPW) on a Multi-Layer Anisotropic Substrate

A coplanar waveguide on a multi-layer anisotropic substrate is shown as in Figure 4.9 (a). This is

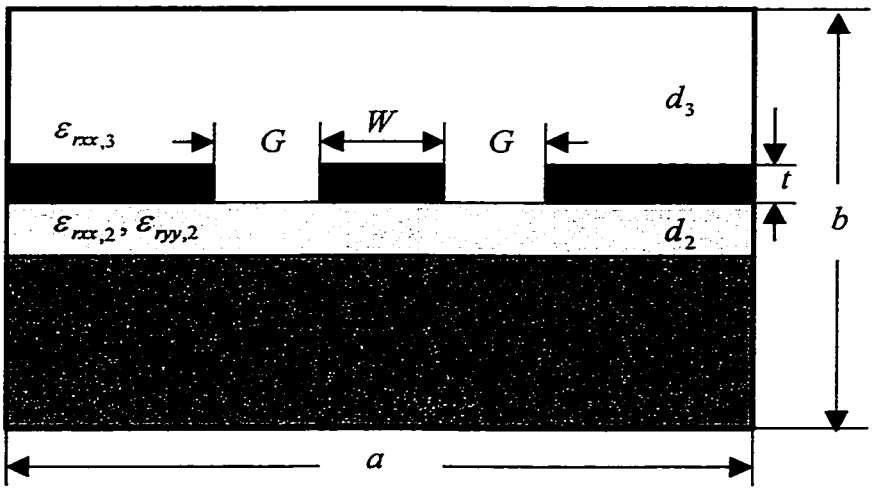

Figure 4.9 (a) A coplanar waveguide of width W, thickness t and ground plane separation G on a multi-layer anisotropic substrate. The physical parameters are: a=100μm, d_1=30μm, d_2=1.2μm, d_3=50μm, W=8μm and G=15μm. The first layer is Z-cut $LiNbO_3$: $\varepsilon_{rxx,1}$=43, $\varepsilon_{ryy,1}$=28, the second layer is an SiO_2 buffer layer: $\varepsilon_{rxx,2}=\varepsilon_{ryy,2}$=3.9, and the third layer has: $\varepsilon_{rxx,3}=\varepsilon_{ryy,3}$=1.

a traveling wave electrooptic modulator [14], [42]. The effective dielectric constant and characteristic impedance have been computed as a function of metallization thickness and the results are plotted in Figure 4.9 (b). A line spacing of h=0.5μm was used for these computations.

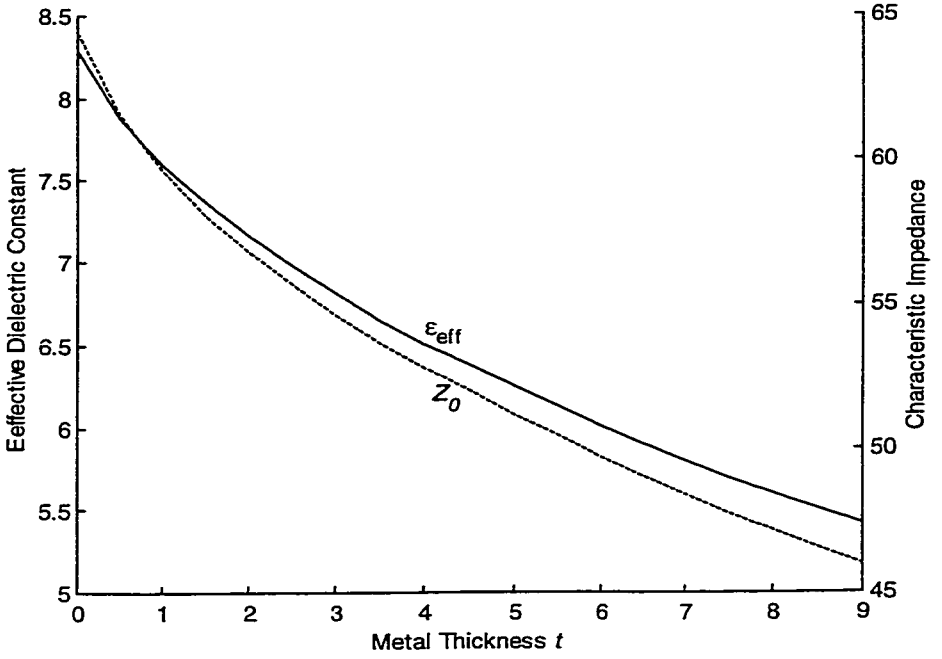

Figure 4.9 (b) The effective dielectric constant and characteristic impedance are plotted as a function of the conductor thickness

4.7.6 Coupled Microstrip on a Multi-layer Anisotropic Substrate

A coupled microstrip on an anisotropic substrate is shown as Figure 4.10(a). This is a typical electrooptic modulator [15]. The electrode parameters are: a=124μm, d_1=50μm, d_3=50μm, W=G=8μm. The substrate is Z-cut $LiNbO_3$: $\varepsilon_{rxx,1}$=43, $\varepsilon_{ryy,1}$=28. The second layer is a buffer layer consisting of SiO_2: $\varepsilon_{rxx,2}=\varepsilon_{ryy,2}$=3.8, and third layer: $\varepsilon_{rxx,3}=\varepsilon_{ryy,3}$=1. The effective dielectric constant and characteristic impedance for different metallization thickness and a line spacing of h=0.5μm are shown in Figure 4.10(b) and Figure 4.10(c) for odd and even modes respectively and d_2=0. Figure 4.10(d) and Figure 4.10 (e) show these quantities for d_2=1.0μm.

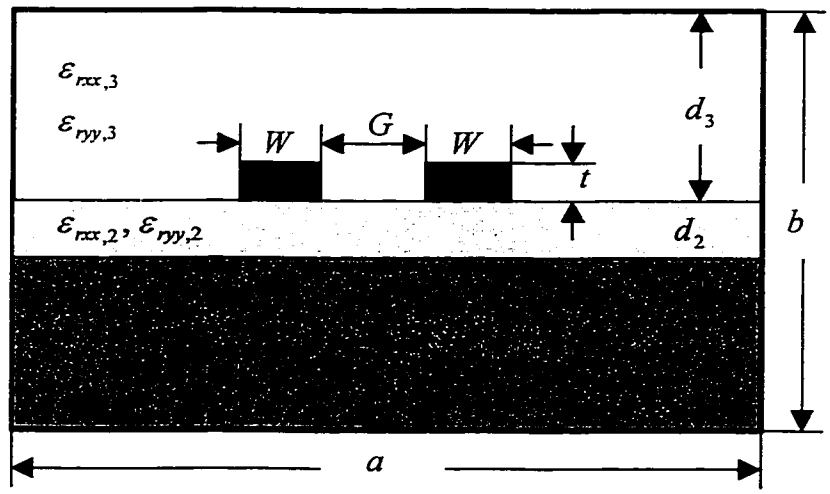

Figure 4.10(a) A coupled microstrip of width W, thickness t and separation G on a multi-layer anisotropic substrate.

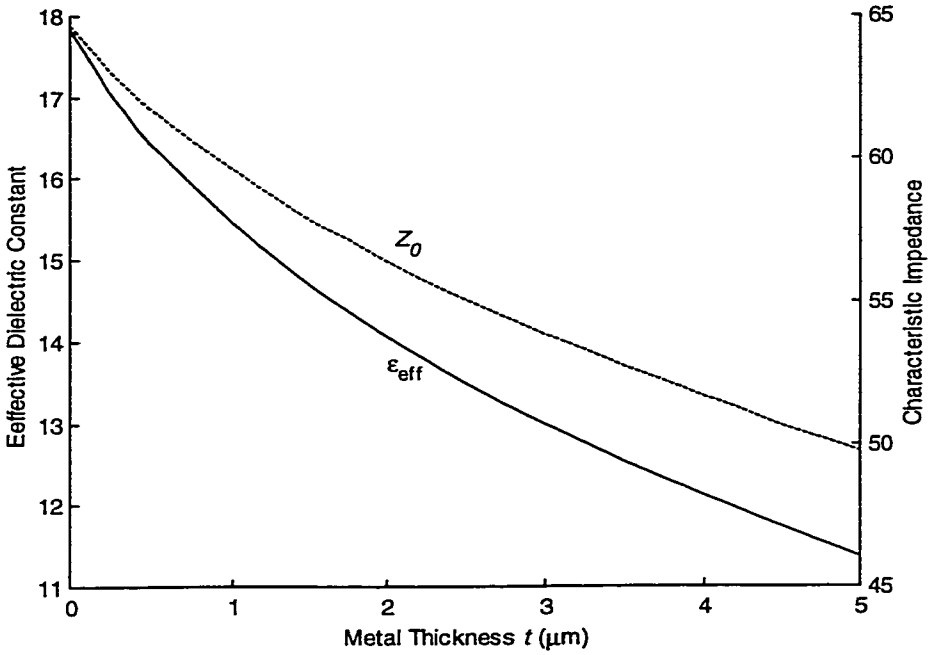

Figure 4.10 (b) The effective dielectric constant and characteristic impedance are plotted as a function of the conductor thickness for the odd mode (d_2=0).

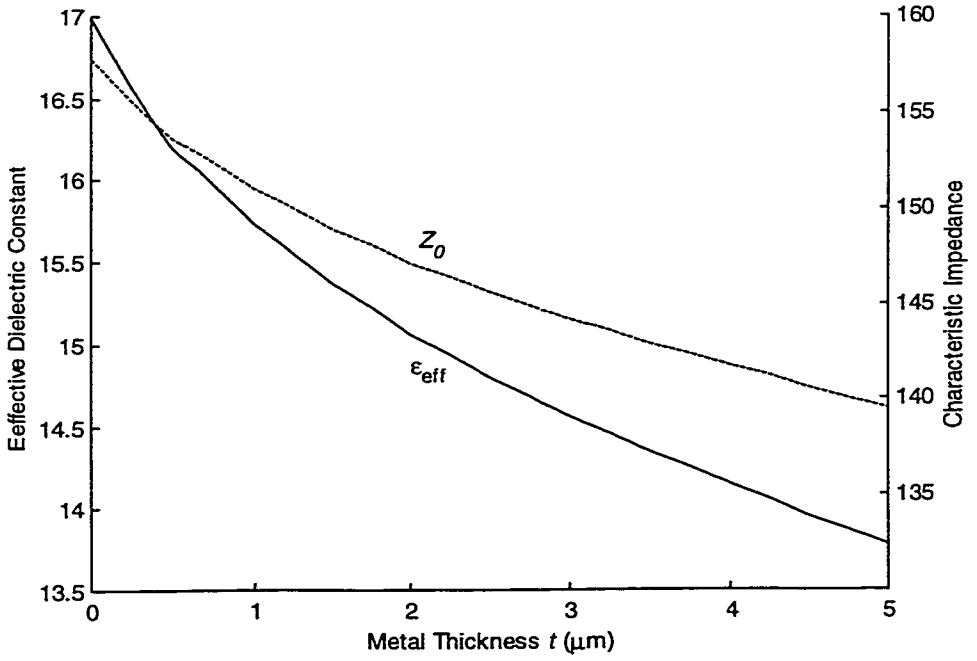

Figure 4.10 (c) The effective dielectric constant and characteristic impedance are plotted as a function of the conductor thickness for the even mode (d_2=0).

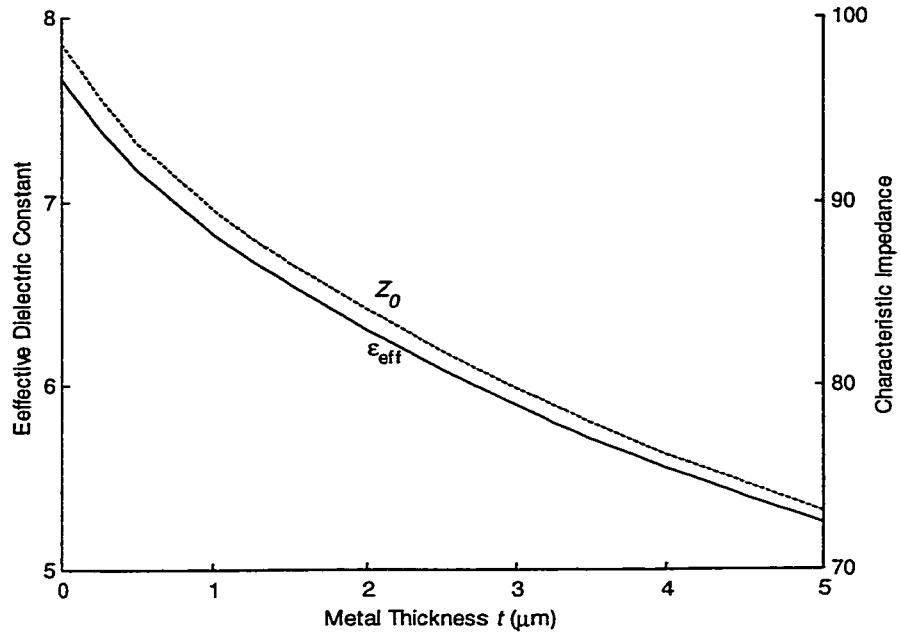

Figure 4.10 (d) The effective dielectric constant and characteristic impedance are plotted as a function of the conductor thickness for the odd mode (d_2=1.0μm).

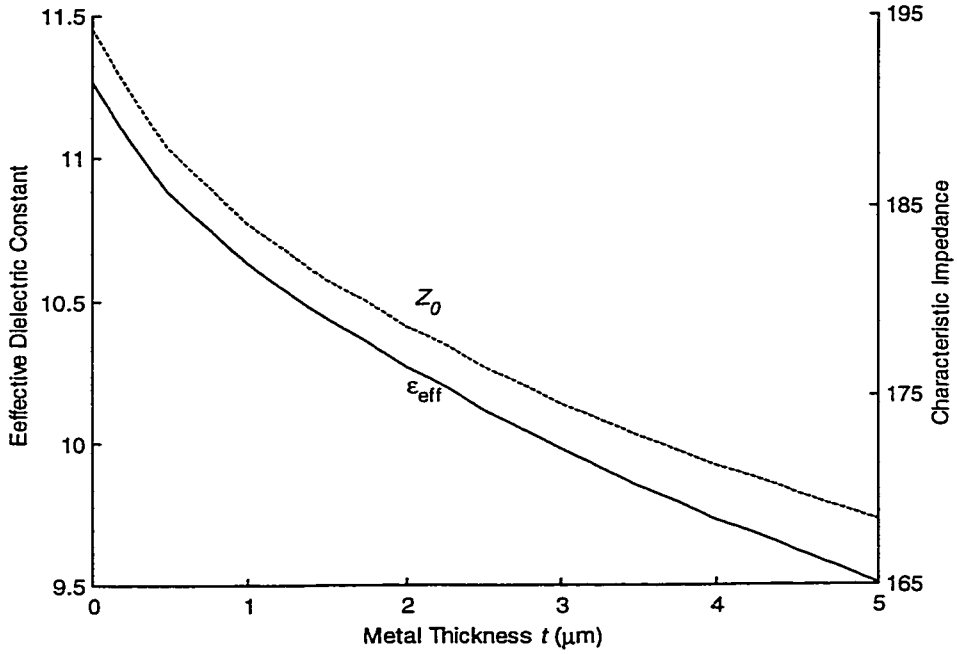

Figure 4.10 (e) The effective dielectric constant and characteristic impedance are plotted as a function of the conductor thickness for the even mode (d_2=1.0μm).

4.8 SUMMARY

In this chapter, a formulation of the method of lines suitable for the electrostatic analysis of multi-conductor transmission lines is presented. The new formulation can handle inhomogenous anisotropic dielectrics and the finite metallization thickness of conductors. The equivalent permittivity at an abrupt dielectric discontinuity along the transverse direction is derived and a non-equidistant discretization scheme is presented. Numerical results for several example structures are given and compared with results reported in the literature in order to validate the method. The method presented is very accurate and numerically efficient compared to other methods currently available in the literature. This method is flexible enough to solve most multi-conductor transmission line problems defined over a rectangular domain and is suitable for inclusion into commercial computer-aided design packages.

CHAPTER 5
CONCLUSION

5.1 MULTILAYER PLANAR OPTICAL WAVEGUIDES

In this thesis, a numerical method based on Cauchy's integration in the complex plane has been developed to analyze the multilayer planar optical waveguides. The new features presented in this thesis include:

(i) The formulation of the multilayer problem for anisotropic media characterized by a diagonal permittivity tensor.

(ii) The derivation and use of an analytical derivative for the dispersion equation.

(iii) The selection of a new integration contour used in conjunction with Cauchy's integration method for locating leaky modes.

Using an analytical derivative improves the accuracy of the method and greatly reduces the CPU time required to find modes. Our new integration contour improves the efficiency of the adaptive integration calculation. This method is applicable to lossless, lossy, active and ARROW waveguide structures and can handle both leaky and guided modes in anisotropic media. Based on the method, object oriented software has been developed for the analysis of multilayer planar optical waveguides.

5.2 MULTI-CONDUCTOR TRANSMISSION LINES

A new formulation of the method of lines suitable for the electrostatic analysis of multi-conductor transmission lines is presented in this thesis.

(i) It can handle inhomogenous anisotropic dielectrics.

(ii) It can handle the finite metallization thickness of conductors.

(iii) The equivalent permittivity at an abrupt dielectric discontinuity along the transverse direction is derived.

(iv) A non-equidistant discretization scheme is presented.

Numerical results compared with results reported in the literature validate this method. The method presented is very accurate and numerically efficient compared to other methods currently available in the literature. This method is flexible enough to solve most multi-conductor transmission line problems defined over a rectangular domain and is suitable for inclusion into commercial computer-aided design packages. Based on this novel numerical technique, a numerical engine has been developed for analyzing the finite-thickness multi-conductor transmission lines.

5.3 THESIS CONTRIBUTIONS

In this thesis, novel numerical techniques for integrated optics and microwave planar structures have been developed and implemented. The novel work for multilayer planar optical waveguides includes [9], [43]:

- The derivation and use of a novel transfer matrix and a new dispersion equation for multilayer planar anisotropic optical waveguides characterized by a diagonal permittivity tensor.
- The derivation and use of an analytical derivative for the dispersion equation.
- The selection of a new integration contour used in conjunction with Cauchy's integration method for locating leaky modes.

The novel work for the electrostatic analysis of multi-conductor transmission lines using method of lines includes [44,45]:

- New formulation of the method of lines suitable for the electrostatic analysis of multi-conductor transmission lines in inhomogenous anisotropic dielectrics.
- New formulation of the method of lines for the finite metallization thickness of conductors.
- Formulation of numerical boundary conditions to handle an abrupt dielectric discontinuity along the transverse direction.
- New formulation of the method of lines for non-equidistant discretization scheme

5.4 SUGGESTIONS FOR FUTURE WORK

The numerical technique presented to analyze multilayer planar optical waveguides can solve both guided and leaky modes for lossless, lossy, active anisotropic and ARROW waveguide structures and thus handle almost all multilayer planar optical waveguides. Future work should focus on how to extend this numerical technique to 2-dimension multilayer optical waveguides such as rib and channel waveguides. For weakly guided optical rib and channel waveguides

including lossy materials, this method can be easily extended based on the effective index method [46] to obtain the complex propagation constant. For strongly guided rib and channel waveguides, this method can be extended based on the weighed index method [46] and the spectral index method [47]. Compared with existing semi-vectorial and full-vectorial mode solves for optical rib and channel optical waveguides, the effective index method, weighed index method and spectral index method combined with Cauchy's integration method will be much more efficient especially when the propagation constant is complex.

For the Quasi-TEM MoL method, possible future work would be to extend the formulation from one conductor layer to two conductor layers. This will make the formulation more complex but it will also make the method more powerful. Another possible extension would be to handle transmission line structures in 3-dimensions. An efficient and accurate modeling and designing tool for analyzing periodic traveling wave structures is needed. Compared with the moment method and finite element methods now widely used in analyzing traveling wave structures, the MoL method would be much more efficient.

REFERENCES

1. J. Chilwell and I. Hodgkinson, " Thin-films field-transfer matrix theory of planar multilayer waveguides and reflection from prism-loaded waveguide," *J. Opt. Soc. Amer. A*, vol. 1, pp. 742-753, July 1984
2. L. M. Walpita, " Solutions for planar optical waveguide equations by selecting zero elements in a characteristic matrix," *J. Opt. Soc. Amer. A*, vol. 2, pp. 595-602, Apr. 1985
3. K. H. Schlereth and M. Tacke, "The complex propagation constant of multilayer waveguides: An algorithm for a personal computer," *IEEE J. Quantum Electron.*, vol. 26, pp. 627-630, Apr. 1990
4. L. Sun and E. Marhic, "Numerical study of attenuation in multilayer infrared waveguides by the circle-chain convergence method", *J. Opt. Soc. Amer. B*, vol. 8, pp478-483, Feb. 1991
5. L. M. Delves and J. N. Lyness, "A numerical method for locating the zeros of an analytic function," *Math. Comp.*, vol. 21, pp. 543-560, 1967
6. L. C. Botten and M. S. Craig, "Complex zeros of analytic functions", *Comput. Phys. Commun.*, vol. 29, pp.245-259, 1983
7. E. Anemogiannis, and E. N. Glytsis, "Multilayer waveguides: efficient numerical analysis of general structures", *J. Lightwave Technol.*, vol. 10, pp. 1344-1351. Oct. 1992
8. R. E. Smith, S. N. Houde-Walter, and G. W. Forbes, " Numerical determination of planar waveguide modes using the analyticity of the dispersion relation," *Opt. Lett.*, vol. 16, pp. 1316-1381, Sept. 1991
9. C. Chen, P. Berini, D. Feng, and V. P. Tzolov, " Efficient and accurate numerical analysis of multilayer planar waveguides", *Proceedings of SPIE*, vol. 3795, pp.676-686, July, 1999

10. W. Huang, R. M. Shubiar, A. Nathan and Y. L. Chow, "The modal characteristics of ARROW structures", *J. Lightwave Technol.*, vol. 10, pp. 1015-1022. Aug. 1992

11. T. Chang and C. Tan, "Analysis of a shield microstrip line with finite metallization thickness by the boundary element method," *IEEE Trans. Microwave Theory Tech.*, vol. 38, pp. 1130-1132, Aug. 1990

12. K. Atsuki and K. Li, "Partial-boundary element method for analysis of striplines with arbitrary cross-sectional dielectric in multi-layered media," *IEEE Trans. Microwave Theory Tech.*, vol. 43, pp. 1153-1161, May 1995

13. Z. Pantic and R. Mittra, "Quasi-TEM analysis of microwave transmission lines by the finite-element method," *IEEE Trans. Microwave Theory Tech.*, vol. MTT-34, pp. 1096-1130, Nov. 1986

14. M. Koshiba, Y. Tsuji, and M. Nishio, "Finite-element modeling of broad-band traveling-wave optical modulators," *IEEE Trans. Microwave Theory Tech.*, vol. 47, pp. 16271633, Sept. 1999

15. H. Jin, R. Vahldieck, M. Bèlanger, and Z. Jakubczyk, "A mode projecting method for the quasi-static analysis of electrooptic device electrodes considering finite metalization thickness and anisotropic substrate," *IEEE J. Quantum Electron.*, vol. 27, pp. 2306-2314, Oct. 1991

16. H. Klingbeil and W. Heinrich, "Calculation of CPW A.C. resistance and inductance using a quasi-static mode-matching approach," *IEEE Trans. Microwave Theory Tech.*, vol. 42, pp. 1004-1007, June 1994

17. N. H. Zhu, W. Qiu, E. Y. B. Pun, and P. S. Chung, "Quasi-static analysis of shielded microstrip transmission lines with thick electrodes," *IEEE Trans. Microwave Theory Tech.*, vol. 45, pp. 288-291, Feb. 1997

18. I. Hong, S. Park, and H. Park, "Quasi-static analysis of coupled microstrip lines with asymmetry finite metallization thickness," *IEEE Trans. Microwave Theory Tech.*, vol. 47, pp. 1739-1742, Sept. 1999

19. G. G. Gentili and G. Macchiarella, "Quasi-static analysis of shielded planar transmission lines with finite metalization thickness by a mixed spectral-space domain method," *IEEE Trans. Microwave Theory Tech.*, vol. 42, pp. 249-255, Feb. 1994

20. J. Kuo, "Accurate quasi-static spectral domain analysis of single and multiple coupled microstrip lines of arbitrary metallization thickness," *IEEE Trans. Microwave Theory Tech.*, vol. 43, pp. 1881-1888, Aug. 1995

21. E. Carlsson and S. Gevorgian, "Conformal mapping of the field and charge distributions in multilayered substrate CPW's," *IEEE Trans. Microwave Theory Tech.*, vol. 47, pp. 1544-1552, Aug. 1999

22. C. Tsai and W. Wang, "An improved multigrid technique for Quasi-TEM analysis of a microstrip embedded in an inhomogeneous anisotropic media," *IEEE Trans. Microwave Theory Tech.*, vol. 45, pp. 678-686, May 1997

23. Y. Naiheng, and R. F. Harrington, "Characteristic Impedance of Transmission lines with arbitrary dielectrics under the TEM approximation," *IEEE Trans. Microwave Theory Tech.*, vol. MTT-34, pp. 472-475, Apr. 1986

24. S. M. Rao, T. K. Sarkar, and R. F. Harrington, "The electrostatic field of conducting bodies in multiple dielectric media," *IEEE Trans. Microwave Theory Tech.*, vol. MTT-32, pp. 1441-1448, Nov. 1984

25. K. Wu, Y. Xu, and R. G. Bosisio, "A technique for efficient analysis of planar integrated microwave circuits including segmented layers and miniature topologies," *IEEE Trans. Microwave Theory Tech.*, vol. 43, pp. 826-833, May 1995

26. G. Keen, M. J. Wale, M. I. Sobhy, and A. J. Holden, "Quasi-static analysis of electrooptic modulators by the method of lines," *J. Lightwave Technol.*, vol. 8, pp. 42-50. Jan. 1990

27. R. Pregla and W. Pascher, "The method of lines," in *Numerical Techniques for Microwave and Millimeter-Wave Passive Structures* T. Itoh, Ed. New York: Wiley, 1989

28. P. Berini and K. Wu, "Modeling lossy anisotropic dielectric waveguides with the method of lines," *IEEE Trans. Microwave Theory Tech.*, vol. 44, pp. 749-759, May 1996

29. Hermann A. Haus, *Waves and Fields in Optoelectronics*, New Jersey, Prentice-Hall Inc., 1984. Chapter 11

30. J. W. Brown and R. V. Churchill, *Complex Variables and Applications*, Sixth Edition, New York: McGraw-Hill, 1996

31. W. H. Press, S. A. Teukolsky, W. T. Vetterling and B. P. Flannery, *Numerical Recipes in C,* Second Edition, Cambridge, 1994

32. J. R. Rice, *Numerical Methods, Software, and Analysis IMSL Reference Edition.* New York: McGraw-Hill, 1983

33. A. S. Kronrod, *Nodes and Weights of Quadrature Formulas*. NewYork: Consultants Bureau, 1965

34. E. K. Sharma and M. P. Singh, "Multilayer waveguide devices with absorbing layers," *J. Opt. Commun.*, vol. 14, pp.134-137, Apr. 1993

35. T. D. Visser, H. Blok and D. Lenstra, "Modal analysis of a planar waveguide with gain and losses," *IEEE J. Quantum Electron.*, vol. 31, pp. 1803-1810, October, 1995

36. T. Baba and Y. Kokubun, "Dispersion and radiation loss characteristics of antiresonsnt reflecting optical waveguides-Numerical Results and Analytical Expressions", *IEEE J. Quantum Electron.*, vol. 28, pp. 1689-1700, July 1992

37. J. Deng and Y. Huang,"A novel hybrid coupler based on antiresonant reflecting optical waveguides," *J. Lightwave Technol.*, vol. 16, no. 6, pp. 1062-1069. June 1998

38. J. Gehler, A. Braüer and W. Karthe, "Remote coupling over 93 μm using ARROW waveguides in strip configuration", *Electron. Letters*, vol. 30, pp. 218-220, 1994

39. B. Ray and G W. Hanson, "Some effects of anisotropy on planar antiresonant reflecting optical waveguides", *J. Lightwave Technol.*, vol. 14, pp. 202-208. Feb. 1996

40. G. G. Gentili and M. Salazar-Palma, "The definition and computation of modal characteristic impedance in quasi-TEM coupled transmission Lines" *IEEE Trans. Microwave Theory Tech.*, vol. 43, pp. 338-343, Feb. 1995

41. F. J. Schmückle and R. Pregla, "The method of lines for the analysis of planar waveguides with finite metallization thickness," *IEEE Trans. Microwave Theory Tech.*, vol. 39, pp. 107-111, Jan. 1991

42. K. Noguchi, O. Mitomi, and H. Miyazawa, "Millimeter-wave Ti:$LiNbO_3$ optical modulators," *J. Lightwave Technol.*, vol. 16, pp. 615-619, Apr. 1998

43. C. Chen, P. Berini, D. Feng, V. I. Tolstikhin, S. Tanev and V. P. Tzolov, "Efficient and accurate numerical analysis of multilayer planar optical waveguides in lossy anisotropic media, " submitted to *J. Lightwave Technol.*, Aug. 1999

44. C. Chen and P. Berini, "A formulation of the method of lines for the electrostatic analysis of finite-thickness multi-conductor transmission lines embedded in inhomogeneous anisotropic dielectrics ," submitted to *IEEE Trans. Microwave Theory Tech.*, Jan. 2000

45. P. Berini and C. Chen, "Quasi-TEM modeling of multi-conductor transmission lines using the method of lines," PIERS 2000, Cambridge Massachusetts, USA, July 2000

46. T. M. Benson and P. C. Kendall, "Variational techniques including effective and weighted index methods," in *Progress In Electromagnetics Research, PIER 10* W. Huang, Ed. Cambridge Massachusetts: EMW Publishing, 1995

47. S. V. Burke, "The spectral index method for semiconductor rib and ridge waveguides," in *Progress In Electromagnetics Research, PIER 10* W. Huang, Ed. Cambridge Massachusetts: EMW Publishing, 1995